

THE ULTRACOOL SPECTROSCOPIC SURVEY. I. VOLUME-LIMITED
SPECTROSCOPIC SAMPLE AND LUMINOSITY FUNCTION OF M7–L5
ULTRACOOL DWARFS.

DANIELLA C. BARDALEZ GAGLIUFFI,^{1,2,*} ADAM J. BURGASSER,²
SARAH J. SCHMIDT,³ CHRISTOPHER THEISSEN,² JONATHAN GAGNÉ,⁴
MICHAEL GILLON,⁵ JOHANNES SAHLMANN,⁶ JACQUELINE K. FAHERTY,¹
CHRISTOPHER GELINO,^{7,8} KELLE L. CRUZ,^{1,9,10,11} NATHALIE SKRZYPEK,¹² AND
DAGNY LOOPER¹³

¹*Department of Astrophysics, American Museum of Natural History, Central Park West at 79th St, New York, NY 10024, USA*

²*Center for Astrophysics and Space Sciences, University of California, San Diego, 9500 Gilman Dr., Mail Code 0424, La Jolla, CA 92093, USA*

³*Leibniz-Institute for Astrophysics Potsdam (AIP), An der Sternwarte 16, D-14482, Potsdam, Germany*

⁴*Institute for Research on Exoplanets, Université de Montréal, Département de Physique, C.P. 6128 Succ. Centre-ville, Montréal, QC H3C 3J7, Canada*

⁵*1 Space sciences, Technologies and Astrophysics Research (STAR) Institute, Université de Liège Allée du 6 Août 17, Bat. B5C, 4000 Liège, Belgium*

⁶*Space Telescope Science Institute (STScI), 3700 San Martin Drive, Baltimore, MD 21218, USA*

⁷*Infrared Processing and Analysis Center (IPAC), California Institute of Technology, 117 Morrisroe Astroscience Lab, Mail Code 100-22, Pasadena CA 91125, USA*

⁸*NASA Exoplanet Science Institute (NExSci), California Institute of Technology, Mail Code 100-22, 1200 East California Blvd., Pasadena, CA 91125, USA*

⁹*Hunter College, City University of New York, 695 Park Ave, New York, NY 10065, USA*

¹⁰*Department of Physics, Graduate Center, City University of New York, 365 5th Ave, New York, NY 10016, USA*

¹¹*Center for Computational Astrophysics, Flatiron Institute, 162 5th Avenue, New York, NY 10010 USA*

¹²*Blackett Laboratory, Imperial College, Prince Consort Rd, Kensington, London SW7 2AZ, UK*

¹³*CBS Studios, 4024 Radford Ave, Studio City, CA 91604*

(Received; Revised; Accepted June 12, 2019)

Submitted to ApJS

ABSTRACT

We present a volume-limited, spectroscopically-verified sample of M7–L5 ultracool dwarfs within 25 pc. The sample contains 410 sources, of which 93% have trigonometric distance measurements (80% from *Gaia* DR2), and 81% have low-resolution ($R \sim 120$), near-infrared (NIR) spectroscopy. We also present an additional list of 60 sources which may be M7–L5 dwarfs within 25 pc when distance or spectral type uncertainties are taken into account. The spectra provide NIR spectral and gravity classifications, and we use these to identify young sources, red and blue $J - K_S$ color outliers, and spectral binaries. We measure very low gravity and intermediate gravity fractions of $2.1^{+0.9}_{-0.8}\%$ and $7.8^{+1.7}_{-1.5}\%$, respectively; fractions of red and blue color outliers of $1.4^{+0.6}_{-0.5}\%$ and $3.6^{+1.0}_{-0.9}\%$, respectively; and a spectral binary fraction of $1.6^{+0.5}_{-0.5}\%$. We present an updated luminosity function for M7–L5 dwarfs continuous across the hydrogen burning limit that agrees with previous studies. We estimate our completeness to range between 69 – 80% when compared to an isotropic model. However, we find that the literature late-M sample is severely incomplete compared to L dwarfs, with completeness of $62^{+8}_{-7}\%$ and $83^{+10}_{-9}\%$, respectively. This incompleteness can be addressed with astrometric-based searches of ultracool dwarfs with *Gaia* to identify objects previously missed by color- and magnitude-limited surveys.

Keywords: astronomical databases: miscellaneous — infrared: stars — stars: binaries (including multiple): close — stars: binaries: general — stars: brown dwarfs — stars: fundamental parameters — stars: late-type — stars: low mass — stars: luminosity function — methods: observational — methods: statistical — surveys — techniques: spectroscopic

* AMNH Kalbfleisch Fellow.

1. INTRODUCTION

Ultracool dwarfs (UCDs) are the lowest-mass, coldest, and faintest products of star formation, encompassing objects with masses $M \lesssim 0.1 M_{\odot}$, effective temperatures ≤ 2700 K, and spectral types M7 and later (Kirkpatrick et al. 1991). UCDs include both very low-mass (VLM) stars that slowly fuse hydrogen for up to a trillion years (Laughlin et al. 1997); and brown dwarfs, which have insufficient mass to sustain hydrogen fusion in their cores ($M_{BD} \lesssim 0.072 M_{\odot}$ for solar metallicity; Kumar 1963; Hayashi & Nakano 1963). Brown dwarfs never reach thermal equilibrium as they are supported by electron degeneracy pressure, and thus continue to cool and dim over time across spectral types M, L, T, and Y (Kirkpatrick et al. 1999; Burgasser 2002, and Cushing et al. 2011, respectively). The absence of an internal energy generation mechanism results in a degeneracy between mass, age and luminosity (and its proxies, effective temperature, absolute magnitude, and spectral type). As a consequence, the characterization of isolated brown dwarfs is challenging, but the population can be evaluated statistically (e.g. Burgasser 2004; Allen et al. 2005; Metchev et al. 2008; Burningham et al. 2010; Reyl e et al. 2010; Day-Jones et al. 2013; Kirkpatrick et al. 2019).

UCDs are yardsticks of Galactic chemical evolution, as their minimal core fusion mostly preserves their natal compositions. Their interiors are fully convective, allowing measurement of both composition and products of fusion (i.e. Li depletion) from their atmospheres. UCDs are ubiquitous, and include some of the closest neighbors to the Sun, such as the L/T transition and flux reversal binary Luhman 16AB (Luhman 2013), and the coldest known brown dwarf, the \gtrsim Y2 WISE J085510.83–071442.5 ($T_{eff} \sim 250$ K; Luhman 2014), both at a distance of 2 pc. UCDs can host disks (e.g., Ricci et al. 2014; Testi et al. 2016) and exoplanets (e.g., TRAPPIST-1, Gillon et al. 2016, 2017; OGLE-2012-BLG-0358Lb, Han et al. 2013); are found in binary and higher-order multiple systems (e.g., Burgasser et al. 2007c, 2012), and in young clusters and associations (e.g., Gagn e et al. 2015a; Zapatero Osorio et al. 2000); they are members of the Galactic halo (e.g., Burgasser et al. 2003; Kirkpatrick et al. 2014; Zhang et al. 2017); and have a broad range of magnetic activity (Schmidt et al. 2015; Gizis et al. 2000) including high levels of radio emission (e.g., Kao et al. 2018; Berger 2006); among other distinct properties. Finally, while UCDs represent the low-mass tail of the stellar initial mass function (IMF; e.g., Chabrier 2005), their formation mechanisms remain poorly understood, since the Jeans mass in typical molecular clouds favors the production of objects with masses $M \sim 0.5 M_{\odot}$ (Jeans 1902). The dense regions that are necessary to produce UCDs are difficult to model (e.g., Bate 2012).

Large area surveys in optical, NIR and mid-infrared (MIR) bands have been crucial to the discovery and population characterization of UCDs. These include the Two-Micron All Sky Survey (2MASS; Skrutskie et al. 2006), the Sloan Digital Sky Survey (SDSS; York et al. 2000), the UKIRT Infrared Deep Sky Survey (UKIDSS; Lawrence

et al. 2007), the Deep Near Infrared Survey of the Southern Sky (DENIS; Epchtein 1994), the Canada France Brown Dwarf Survey (CFBDS; Delorme et al. 2008), and the *Wide-Field Infrared Survey Explorer* (WISE; Wright et al. 2010). *Gaia* (Gaia Collaboration et al. 2016), whose second data release (DR2; Gaia Collaboration et al. 2018) has delivered 5-parameter astrometric solutions for 1.3 billion sources, has further uncovered and characterized nearby UCDs (Gaia Collaboration et al. 2018; Reylé 2018).

A homogeneous and unbiased sample is key to understanding the essential mechanisms, physical processes, and environmental conditions favorable to UCD formation and evolution. The IMF is a consequence of formation, and ultracool IMF studies indicate there are fewer brown dwarfs than stars (e.g., Luhman et al. 2000; Chabrier 2005). The incidence of rare subpopulations such as color outliers, young, and metal-poor sources, and binary and higher order systems, all probe formation and evolution mechanisms. The Solar neighborhood is the ideal region to measure these statistics. Bearing in mind the location and motion of the Sun with respect to the Galactic center, and the distinct kinematics and metallicity distributions of the thin disk, thick disk and halo populations (Gilmore & Reid 1983), the local volume can be treated as broadly representative of the Milky Way. Since brown dwarfs are intrinsically faint ($M_K \gtrsim 10$ mag; Faherty et al. 2013b), collecting data on the nearest sources is particularly advantageous to building a well-characterized sample. Spectroscopy, broad-band spectral energy distributions, kinematics, multiplicity, magnetic activity, and excesses and variability attributable to weather, magnetic activity, and presence of disks are best investigated with the nearest stars and brown dwarfs.

Previous studies of the nearby UCD population have already revealed some of the statistical properties of these low-mass objects. Reid et al. (2003a) compiled the northern sample of systems within 8 pc of the Sun in V -band magnitude, including 142 main sequence stars, 3 brown dwarfs, and 8 white dwarfs, and estimated $\sim 15\%$ incompleteness. Cruz et al. (2003) compiled a volume-limited sample of 186 M7–L6 dwarfs within 20 pc using a NIR photometric color and magnitude selection in 2MASS. Subsequently, Cruz et al. (2007) built the first UCD NIR luminosity function, finding number densities of $n = 4.9 \times 10^{-3} \text{ pc}^{-3}$ for M7–M9.5 and a lower limit of $n \geq 3.8 \times 10^{-3} \text{ pc}^{-3}$ for L dwarfs¹. Using the sixth data release of SDSS, Bochanski et al. (2010) compiled luminosity and mass functions of field low-mass stars spanning the M dwarf spectral class. Other studies have focused on the coldest brown dwarfs, to eventually obtain the low-mass end of the substellar mass function. Metchev et al. (2008) measured a T dwarf number density of $n = (7.0_{-3.0}^{+3.2}) \times 10^{-3} \text{ pc}^{-3}$ based on the detection of 15 T dwarfs in 2099 deg^2 sampled by 2MASS and SDSS. Reylé et al. (2010) measured a late-L dwarf density of $n = (2.0_{-0.7}^{+0.8}) \times 10^{-3} \text{ pc}^{-3}$, and T dwarf densities of $n = (1.4_{-0.2}^{+0.3}) \times 10^{-3} \text{ pc}^{-3}$ for T0.5–T5.5 dwarfs and $n = (5.3_{-2.2}^{+3.1}) \times 10^{-3} \text{ pc}^{-3}$

¹ This study also converted an earlier luminosity function of the 8 pc sample in V -band from Reid et al. (2003a) into J -band magnitudes.

for T6-T8 dwarfs in CFBDS. Recently, Kirkpatrick et al. (2019) used a 20 pc volume limited sample of sources T6 and later and estimated a number density of $0.97 \times 10^{-3} pc^{-3}$ for objects with temperatures 900-1050 K or roughly T6 dwarfs, increasing to $3.26 \times 10^{-3} pc^{-3}$ for objects with temperatures in the 300-450 K range, roughly corresponding to Y dwarfs.

Despite these concerted efforts, source identification and follow-up has been inhomogeneous for the local 25 pc sample, as evidenced by ongoing nearby discoveries. The M7 dwarf 2MASS J154043.42–510135.7 at 5 pc (Pérez Garrido et al. 2014), the M9.5+T5 binary system WISE J072003.20–084651.2 (Scholz 2014; Burgasser et al. 2015b), the L/T transition binary WISE J104915.57–531906.1 (Luhman 2013), and the 250 K WISE J085510.83–071442.5 (Luhman 2014), all at distances of 6 pc or less, show that the nearby sample remains incomplete. Given the availability of abundant multi-epoch survey data and astrometry from *Gaia*, it is time to revisit the compilation of UCDs in the local volume.

In this paper we present a new volume-limited sample of M7–L5 ultracool dwarfs within 25 pc, accompanied by NIR spectra homogeneously acquired with the SpeX spectrograph (Rayner et al. 2003) on the NASA Infrared Telescope Facility (IRTF). We follow a similar analysis to those of Cruz et al. (2003) and Reid et al. (2008) by creating an unbiased, homogeneous, NIR spectroscopic sample of M7–L5 dwarfs selected from multiple sources in the literature. Section 2 describes the sample selection and construction of our 25 pc and $+1\sigma$ samples. Section 3 describes the construction of the spectral sample, which is analyzed in Section 4, for spectral and gravity classifications, color outliers, low gravity sources, spectral binaries, and resolved binaries and higher order multiples previously identified in the literature. In Section 5, we estimate our biases, the completeness of the observed sample, and compute its selection function through a population simulation. We present an updated infrared luminosity function of ultracool dwarfs and compare it to previous work. Conclusions are summarized in Section 6.

2. LITERATURE SAMPLE CONSTRUCTION

2.1. *Compilation of UCD Targets from the Literature*

Targets for the sample were drawn from a number of literature sources, including surveys and previous compilations, each designed for its own scientific purposes and with a variety of follow-up. We attempt to average over the various biases from the original surveys by compiling as many sources as possible. Some of the known biases include a red $J - K_S$ color bias (e.g., Cruz et al. 2003; Lépine et al. 2013, identified by Schmidt et al. 2015); incomplete compilations (e.g., Gagné et al. 2015b) or partial sky coverage, e.g. Sloan Digital Sky Survey (SDSS; Ahn et al. 2012; Alam et al. 2015), Deep Near-Infrared Southern Sky Survey (DENIS; Epchtein 1994), UKIRT Infrared Deep Sky Survey (UKIDSS; Lawrence et al. 2007); and targeted surveys (e.g., young objects, Shkolnik et al. 2009; wide binaries, Deacon et al. 2014; high proper motion

Table 2. Cuts leading to the final sample

Cut	Targets remaining
Initial compilation	16,322
Deletion of duplicates	12,711
Optical, NIR or “photometric” spectral type between M7–L5	6,226
Estimated distance ≤ 50 pc	1,664
<i>Compilation of photometry, recalculation of spectrophotometric distances</i>	
Deletion of non-stellar sources, giants, compact and young stellar objects	1,571
Estimated Distance ≤ 30 pc	833
<i>Compilation of Gaia astrometry, recalculation of trigonometric distances</i>	
Objects with literature optical, NIR, or SpeX spectral type within M7–L5 (including photo-types only)	595
Objects with trigonometric or NIR spectrophotometric distance ≤ 25 pc	435^{+21}_{-20} a
Objects with trigonometric or NIR spectrophotometric distance ≤ 25 pc+ 1σ	470^{+22}_{-21} a
<i>Final samples</i>	
25 pc sample of M7–L5 dwarfs	410^{+21}_{-20} a
25 pc plus 1σ sample of M7–L5 dwarfs	470^{+22}_{-21} a

^aUncertainties based on Poisson statistics.

surveys, i.e. SUPERBLINK, Lépine & Gaidos 2011). We believe biases due to proper motion selection are negligible due to the completeness of the photometric selection surveys. While proper motion surveys tend to be more incomplete, they also are less likely to scatter distant objects into the sample. Table 1 lists the literature sources used to consolidate a database of $\sim 16,000$ candidate nearby UCDs. Table 2 summarizes the sequence of cuts leading to our final samples.

Duplicate sources were removed with TOPCAT (Taylor 2005) through an internal match that organized sources in near-neighbor groups with a matching radius of $15''$, large enough to catch binary components before deletion. This step reduced the number of entries to $\sim 12,700$. We applied a spectral type cut requiring optical or NIR spectral types or photometric spectral type estimates (e.g., Skrzypek et al. 2015; Theissen et al. 2017) to be in the M7–L5 range, shrinking the database to $\sim 6,200$ sources. A rough distance cut eliminating objects farther than 50 pc, trimmed this list to 1,664 sources.

Galaxies, giants, T-Tauri stars and other non-UCD sources as reported in the literature were identified using SIMBAD and removed, reducing the sample to 1,571 sources. After compiling photometric and astrometric data and recalculating spectrophotometric distances (see below), another distance cut at 30 pc was applied for those sources with astrometric parallaxes, yielding 833 sources.

2.2. Photometric and Astrometric Data

Photometry from the 2MASS (Skrutskie et al. 2006), SDSS DR9 (Ahn et al. 2012), *AllWISE* (Wright et al. 2010; Mainzer et al. 2011), UKIDSS-LAS (Lawrence

et al. 2007), and *Gaia* DR2 (Gaia Collaboration et al. 2018) catalogs were collected for all sources, selecting the closest match up to 15'' through the VizieR interface to account for objects with large proper motions, using a custom routine² built with the *Astroquery* Python package (Ginsburg et al. 2018). We obtained coordinates, epochs, identifiers, and *GrizJHK_sKW1W2W3* magnitudes from *Gaia*, SDSS, 2MASS, UKIDSS, and *AllWISE*. Spectral types from SDSS spectroscopy were obtained when available. In addition to these surveys, we also obtained *rizJHK_s* magnitudes and uncertainties, spectral type, object type, and proper motions from SIMBAD with the same search radius.

Table 4 provides the photometry data for the sample. All sources in our final 25 *pc* sample (See Table 2) have NIR magnitudes³, 88% have MIR magnitudes from *AllWISE*, and 39% have optical magnitudes from SDSS. Resolved NIR photometry on the Mauna Kea Observatory (MKO) filter system (Tokunaga et al. 2002) was obtained from the literature (e.g. Dupuy & Liu 2012; Best et al. 2018) and selected compilations⁴, particularly for closely-separated components of binary systems. We adopted 2MASS *JHK_s* magnitudes as the standard, and use MKO *JHK* magnitudes if those were the only NIR ones available.

AllWISE includes a crossmatch with the 2MASS catalog that we used to check for mismatches. We compared the *JHK_s* magnitudes from the 2MASS and *AllWISE* catalogs and kept the 2MASS magnitudes when the difference was within 0.05 mag (typical magnitude uncertainty for 2MASS *JHK_s*). Objects whose magnitude differences were > 0.05 mag were flagged for visual examination in multi-wavelength finder charts, and comparison of SIMBAD and VizieR data sets. The mismatches between *AllWISE* and 2MASS *JHK_s* magnitudes were typically caused by the blending of a bright and faint source ($\Delta m \sim 3$ mag) in the larger *AllWISE* pixels. In these cases, we assigned the 2MASS *JHK_s* magnitudes to the source, and replaced the *AllWISE* *W1W2W3* magnitudes with null entries. The same procedure was followed to consolidate *JHK* magnitudes from UKIDSS, and literature sources. While UKIDSS uses MKO filters, we keep these measurements separate because the quantum efficiency of the various NIR detectors may differ.

Further inspection on mismatched photometry between SDSS, 2MASS and *AllWISE* was done with color-color diagrams, as shown in Figure 1, and corrected by visual inspection using finder charts. Figure 1 illustrates the color loci of M7–L5 dwarfs from Schmidt et al. (2015). The most discriminating colors (e.g., $z - J$) use filters across surveys. Mismatches were corrected in a similar way as described above, using multi-wavelength finder charts and comparing magnitudes.

Astrometric data (positions, proper motions, and parallaxes) and radial velocities were drawn from SIMBAD when available. The sample was also crossmatched against

² Available at https://github.com/daniellabardalezgagliuffi/M7L5_download_phot

³ Except for GJ 1116B, where only unresolved photometry for the system was available (Newton et al. 2014). Several companions and close binaries do not have magnitudes in all three 2MASS bands (e.g., Gl 779 B, LSPM J1314+1320AB, LHS 1901AB).

⁴ <https://jgagneastro.wordpress.com/list-of-ultracool-dwarfs/>

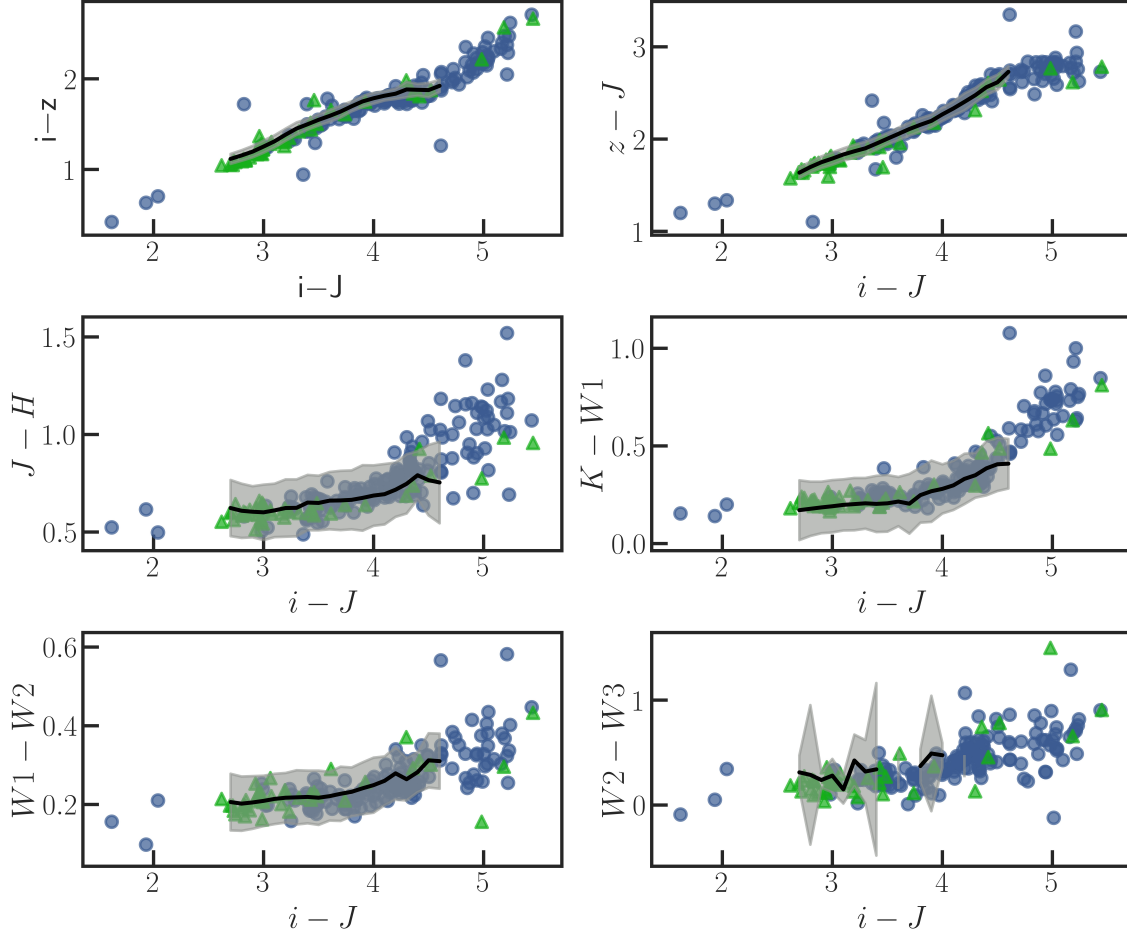


Figure 1. Color locus of the known M7–L5 25 pc sample in SDSS, 2MASS, and *WISE* colors as a function of $i - J$ (Schmidt et al. 2015). Blue circles are members of the 25 pc sample, green triangles are members of the extended 1σ sample. The black line represents mean colors from Schmidt et al. (2015) (complete between M7–L2), with the extent of their uncertainties shaded in light gray.

the astrometric samples of Dupuy & Liu (2012) and Weinberger et al. (2016). Upon the release of *Gaia* DR2 (Gaia Collaboration et al. 2018), we crossmatched our preliminary sample against this dataset to obtain 5-parameter astrometric solutions. We used the following Astronomical Data Query Language (ADQL) query through the `astroquery.Gaia` package.

```
SELECT g.*, t.*
FROM gaiadr1.tmass_original_valid AS t
LEFT OUTER JOIN gaiadr2.tmass_neighbourhood AS xt ON xt.tmass_oid =
t.tmass_oid
LEFT OUTER JOIN gaiadr2.gaia_source AS g ON xt.source_id = g.source_id
where 1=CONTAINS(POINT('ICRS', t.ra, t.dec),CIRCLE('ICRS', {}, {},
5./3600))
```

The *Gaia* crossmatch was done in two steps. First, we crossmatched the sample with the 2MASS-*Gaia* DR2 crossmatch table (`gaiadr2.tmass_neighbourhood`) within a radius of $5''.0$ using 2MASS coordinates from our sample. Second, we joined this crossmatch with the *Gaia* DR2 source table. We obtained 843 matches in 2MASS (10 objects with 2 matches each), 715 matched *Gaia* DR2 with a G magnitude, and 705 with parallaxes. To check the validity of our matches, we examined a color magnitude diagram of $G - RP$ versus absolute G magnitude. We considered sources as outliers if $G - RP \leq 1.25$, and if $M_G \leq 5$ to avoid giant stars. The 36 sources that failed our color/magnitude constraints were examined for crossmatch accuracy, and we found 22 mismatches of true UCDs with erroneous *Gaia* data. The remaining 14 sources were dropped from the sample due to their small *Gaia* parallaxes ($\bar{\omega} \ll 10 \text{ mas}$), resulting in 825 sources.

2.2.1. Spectral Types

Most catalogs provide information on optical or NIR spectral classification, or classification estimates from photometry (Skrzypek et al. 2015; Theissen et al. 2017). Given variations in classification schemes and intrinsic differences between optical and NIR classification (particularly for L dwarfs), we required at least one optical, NIR or photometric type belonging to the M7–L5 range for sources to be included in the sample. Adopted literature spectral types were chosen by prioritizing optical, NIR and photo-types, in that order. In the final 25 *pc* sample, the adopted spectral type is optical for 334 objects, NIR for 73, and photometric for 4. The objects whose adopted literature type is photometric have SpeX observations (see Section 3) confirming their status as M7–L5 dwarfs. Figure 8 shows the distribution of adopted literature spectral types color-coded by the nature of their measurement.

One hundred and eighty-nine objects have both optical and NIR measurements from the literature. With our SpeX observations (see Section 3), we have added 109 NIR classifications (see Section 4.2). Figure 4 shows a comparison between literature optical and NIR spectral types. The size of each circle is proportional to the number of overlapping sources. The scatter between spectral types is 0.95 subtypes; the 3σ boundaries are delineated by the dashed light grey lines.

2.2.2. Distances

Trigonometric and spectrophotometric distances were calculated from parallaxes and from spectrophotometric empirical relations in the NIR, respectively. *Gaia* DR2 provided most of the parallaxes in the sample, 80% of the total or 327 in our 25 *pc* sample. Distances from *Gaia* were calculated simply as $d = 1000/\omega$ (*mas*), rather than using a likelihood function with Bayesian probabilities (e.g., Bailer-Jones et al. 2018), since we are concerned with sources with large parallaxes ($\omega \geq 35 \text{ mas}$ or $d \leq 28.5 \text{ pc}$ to account for uncertainties beyond $d = 25 \text{ pc}$) with small relative errors of the order of 0.04% – 4%. Trigonometric distances from parallaxes predating *Gaia*

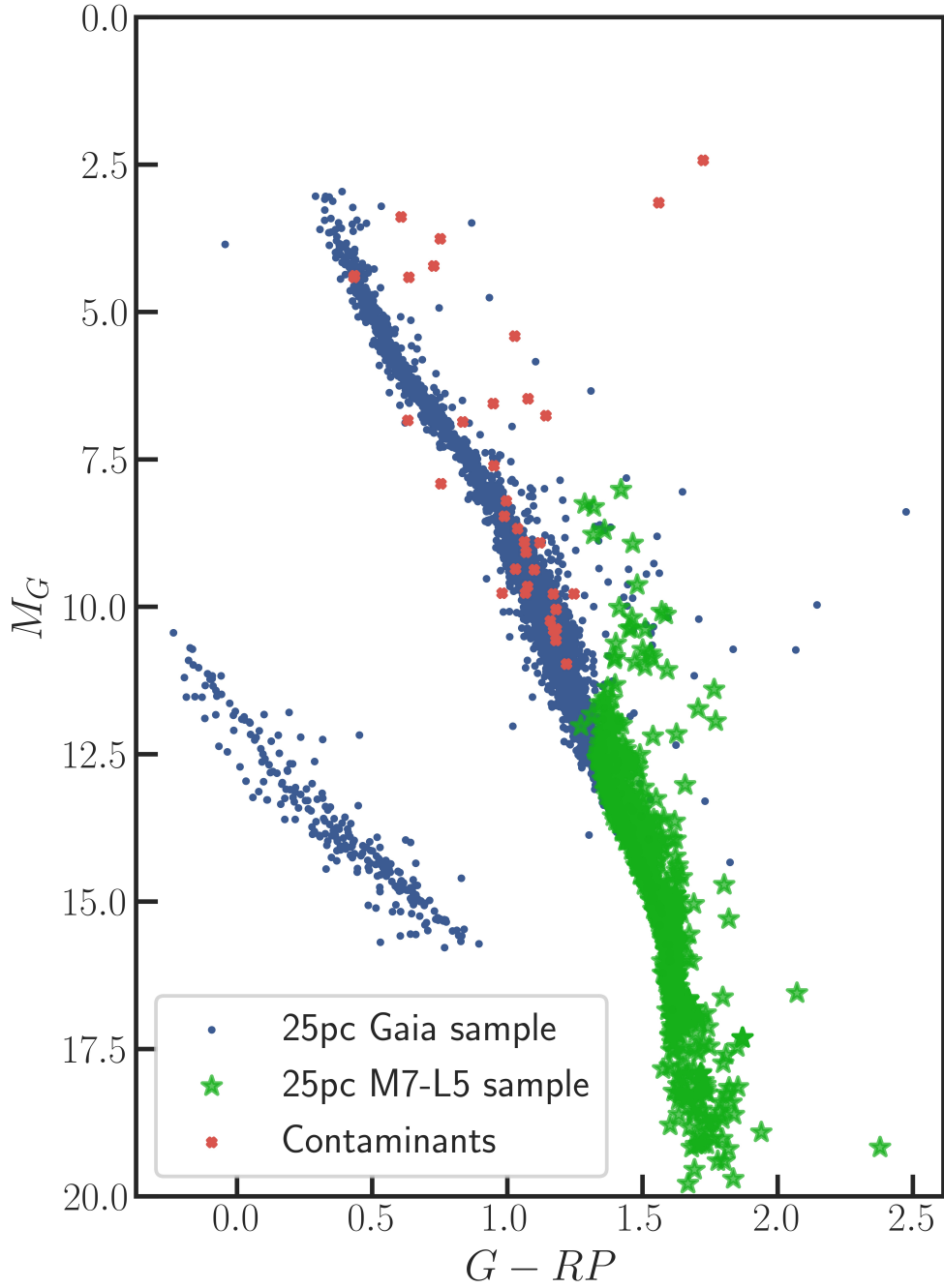


Figure 2. *Gaia* Hertzsprung-Russell Diagram of the 25 pc sample of M7–L5 dwarfs superimposed on the full 25 pc sample from *Gaia*. *Gaia* sources are shown as blue points, and sources from the M7–L5 dwarf 25 pc sample with valid *Gaia* matches are shown as green stars. Sources in orange correspond to *Gaia* mismatches.

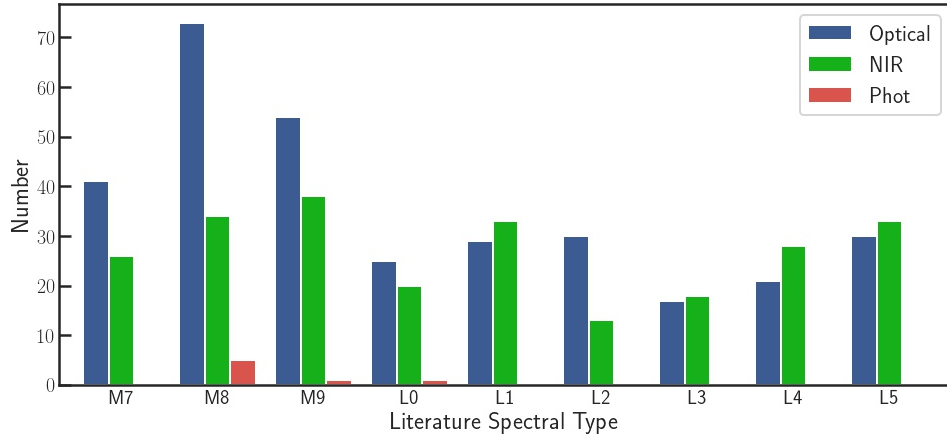


Figure 3. Adopted literature spectral type for the M7–L5 25 pc sample, broken down by optical (blue), NIR (green), and photometric types (red).

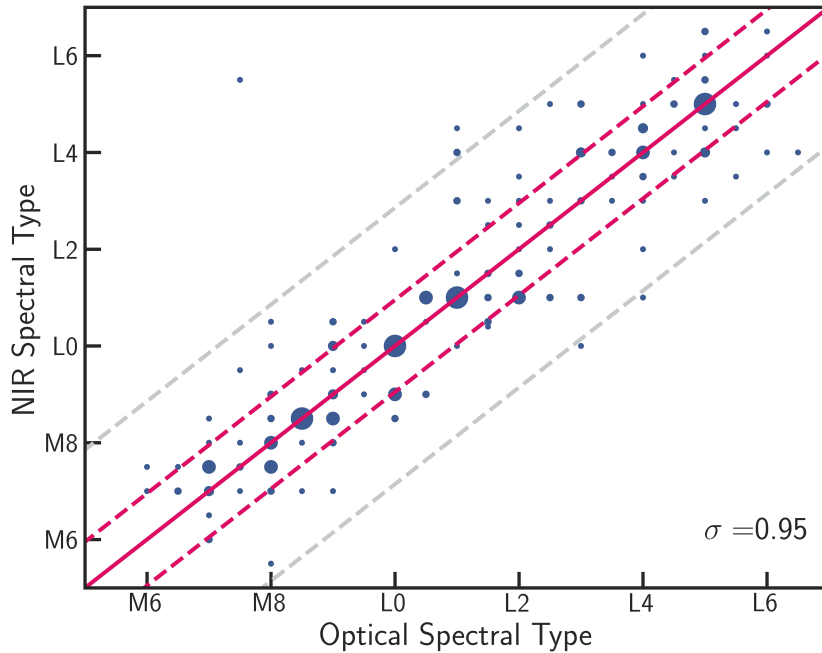


Figure 4. Comparison of optical and NIR spectral types from the literature for the M7–L5 25 pc sample. The size of the circles scales as the cube of the number of repeated points. The solid line marks where the slope equals one, while the dashed lines encompass the 1σ and 3σ limits in magenta and light grey, respectively.

DR2 were calculated in the same way. We also calculated trigonometric distances from *WISE* following the prescription of Theissen (2018) for 16 sources.

We calculated spectrophotometric distances using the adopted literature spectral type and the absolute magnitude empirical relations from Dupuy & Liu (2012). Dis-

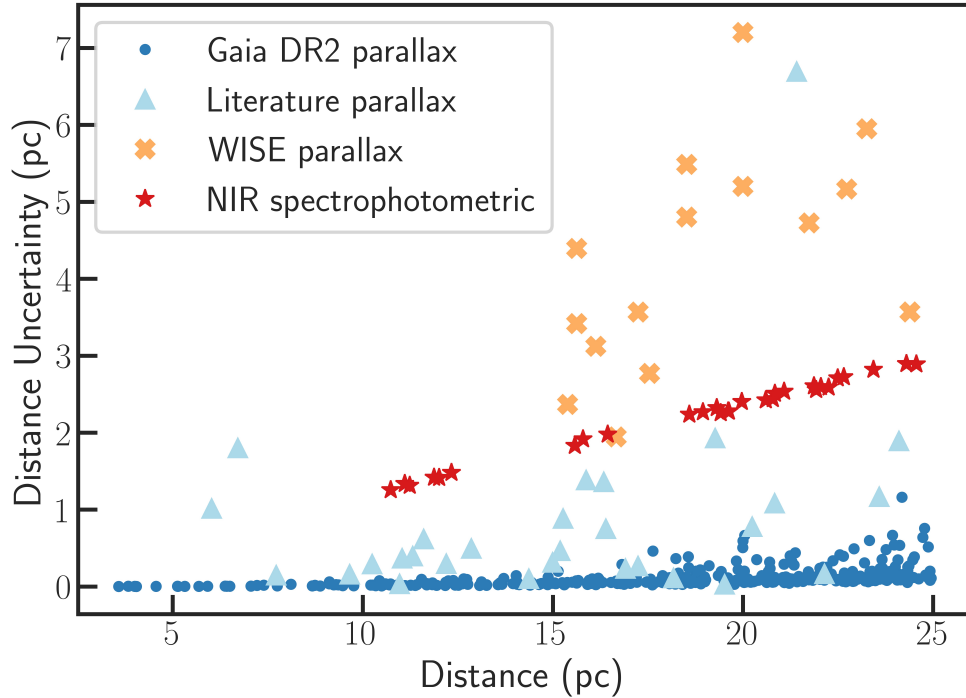


Figure 5. Comparison of distance values and uncertainties. The most precise distances are those found through *Gaia* parallaxes shown as blue dots. Distances found through parallaxes from the literature (i.e. SIMBAD) are plotted as light blue triangles, and show a large scatter since they come from a variety of studies with different systematics. Parallaxes obtained through *WISE* (Theissen 2018) are shown as orange crosses and have the largest uncertainties. NIR spectrophotometric distance estimates are shown as red stars also with large uncertainties, and growing as a function of distance.

tances were calculated for the NIR filters J , H , and K_s , and averaged, weighted by their uncertainties. We adopt trigonometric distances if available (for 93% of the sample), and use spectrophotometric distances for 29 sources that do not have a parallax measurement. Distances are reported in Table 6. Figure 5 summarizes the distance uncertainties for these measurements, and Figure 6 compares trigonometric to spectrophotometric distances for the 25 pc and 1σ samples. Trigonometric and spectrophotometric distances agree within 6.9% of each other, except for obviously overluminous sources.

Using the best distance measure, a strict cut on 25 pc was applied to select our volume-limited sample with 410 sources whose measured literature optical or NIR spectral types lie within M7–L5, and whose distance was within 25 pc, i.e. excluding objects with only a photometric estimation of their spectral type. We assess Poisson uncertainties as described in Gagné et al. (2017) for our sample size in subsequent analysis. Sources whose 1σ uncertainties placed them within 25 pc, amounting to 60 objects, were added to an expanded 25 pc + 1σ sample of 470 objects.

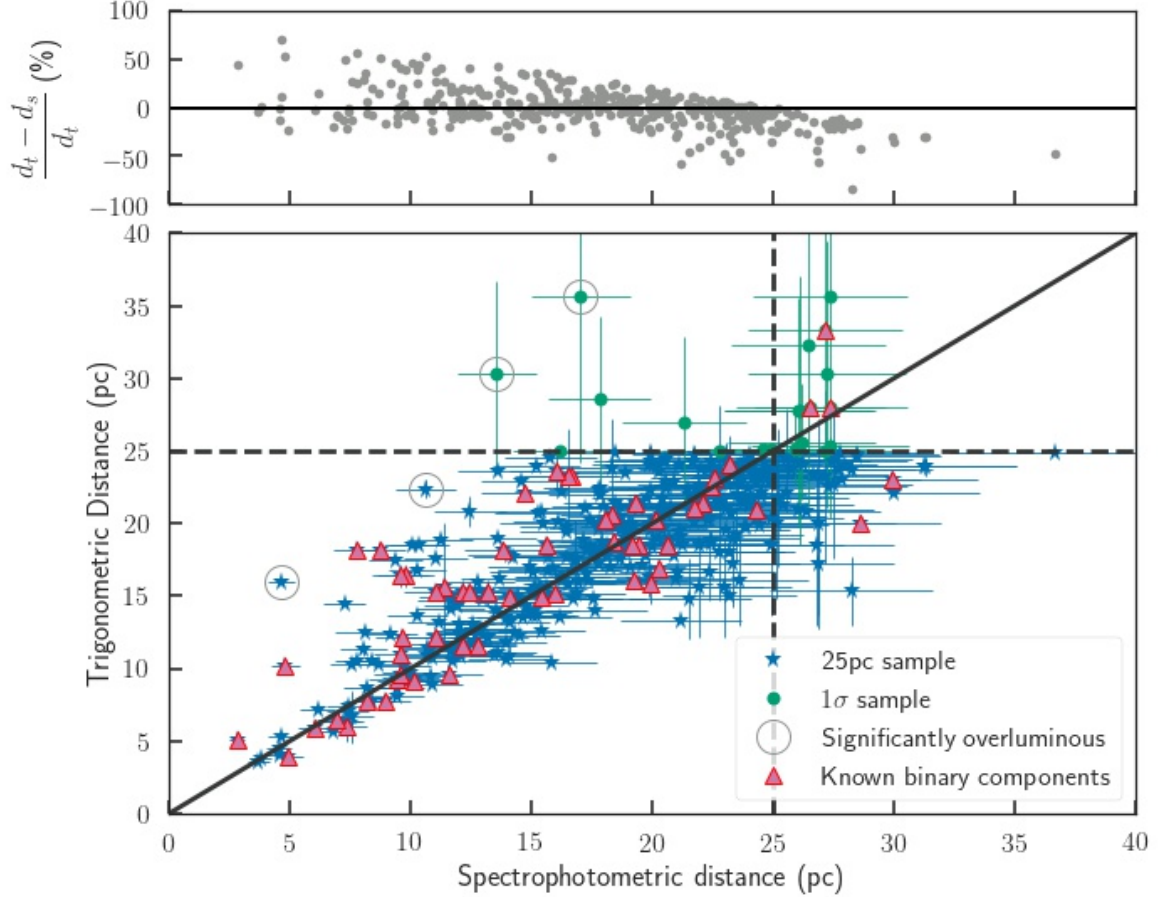


Figure 6. Spectrophotometric distance estimates compared to trigonometric distance measurements. (*Top*) Fractional percentage errors between trigonometric (d_t) and spectrophotometric (d_s). (*Bottom*) The 25 pc sample is shown in green and the 1σ sample is shown in blue. The black solid line delineates the one-to-one correspondence between trigonometric and photometric distances. Sources significantly above the line and beyond three standard deviations are likely unresolved binaries. In particular, the sources encircled in grey are 2MASS J1733+1655 ($d_t = 16.03 \pm 0.10$ pc), NLTT 40017 ($d_t = 22.4 \pm 0.7$ pc), SDSS J1221+4632 ($d_t = 30.3 \pm 6.4$ pc), and SDSS J0911+2248 ($d_t = 35.7 \pm 11.5$ pc). None of these objects have mentions of binarity in the literature.

3. SPECTRAL SAMPLE

Two hundred and forty 25 pc sample members had SpeX spectra in the SpeX Prism Library (SPL; Burgasser 2014) prior to 2015. We observed an additional 286 sources with SpeX between UT 2015 February 24 and 2018 November 22 as part of NASA IRTF programs 2015A074, 2015B087, 2016A079, 2016B114, 2017A102, 2018B120 (PI: Bardalez Gagliuffi), and 2016A038 (PI: Burgasser), over a total of 15 nights. The observations log is summarized in Table 7. The latitude, equatorial mount, and location of IRTF allow for observation of declinations in the $-50^\circ < \delta < +67^\circ$ range. Ninety percent of the 25 pc sample lies within these declinations, and between existing work and our contributions, we obtained spectra for 89% of these sources, or 81% of the 25 pc sources overall. Sources were observed in prism mode, which completely

samples wavelengths $0.75 - 2.5\mu\text{m}$ at a dispersion of $20 - 30\text{\AA pixel}^{-1}$ in a single observation. Most stars were observed with the $0''.5$ slit, 10 sources were observed with the $0''.8$ slit if the seeing rose above $1''.2$. The slit was aligned with the parallactic angle. Integration times ranged between $60 - 150\text{ s}$ per exposure, depending on the brightness of the source and atmospheric conditions. Observations were carried out in an ABBA dither pattern along the slit, with additional AB cycles if more counts were needed to achieve $S/N \sim 100$. Bright A0 stars were observed close in time at a similar airmass and used for flux calibration of the raw science spectra and correction for telluric absorption. Internal flat fields and Ar arc lamps were observed with each flux standard for pixel response and wavelength calibration, respectively. All data were reduced with SpeXtool package v4.1 (Cushing et al. 2004; Vacca et al. 2003) using standard settings.

4. SAMPLE CHARACTERIZATION

4.1. Spatial Distribution

Figure 7 shows the spatial distribution of all our targets. The 25 pc literature sample is evenly distributed across the sky, with the exception of the Galactic plane. Since 25 pc is a relatively small radius compared to the radius of the Milky Way ($R_{MW} \sim 25\text{ kpc}$) and its vertical scale height ($\sim 300\text{ pc}$; Kent et al. 1991; Bochanski et al. 2010), we assume an isotropic distribution of sources within this volume. There are 217 sources at northern declinations and 193 at southern declinations. In Galactic coordinates, there are 228 sources above the plane of the galaxy and 182 below it. We convert the 381 sources with measured parallaxes in our 25 pc from equatorial to galactic X, Y, Z right-handed coordinates centered at the Sun. In the \vec{X} direction we find 161 objects between the Sun and the Galactic center, and 220 between the Sun and the outer edge of the Galaxy. In the \vec{Y} direction we find 206 objects in the direction of the Sun's motion, and 175 objects trailing behind it. In the \vec{Z} direction, we find 207 objects above the plane of the Sun, and 174 below it. All of these values are within 3σ of each other, considering Poisson uncertainties, yet not consistent at the 1σ level. Bihain & Scholz (2016) have suggested an inhomogeneity in the spatial distribution of brown dwarfs compared to stars, most likely an effect of small number statistics and incomplete coverage of observations. The slight preference for northern sources is due to the larger number of panchromatic survey observations in the northern hemisphere (in particular SDSS). The Galactic plane looks sparse due to overcrowding and background source contamination, and this region is excluded from our space density analysis below (c.f. Kendall et al. 2007, 2003).

4.2. Spectral Classification

We compared our SpeX spectra to NIR spectral standards defined in Kirkpatrick et al. (2010), following the method described therein, which compares the $0.9 - 1.4\mu\text{m}$ spectrum of an object to standards using a χ^2 minimization routine. The resulting distribution of spectral types is shown in Figure 8.

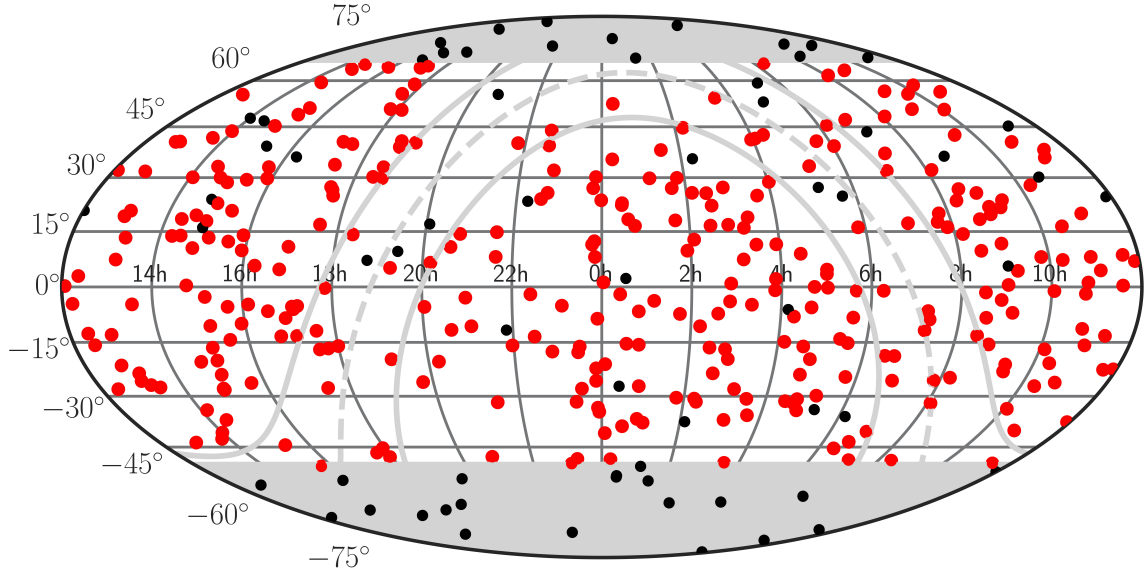


Figure 7. Spatial distribution of 25 pc targets in the M7–L5 25 pc sample. The sample is shown as black dots, objects for which we have SpeX spectra are shown as red dots. The sky regions inaccessible by IRTF are shaded in grey. The galactic plane ($b = 0^\circ$) is shown as a dashed light gray line, and the $\pm 15^\circ$ parallels from the galactic plane are shown as solid light gray lines.

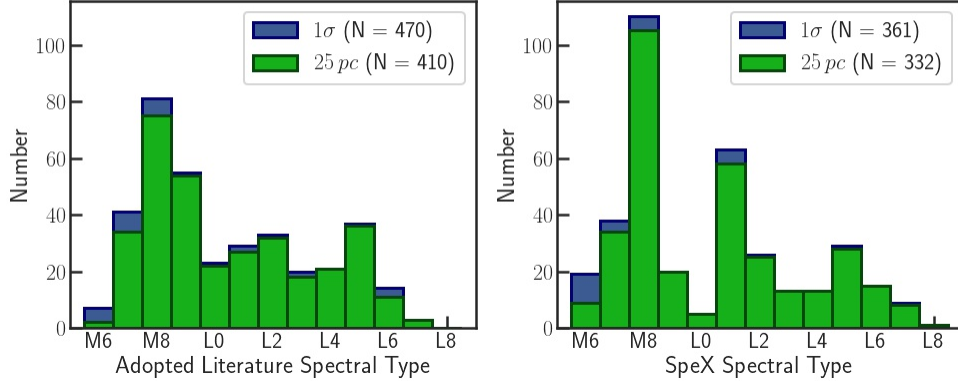


Figure 8. (Left) Adopted literature spectral type distribution of 25 pc and 1σ samples. (Right) Spectral type distribution of 25 pc and 1σ samples according to their SpeX classification. Objects outside of the M7–L5 range have at least one spectral classification within that range.

After classifying the spectra, we compared their literature and measured spectral types. For most objects, we measured a NIR spectral type within one subtype of the published literature type. Objects with only a photometric estimate from the literature and whose SpeX spectral type placed them outside of the M7–L5 range are in the 1σ sample.

Figure 9 compares the literature adopted optical or NIR classifications to the SpeX classification. The scatter for the optical-SpeX comparison is $\sigma = 0.77$ subtypes, the scatter for the NIR-SpeX comparison is $\sigma = 1.06$ subtypes, and the scatter in the

adopted-SpeX comparison is $\sigma = 0.82$ subtypes. The larger scatter between NIR-SpeX classifications may be due to poorly defined prior NIR types, sensitivity to surface gravity, metallicity, clouds; and variance in the spectral region used for NIR classification.

We also classified our SpeX spectra using spectral indices from Burgasser (2007a), Allers et al. (2007), and Reid et al. (2001). These indices are applicable in the L0–T8, M5–L5, and M7–L8 spectral type ranges, respectively. Figure 10 shows the comparisons from these index-classification systems against optical and NIR spectral types reported in the literature. The points outside of the allowed classification ranges are plotted in light grey and are not included in the median offset and scatter calculations. The indices from Burgasser (2007a) have a systematic offset of +1.30 and +1.40 subtypes compared to optical and NIR types, respectively, and overestimate the spectral type of our sources. The Allers et al. (2007) indices are the most accurate at predicting optical spectral types with $\sigma = 0.90$ subtypes. The scatter is larger for NIR types ($\sigma = 1.05$ subtypes), with a slight tendency to predict spectral types earlier than measured in the literature (offset = -0.30 in both cases). For both optical and NIR types, the Reid et al. (2001) indices have the smallest offset (0.10 and 0.05 subtypes for optical and NIR spectral types, respectively) but slightly larger scatters than Allers et al. (2007), at $\sigma = 1.21$ and $\sigma = 1.42$ subtypes, respectively. All spectral types for sample sources are summarized in Table 5.

4.3. Gravity Classification and Young Moving Group Membership

Young brown dwarfs ($\tau \lesssim 200$ Myr) are undergoing cooling and contraction, and are both larger in radius and less massive than their older counterparts at a similar spectral type. These physical properties translate into lower surface gravities, affecting spectral features such as reduced collision-induced absorption, and narrower alkali lines (Allers et al. 2007; Kirkpatrick et al. 2010). Due to their low surface gravity and typically dusty atmospheres, young brown dwarfs share physical properties with directly-imaged exoplanets, making the former ideal analogs to the latter (Faherty et al. 2013a, 2016).

We obtained gravity classifications of our SpeX spectra, following the NIR scheme of Allers & Liu (2013), defined for the spectral type range M5–L7, except that spectral types were determined from H₂O indices without a visual comparison of the *J*-band with NIR standards.

Additionally, we obtain 7 very low gravity (VL-G) and 64 intermediate gravity (INT-G) candidate classifications from our spectra in the combined 25 *pc* and 1 σ samples (Table 8). All low-gravity candidates were examined for visual signatures of low gravity, comparing the spectra band-by-band to low-gravity standards (see Gagné et al. 2015c and Cruz et al. 2018), leading to the rejection of 26 INT-G classifications. We labeled 11 sources with conflicting signatures as peculiar, such as blue *J* – *K_S* colors, indicating low metallicity effects rather than low gravity (Aganze et al. 2016).

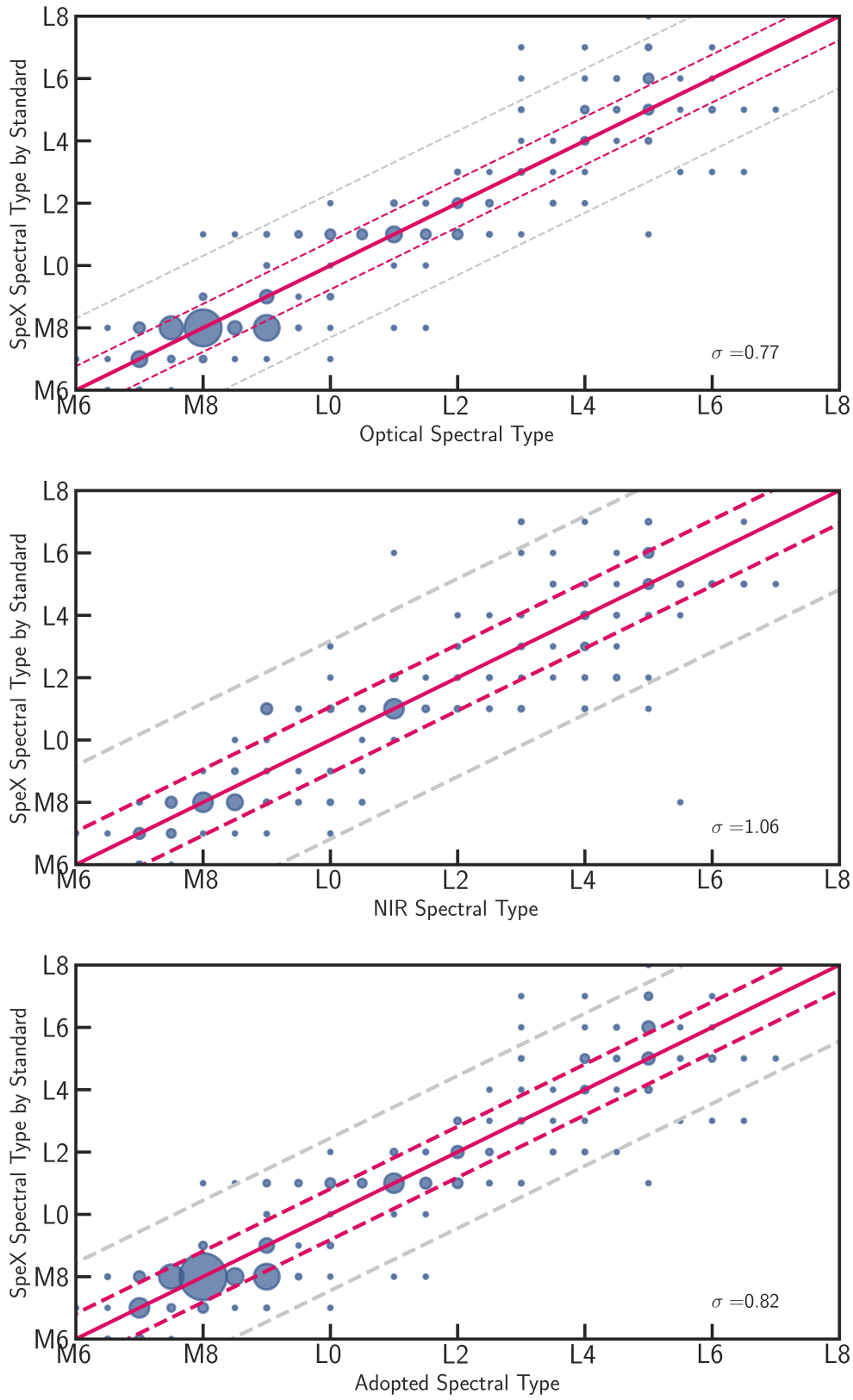


Figure 9. Literature optical and NIR spectral types compared to SpeX spectral types with Kirkpatrick et al. (2010) NIR standards. Circle sizes are proportional to the number of sources in a given optical-NIR spectral type pair. The solid line indicates equal classification, and the pink and grey dashed lines are the 1σ and 3σ limits, respectively.

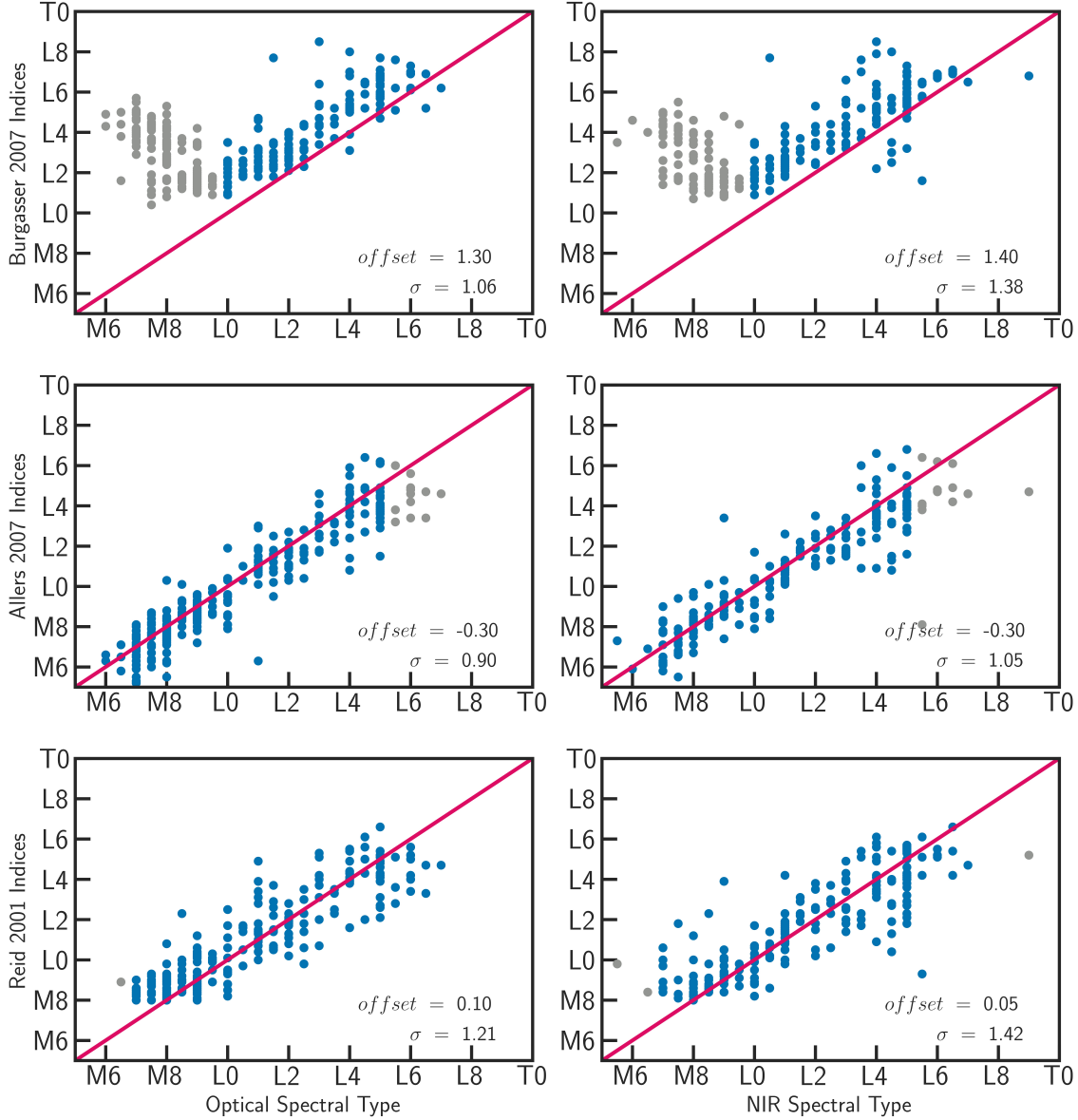


Figure 10. Literature optical and NIR spectral types compared against measured spectral types with the index sets of [Burgasser \(2007a\)](#), [Allers et al. \(2007\)](#) and [Reid et al. \(2001\)](#). Points outside the spectral type ranges defined for each index classification are plotted in grey and do not enter the σ calculation.

Most VL-G sources are previously known, but we have identified 2MASS J1739+2454 as a new very low-gravity source. Thirteen of the 26 INT-G sources are first reported in this paper. The unresolved spectrum of the M8+M8 binary system 2MASS J0027+2219AB ([Forveille et al. 2005](#)) was also classified as an INT-G source. Since both components have the same spectral type, and since the system is coeval, we assume that both components would be independently classified as INT-G, leading to a final number of INT-G objects of 26 plus one more including the 1σ sample.

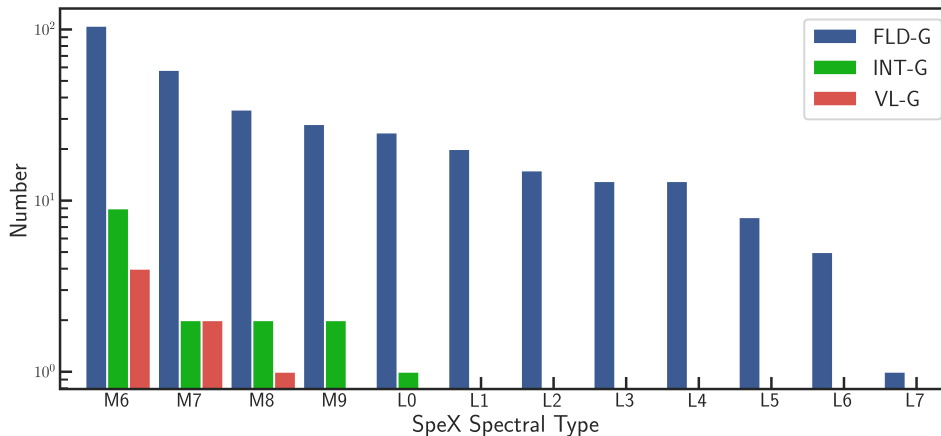


Figure 11. Distribution of spectral types as classified by field spectral standard for different gravity types. Objects with gravity classifications of very-low gravity (VL-G) or intermediate gravity (INT-G) are plotted in red and green, respectively.

While 2MASS J1022+5825 (Reid et al. 2008), 2MASSW J2148+4003 (Looper et al. 2008) and 2MASS J0512–2949 (Cruz et al. 2003) were previously classified as having field gravity (FLD-G; Allers & Liu 2013; Faherty et al. 2016), our spectra yield INT-G classifications. Similarly, SDSS J0443+0002 was classified as a VL-G in Allers & Liu (2013), but our spectra yields an INT-G classification. These discrepancies may be due to instrumental or reduction differences.

We used BANYAN Σ (Gagné et al. 2018) on our low-gravity candidates to assess possible membership in 27 young moving groups, using new kinematic data from *Gaia* DR2 (Gaia Collaboration et al. 2018), and report the probabilities for young moving group membership in Table 8. The Allers & Liu (2013) gravity classification scheme is a spectroscopic test for youth, while BANYAN Σ uses kinematic information to determine membership in a young moving group. Many of our low-gravity sources are classified as 0% probability members of any young group by BANYAN Σ , which implies that these objects might be young and unassociated, field interlopers, or belonging to moving groups other than the 27 known associations included in BANYAN Σ , possibly as a result of ejection.

Figure 11 shows the distributions of gravity types from our SpeX spectra by spectral type, as classified by field standards. We find the very-low-gravity and intermediate-gravity fractions for our 25 pc sample to be $2.1^{+0.9}_{-0.8}\%$ and $7.8^{+1.7}_{-1.5}\%$, respectively, with uncertainties based on Poisson statistics.

The spectral types of our low-gravity objects were further refined using VL-G and INT-G spectral standards from Allers & Liu (2013). The comparison between classifications is shown on Figure 12. The 7 VL-G sources in our sample have much earlier types (by 1-3 subtypes) when classified with a VL-G standard than with a field standard, although this is too small of a sample to precisely quantify the bias. Figure 12 shows the 7 VL-G sources classified with a field standard and VL-G standard.

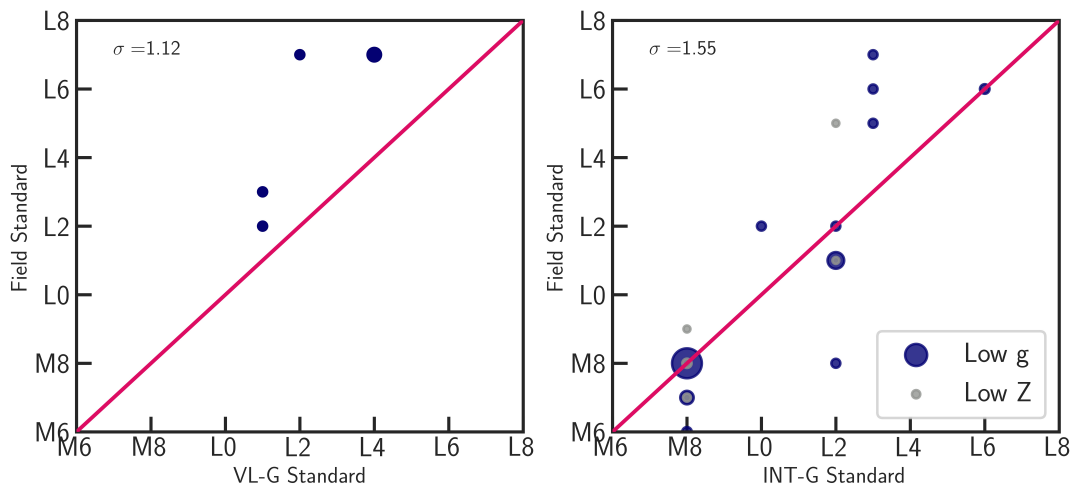


Figure 12. (*Left*) Comparison between spectral classification by very low gravity and field gravity standards for the 4 objects classified as having very low gravity by the prescription of Allers & Liu (2013). Size of markers is proportional to the number of equally-classified sources. The magenta line represents a one-to-one match between classifications. (*Right*) Same comparison between intermediate gravity and field gravity standards. Objects with an INT-G classification most likely not young, but metal-poor instead, are shown in grey, with a lower proportionality of number of sources to marker size.

For INT-G sources, there is a better correlation but larger scatter ($\sigma = 1.67$), particularly among L dwarfs, which are expected to show stronger gravity features even as INT-G. These differences highlight the strong role of gravity-sensitive features and reinforce the importance of comparing low gravity sources to equivalent standards.

4.4. Color Outliers

Red and blue $J - K_S$ color outliers are empirically-defined subpopulations. Their unusual color is likely a proxy for physical properties such as age, low or high surface gravity, atmospheric cloud content, opacity, and metallicity (Metchev & Hillenbrand 2006; Burgasser et al. 2008b; Looper et al. 2008; Faherty et al. 2009).

Clouds play a key role in $J - K_S$ color evolution from late-M to L-type, as increased opacity originating from condensates and possibly clouds reddens spectral energy distributions (e.g., Tsuji et al. 1996; Lodders & Fegley 2006). This is intrinsic reddening, as objects in the 25 pc sample should be minimally reddened by interstellar dust. The thickness of clouds may be an independent parameter (e.g., Ackerman & Marley 2001; Hiranaka et al. 2016), or may correlate with youth (e.g., Faherty et al. 2013b), and/or metallicity (e.g., Burgasser et al. 2003). Color outliers may also indicate the presence of an unresolved companion (e.g., Bardalez Gagliuffi et al. 2014). Unusually blue objects and subdwarfs have enhanced collision-induced H_2 opacity (Saumon et al. 1994; Burgasser et al. 2003) due to their metal-poor atmospheres.

To isolate the color outliers of our sample, we compared their $J - K_S$ colors to the average colors and standard deviations as a function of spectral type from Faherty

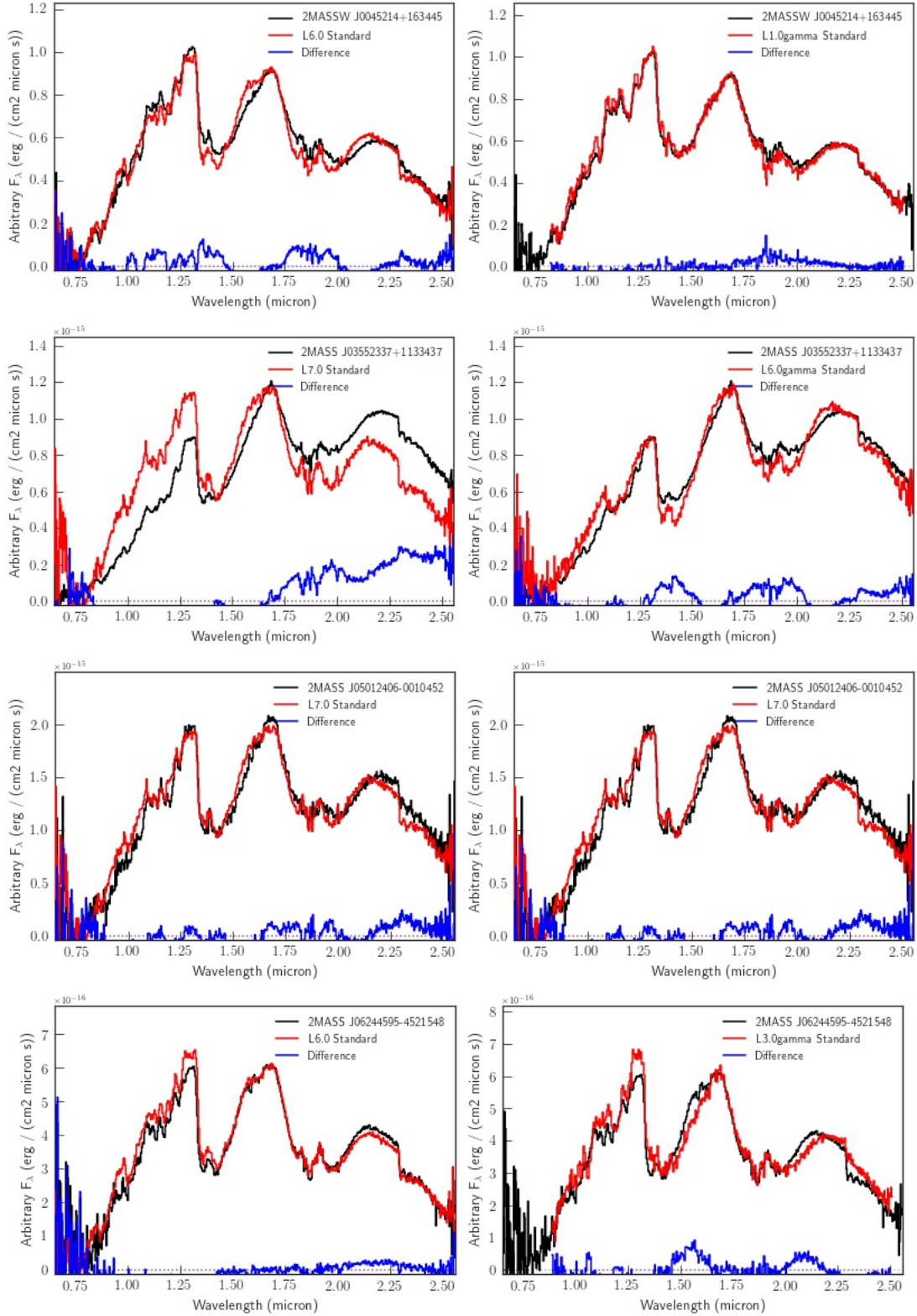


Figure 13. Sources classified as very-low gravity (VL-G) compared against field (*Left*) and VL-G (*Right*) standards. Spectra (black) are consistently redder than their field standards (red). The positive difference between spectra and standards (blue) is clear, emphasizing the need to fit spectra to appropriate gravity standards.

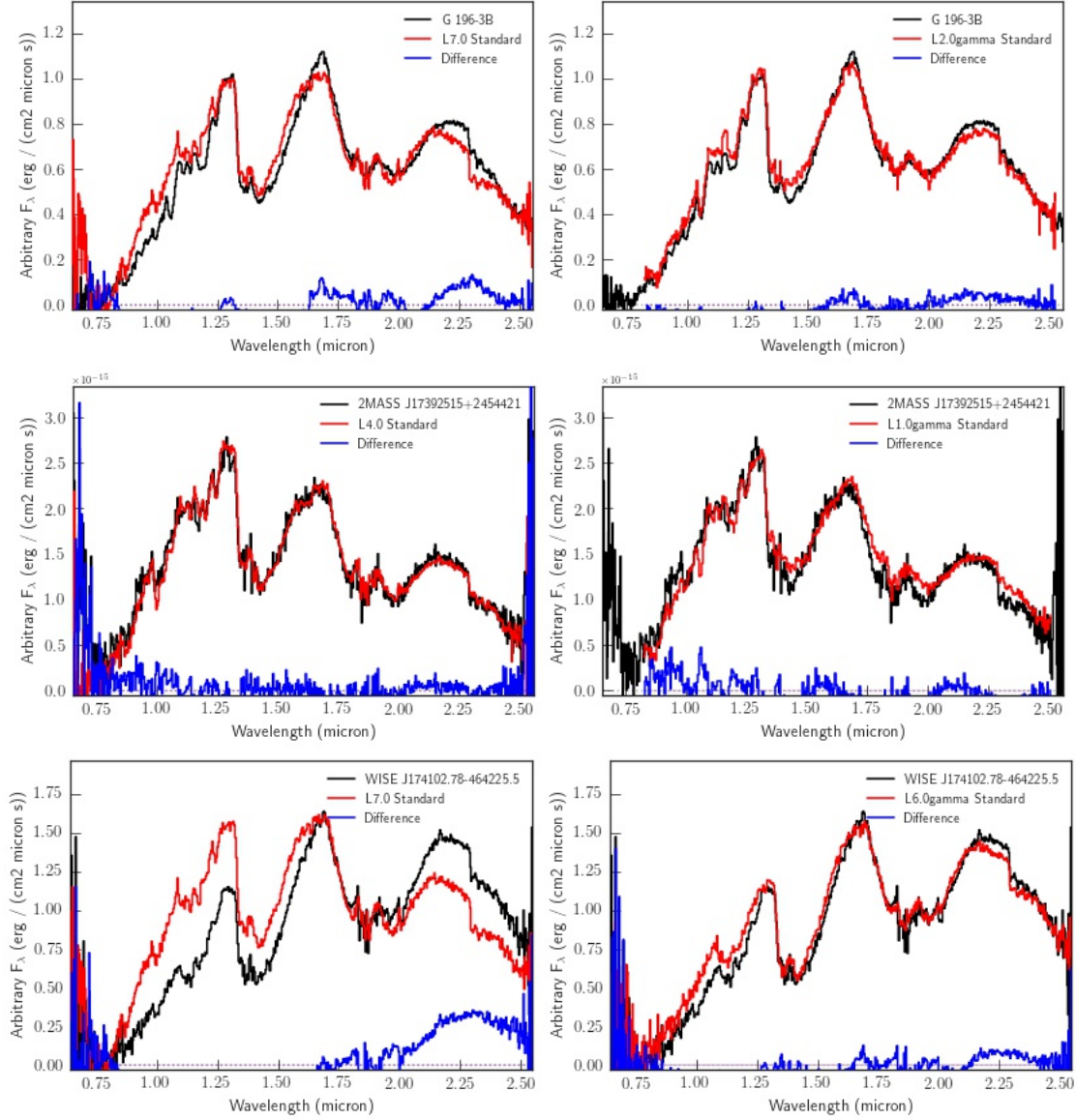


Figure 12. Continued.

et al. (2016), defined over the M7–L8 range. We identified outliers as 2σ deviants, shown in Figure 14. From the 387 objects in the $25 pc$ whose adopted spectral type is within M7–L5⁵, and with both J and K_S photometry⁶, 188 have $J - K$ positive excesses, while 184 have negative color excesses, and 15 do not have a color excess. This even distribution of sources indicates that our sample does not have a NIR color bias, despite widely used 2MASS color selections (Schmidt et al. 2015), for which redder selection criteria were necessary to excise background population.

⁵ Objects with an adopted spectral type outside of the M7–L5 range have an optical spectral type also outside the range, but either a NIR or photometric type estimation within the range.

⁶ GJ 1116AB only has unresolved photometry, so we do not count the B component in this calculation. Gl 779B only has K_S photometry, so it is excluded as well.

The individual outliers are listed in Table 9. In our 25 *pc* sample, 15 objects were found to have unusually blue $J - K_S$ colors and 6 have unusually red $J - K_S$ colors. In the 1σ sample we find 2 more unusually blue objects. Given the numbers of color outliers from the 25 *pc* sample, we infer fractions of $1.4_{-0.5}^{+0.6}\%$ for red and $3.6_{-0.9}^{+1.0}\%$ for blue M7–L5 dwarfs in the Solar neighborhood (with Poisson uncertainties). Among the 5 red outliers, 2MASS J0355+1133, G 196–3B, and 2MASS J1741–4642 have been reported as young in the literature (Gagné et al. 2015c; Faherty et al. 2016), while LHS2397aA and Kelu–1A are classified as having field gravity, but are also known binaries (Freed et al. 2003; Stumpf et al. 2008). From all the sources with *Gaia* kinematics, we explored a reduced proper motion diagram and found no potential subdwarfs, i.e. sources with high proper motion, high reduced proper motion, and blue $G - G_{RP}$ colors.

Five blue sources were also classified as INT-G, cementing their status as metal-poor objects (see Section 4.3 and Aganze et al. 2016). Two unusually blue sources, G 203–50B and 2MASS J1721+3344, are also rejected spectral binary candidates, as blue sources tend to be contaminants in the identification of spectral binaries (Bardalez Gagliuffi et al. 2014)⁷.

Additionally, we calibrated our SpeX spectra to 2MASS J and K_s magnitudes to find spectrophotometric $J - K_S$ colors. These were compared against 2MASS $J - K_S$ colors, and found to have a scatter of 0.18 mag. 2σ outliers or higher are highlighted in Figure 15, and could be due to intrinsic atmospheric variability (e.g., Radigan et al. 2012). These sources are: LHS 5166B, 2MASS J1152+2438, 2MASS J1200+2048, Kelu-1 A (unusually red), 2MASS J1416+1348A (unusually blue), and 2MASS J1438+6408. Kelu-1 has a variability detection in 410Å with a peak-to-peak amplitude of 11.9 ± 0.8 mmag (Clarke et al. 2003), reported before the discovery of its nearby companion (Liu & Leggett 2005). Khandrika et al. (2013) reported marginal variability in J -band for 2MASS J1416+1348A. The remaining outliers have not been targeted in variability surveys.

4.5. Spectral Binaries

Spectral binaries of ultracool dwarfs are systems composed of a late-M/L-type primary and a hidden T-dwarf secondary, identifiable only by their peculiar blended-light spectrum in NIR wavelengths (Cruz et al. 2004; Burgasser et al. 2010; Bardalez Gagliuffi et al. 2014). Identifying these potentially closely-separated binaries allows us to probe the very low mass binary separation distribution at all scales and select potential systems for orbital measurement (see Bardalez Gagliuffi et al. 2015).

We applied the spectral binary technique of Bardalez Gagliuffi et al. (2014)⁸ to the SpeX spectral sample. The spectral binary technique consists of two parts: spectral index selection and binary template fitting, the second of which incurs a hypothe-

⁷ When identifying spectral binaries via spectral indices alone, objects with a bluer spectral slope are often false positives that are rejected by visual inspection of their binary template fits.

⁸ The boundaries of the parameter spaces were modified in Bardalez Gagliuffi et al. (2015) to include the M9+T5 spectral binary WISE J072003.20–084651.2 (Scholz 2014; Burgasser et al. 2015b).

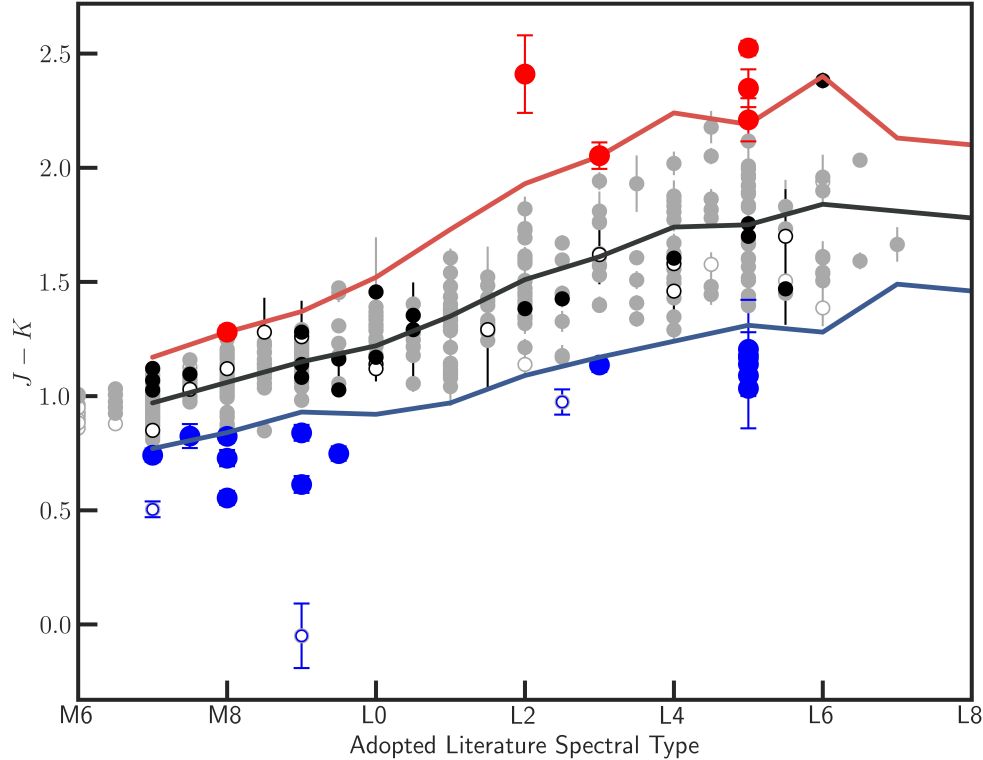


Figure 14. $J - K$ color outliers per spectral type. 25 pc sources with 2MASS photometry are filled grey circles, and 1σ sources are open grey circles. Black filled and open circles are sources where the adopted magnitudes are in the MKO system for the 25 pc and 1σ samples, respectively. Red and blue circles are color outliers for their spectral type, as defined by the color averages of Faherty et al. (2016). The average $J - K_S$ color is the dark grey line, and the 2σ limits are the red and blue lines. The red outlier at L2 is the binary Kelu-1A.

sis test to determine whether binary template fits are statistically better fits to a candidate than single templates. Spectral binary candidates are listed in Table 10. Forty-two objects were selected by the index-index parameter spaces as candidates, but rejected by the low confidence from hypothesis testing. Seven objects were rejected despite passing the spectral binary fitting due to their blue colors, as blue objects are known contaminants of the spectral binary technique (Bardalez Gagliuffi et al. 2014).

We found five previously identified and confirmed spectral binaries in our 25 pc sample: 2MASSW J0320284–044636 (Blake et al. 2008; Burgasser et al. 2008a), WISE J072003.20–084651.2 (Burgasser et al. 2015b), 2MASS J08053189+4812330 (Burgasser 2007b; Burgasser et al. 2016; Dupuy & Liu 2012), 2MASS J13153094–2649513 (Burgasser et al. 2011b), and 2MASS J22521073–1730134 (Reid et al. 2006). We recover the L4+T3 spectral binary 2MASS J0931+2802 Bardalez Gagliuffi et al. (2014) outside our 25 pc sample. We

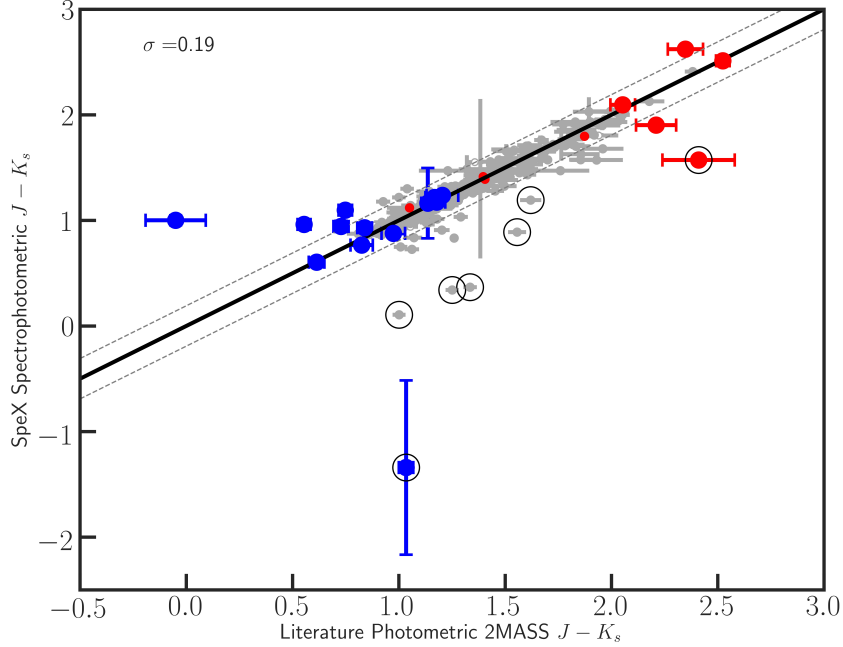


Figure 15. Photometric 2MASS $J - K_S$ color from the literature compared to spectrophotometric $J - K_S$ color from our SpeX observations. Same color-coding as Figure 14. Objects inside open black circles are $> 2\sigma$ outliers.

identify two previously unreported spectral binary candidates in our spectral sample, both of which lie formally outside our 25 pc distance limit:

2MASS J14111847+2948515. Its spectrum shows a deep H -band dip at $1.62 \mu\text{m}$, and an angled J -band peak at $1.25 \mu\text{m}$, both signs of a hidden T-dwarf companion. The K_S -band of the object is slightly fainter compared to the binary template, which could be an indication of slightly blue L dwarf, known contaminants to the spectral binary technique. However, the best single fits to its SpeX spectrum fail to reproduce the dip in the H -band, and are fainter in J and K_S -bands in comparison to 2MASS J1411+2948. Its component spectral types are likely to be L4+T4. No parallax has been measured for this source, whose distance would be larger than the estimated spectrophotometric distance of 49 ± 6 pc if it is a binary.

2MASS J14211873–1618201. The spectrum of this source shows an angled J -band peak and a small dip in the H -band. Its inferred component spectral types are M8+T5, similar to 2MASS J0320–0446 (Blake et al. 2008; Burgasser et al. 2008a) and 2MASS J0006–0852 (Burgasser et al. 2012), and WISE J0720–0846 (Scholz 2014; Burgasser et al. 2015b). Our strict distance cut left this source outside of the 25 pc sample, yet it rests right at the 25 pc limit ($d_t = 25.15 \pm 0.14$ pc; Gaia Collaboration et al. 2018).

To calculate the frequency of spectral binary systems, we used the definition of Reipurth & Zinnecker (1993) (See Section 4.6), where the binary fraction is the number of binaries over the total number of systems. For this calculation, we only consider systems with a measured SpeX spectrum, since otherwise we would not be able to assess spectral binarity⁹. Since 2MASS J1421–1618 lies at our limit distance, we calculate two spectral binary fractions, assuming 24 pc (5 spectral binaries/282 spectra) and 26 pc (6 spectral binaries/312 spectra) volumes. The fractions are $1.7_{-0.7}^{+0.9}$ and $1.9_{-0.7}^{+0.8}$ for 24 pc and 26 pc, respectively, or an average of $1.8_{-0.5}^{+0.6}\%$ assuming Poisson errors. This fraction is significantly lower than the total fraction of resolved binaries in the sample ($7.5_{-1.4}^{+1.6}\%$, see Section 4.6), but this is likely because spectral binary systems encompass a specific range of component spectral types to be selected. We analyze the spectral binaries in this sample and their implication for the brown dwarf binary fraction in a companion paper.

4.6. Binary systems containing UCDs in the 25 pc volume

Binaries and multiple systems reported in the literature were identified in our sample through crossmatches with the Washington Double Star Catalog¹⁰ (WDS; Mason et al. 2001), SIMBAD (Wenger et al. 2000), and vlmbinaries.org. Table 11 lists the UCD binaries with primary components between M7–L5 found in our sample previously reported in the literature, as well as UCD companions to main sequence stars. Our 25 pc sample contains 410 objects in 393 systems, 341 single systems, 42 binary systems, and 10 triple systems. Only 28 binaries and no triples have a primary with a spectral type M7 or later. Including the 1σ sample, we find 4 more binaries and one quintuple system, HD 114762, comprised of Aa, Ab, and Ac components F9+F8+F4 stars, an $11\pm 0.1 M_J$ (Kane et al. 2011) brown dwarf orbiting the F9 star (Latham et al. 1989), and an M6:: dwarf as the B component 130 AU away from the F triple system (Patience et al. 2002).

We calculate several statistics to represent the multiplicity of the sample: the multiplicity fraction, which provides the probability that a given source is a multiple system; the companion star fraction, which is the probability for an object to be in a multiple system; the pairing factor, which is the mean number of companions per primary; and the companion frequency that indicates the mean number of companions per object. These equations are defined and explained in detail in Reipurth & Zinnecker (1993) and Goodwin et al. (2004). Since we have no triple systems with primaries M7 or later, our multiplicity fraction is effectively a binary fraction. We determine the binary fraction of the 25 pc sample to be $7.5_{-1.4}^{+1.6}\%$, including both spectral binaries and RV variable systems. The companion star fraction for this sample is $14.1_{-1.9}^{+2.1}\%$, the pairing factor is 1 ± 0.3 , since there are no triple systems with primaries

⁹ I.e. spectra of secondaries are not counted in the calculation since we are only concerned with the number of systems, neither do spectra of UCD components of higher order systems.

¹⁰ Eight matches to the WDS were ruled out in the notes from the Sixth Catalog of Orbits of Visual Binary Stars, found at <https://ad.usno.navy.mil/wds/orb6/orb6notes.html>. 2MASS J0355+1603 was refuted as a binary in Faherty et al. (2013b), and 6 other sources are only binary candidates, so are not considered in our binary statistics.

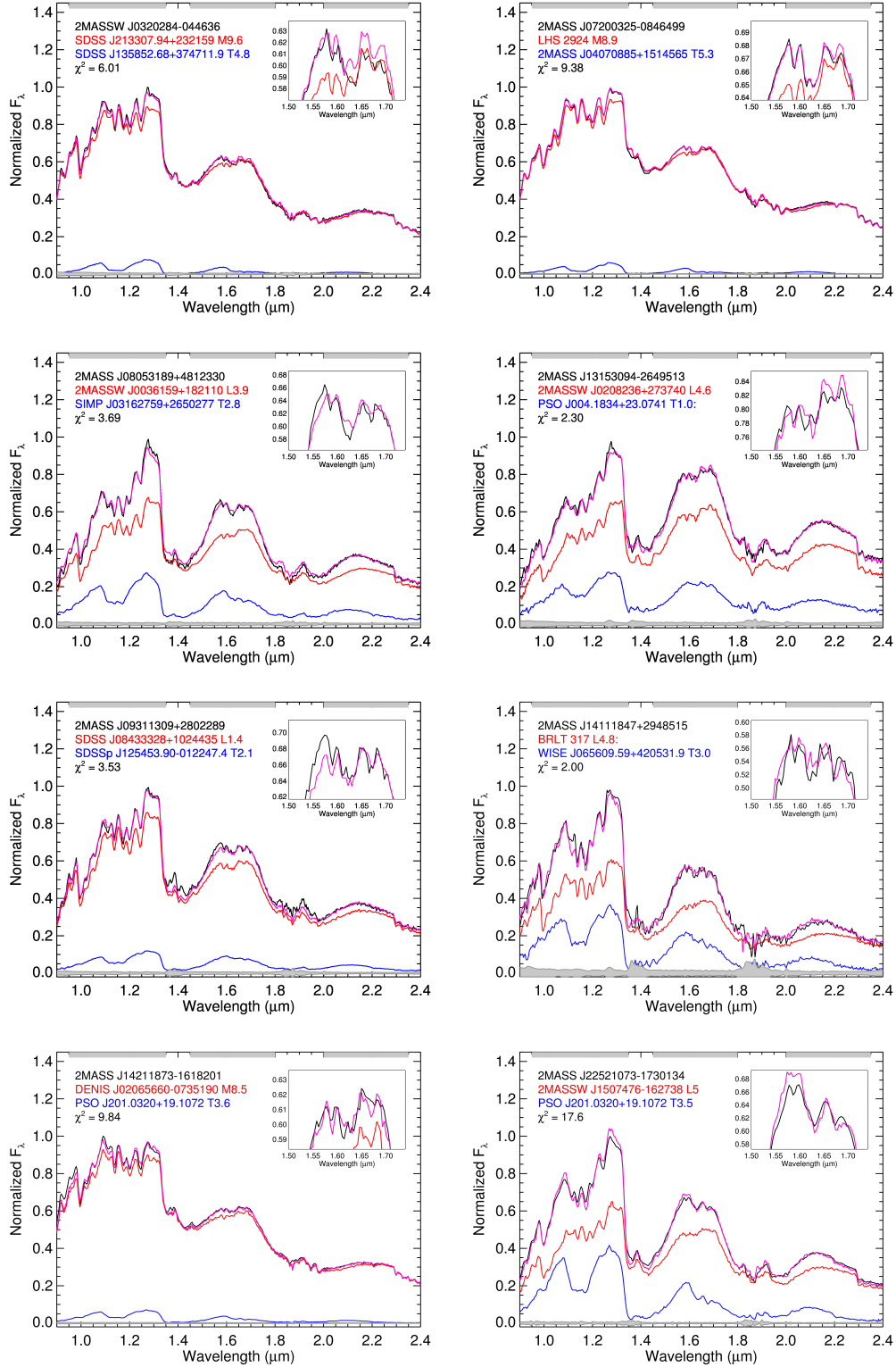


Figure 16. Best fit templates to spectral binaries with M7–L5 primaries with a confidence $> 90\%$. 2MASSW J0320–0446, WISE J0720–0846, 2MASS J0805+4812, 2MASS J1315–2649, 2MASS J2252–1730 are all within 25 pc, whereas 2MASS J0931+2802, 2MASS J1411+2948, and 2MASS J1421–1618 are outside 25 pc. All the spectral binary candidates in the 25 pc sample have already been confirmed as true binaries.

$\geq M7$, and the companion frequency is 0.14 ± 0.02 companions per object (following the definition of Goodwin et al. 2004).

Figure 18 shows the cumulative binary fraction as a function of distance. Out to a distance of 9 pc, the binary fraction oscillates around 13–25%, and at larger distances it begins to drop and settle around $\sim 7\%$. The resolved UCD binary fraction has been thoroughly studied (e.g., Bouy et al. 2003; Burgasser 2007a) leading to $\sim 10–20\%$ for separations > 1 AU, while sub-AU systems comprise 1–4% of the population (Blake et al. 2010; Allen 2007). However, this is the first time the UCD binary fraction has been calculated in a volume-limited sample¹¹, and as seen in Figure 17, there may be a significant fraction of overluminous binaries that have not been confirmed by high resolution imaging, astrometry, or RV monitoring yet. Additionally, in the previous Section we found that 5 out of the 25 binaries within 25 pc are spectral binaries. Since spectral binaries require specific combinations of spectral types to be identified as such, we do not expect them to dominate the binary detection yield. Yet in this study, $\sim 20\%$ of our binaries are spectral binaries, supporting our hypothesis that the population of binaries in the 25 pc sample literature is incomplete. The incompleteness of binaries is shown in Figure 19 as a cumulative histogram over distance which flattens beyond 20 pc compared to the general 25 pc sample. Fitting curves to the 5–10 pc, 5–15 pc, and 5–20 pc regions, and extrapolating to 25 pc, we estimate a large binary incompleteness of 76%, 65%, or 56%, respectively.

5. SELECTION AND LUMINOSITY FUNCTIONS

The luminosity function measures the number density of sources as a function of luminosity, or equivalently, absolute magnitude, temperature, or spectral type. For main sequence stars there is generally a one-to-one mapping between luminosity and mass functions; for UCDs, because brown dwarfs cool as they age, there is not a one-to-one mapping between a brown dwarf luminosity function and a brown dwarf mass function. However, the luminosity function is the initial crucial measurement towards a fundamental understanding of low mass star and brown dwarf formation through a field present-day mass function. The luminosity function of UCDs covering the M7–L5 spectral type range, has been most notably measured by Cruz et al. (2007), hence here we provide an updated reevaluation.

5.1. Area Coverage

The area covered by our spectral survey is limited by the declinations accessible from IRTF, roughly $-50^\circ < \delta < +67^\circ$. Additionally, our survey suffers from an inherent incompleteness of sources in the Galactic plane. We therefore restrict our analysis to the area of sky outside $-15^\circ < b < +15^\circ$ and within $-50^\circ < \delta < +67^\circ$ which corresponds to an area of $26,051.54 \text{ deg}^2$, or 63.2% of the sky.

¹¹ In their 6.5 pc volume literature study, Bihain & Scholz (2016) identify 48.5% of stars and 15.4% of brown dwarfs as part of multiple systems, but no combined UCD fraction.

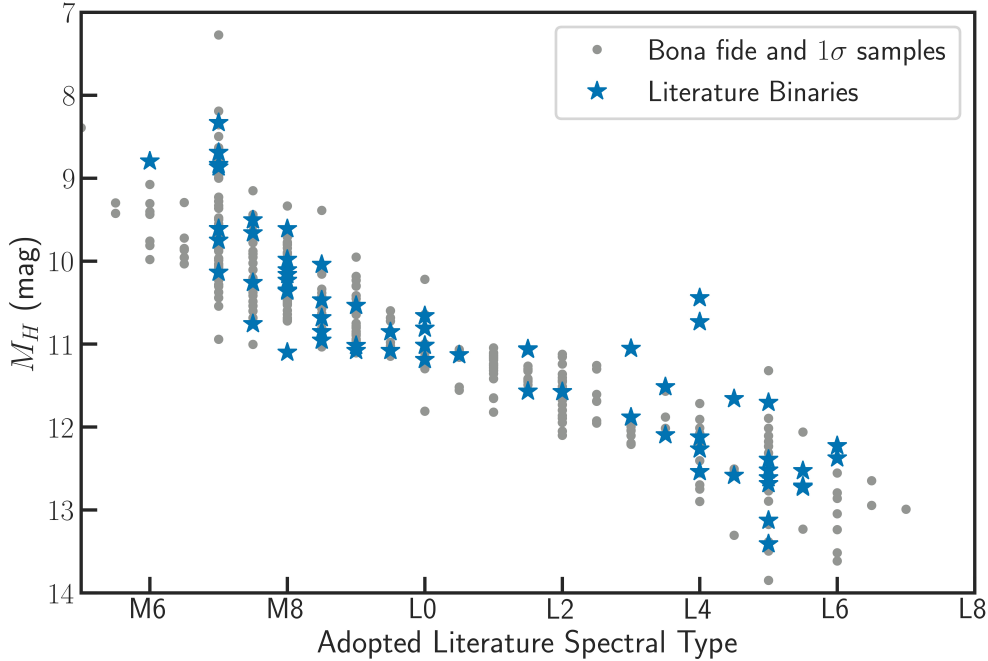


Figure 17. Adopted literature spectral type vs. 2MASS H absolute magnitude for our extended 1σ sample highlighting the UCD binary systems reported in the literature. Most binaries in this plot have resolved absolute magnitudes, and thus their individual components look normal. The two L4 dwarfs well above the sequence are HD 130948B and C are companions to the young F9 variable star (Goto et al. 2002), known to be overluminous on color-magnitude diagrams (Faherty et al. 2016).

Bright stars reduce the total available sky area by obscuring patches of sky where a UCD could otherwise be found. To account for this effect, we drew one million sources from our sample and reassigned them to random coordinates within our observable area. This list was crossmatched with the 2MASS catalog using TOPCAT with a $5''.0$ radius, returning 22,126 matches. Of these, 2,345 stars were as bright or brighter than the simulated input targets within the search radius, thus effectively obscuring nearby UCD. Accounting for this effect reduces the effective observable sky by 0.15% to 25990.45 deg^2 . While we note that 0.5% of the sky is obscured by bright stars and excluded from the 2MASS survey¹², we do not take it into account in our calculations, since our sources also come from optical and mid-infrared surveys.

5.2. Volume Completeness

A volume within 25 pc around the Sun is well embedded within the thin disk of the Galaxy (scale height ~ 300 pc; Kent et al. 1991; Bochanski et al. 2010), and therefore should be relatively uniform in density. Assuming a uniform distribution of sources,

¹² See 2MASS Explanatory Supplement, <https://old.ipac.caltech.edu/2mass/releases/second/doc/>

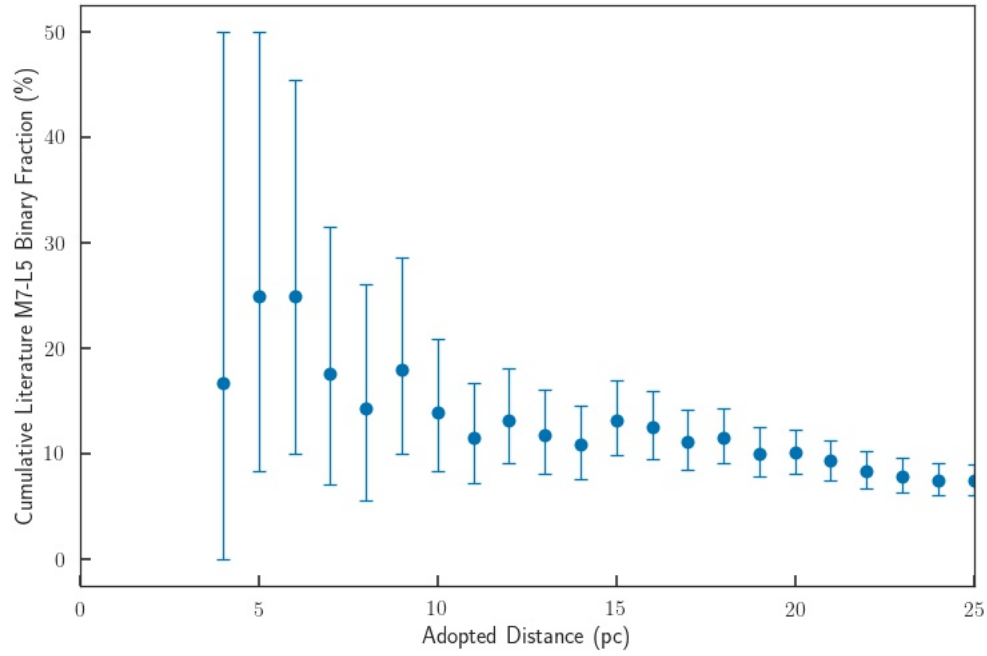


Figure 18. Cumulative binary fraction as a function of distance.

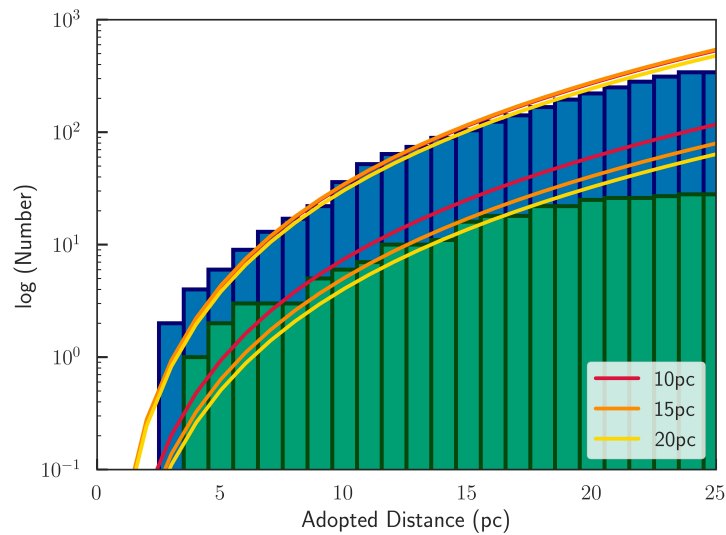


Figure 19. Cumulative histogram of sources per unit adopted distance. The full 25 pc sample is shown in blue, and the binaries with primaries M7 or later are shown in green. Three curve fits are shown for each histogram, assuming completeness between 5 – 10 pc (red), 5 – 15 pc (orange), and 5 – 20 pc (yellow).

Table 12. Estimated volume completeness.

Fit Range (pc)	Predicted Numbers		Completeness	
	Trigonometric	Adopted Distance	Trigonometric	Adopted Distance
<i>25 pc sample (N = 410)</i>				
5 – 10	592	592	64 ⁺⁸ ₋₇ %	69 ⁺⁹ ₋₈ %
5 – 15	552	583	69 ⁺⁹ ₋₈ %	70 ⁺⁹ ₋₈ %
5 – 20	484	511	79 ⁺⁹ ₋₈ %	80 ⁺⁹ ₋₈ %
<i>25 pc M dwarfs (N = 223)</i>				
5 – 10	...	509	...	44 ⁺⁷ ₋₆ %
5 – 15	...	357	...	62 ⁺⁸ ₋₇ %
5 – 20	...	283	...	78 ⁺⁹ ₋₈ %
<i>25 pc L dwarfs (N = 187)</i>				
5 – 10	...	83	...	226 ⁺¹⁶ ₋₁₅ %
5 – 15	...	226	...	83 ⁺¹⁰ ₋₉ %
5 – 20	...	228	...	82 ⁺¹⁰ ₋₉ %

the cumulative number of objects should increase with distance following an r^3 relation. We estimate our volume completeness in trigonometric, spectrophotometric, and adopted distances by fitting power law curves to the cumulative distribution of sources between 5 – 10 pc, 5 – 15 pc and 5 – 20 pc, assuming completeness in those ranges, considering Poisson uncertainties (Figure 21), and extrapolating expected numbers to 25 pc. The ratio of number of objects in our sample to expected number is used to estimate our completeness. These values are summarized in Table 12.

The completeness of late-M dwarfs is lower than that of L dwarfs. Using the 5 – 15 pc fit, which is a good trade-off between completeness and sample size, our sample contains 62⁺⁸₋₇% of the late-M dwarfs within 25 pc, and 83⁺¹⁰₋₉% of L dwarfs. Late-M dwarfs may have been missed in previous surveys, due to color-selection biases designed to exclude more numerous and brighter mid-M dwarfs, as indicated by Schmidt et al. (2015). While most L dwarfs in the Solar neighborhood have already been identified in previous searches, many may be hidden in crowded areas like the Galactic plane (e.g. the L8 dwarf recently identified at 11 pc; Faherty et al. 2018). From the trigonometric distances, we estimate our total sample completeness to be between 64 – 79%. Including spectrophotometric distances when parallaxes are not available, the sample completeness is between 69 – 80%, but we adopt the value for the 5 – 15 pc fit, 70⁺⁹₋₈%. This completeness value is used in Section 5.5 to scale the corrected number of sources in the 25 pc volume when measuring the luminosity function (see Equation 4). We expect most of the incompleteness to come from missing sources beyond 20 pc, as seen in Figure 20, possibly including sources in the Galactic plane, the

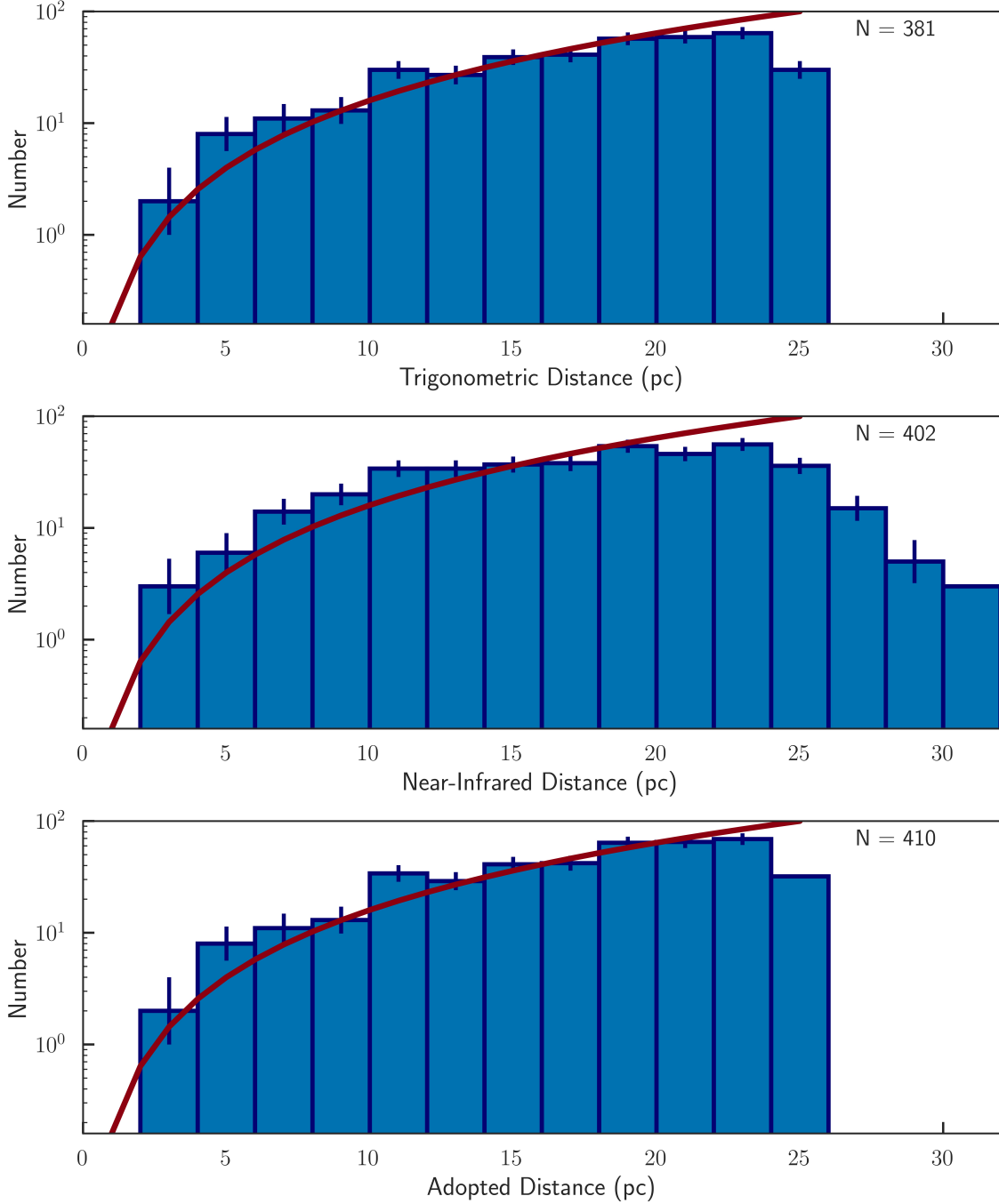


Figure 20. Distributions of trigonometric (*top*), spectrophotometric (*middle*) and adopted distances (*bottom*). Solid line is an r^2 fit normalized at the 25 pc bin. Note the drop off in the largest distance bins, which reflects incompleteness likely due to brightness limits and selection biases.

southern hemisphere, or UCD candidates recently identified in [Reylé \(2018\)](#) in need of spectroscopic validation.

Additionally, we estimate $\langle V/V_{max} \rangle$ averages suggested by [Schmidt \(1968\)](#) to evaluate the homogeneous spatial distribution of our sample. $\langle V/V_{max} \rangle$ measures the

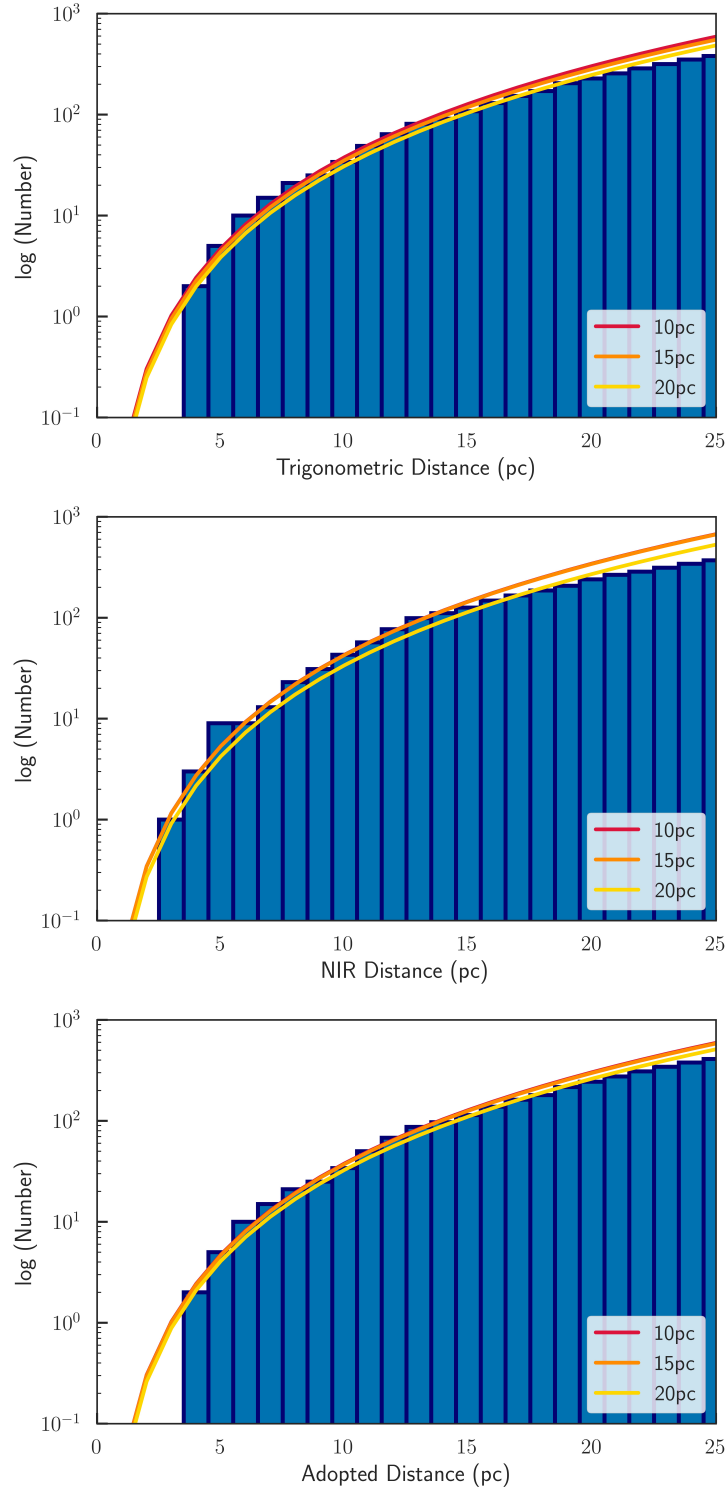


Figure 21. Cumulative distance histograms for trigonometric, spectrophotometric, and adopted distances. The red, orange and yellow curves show the cube fit to the histograms in blue up to 10 pc, 15 pc and 20 pc, including their Poisson uncertainties.

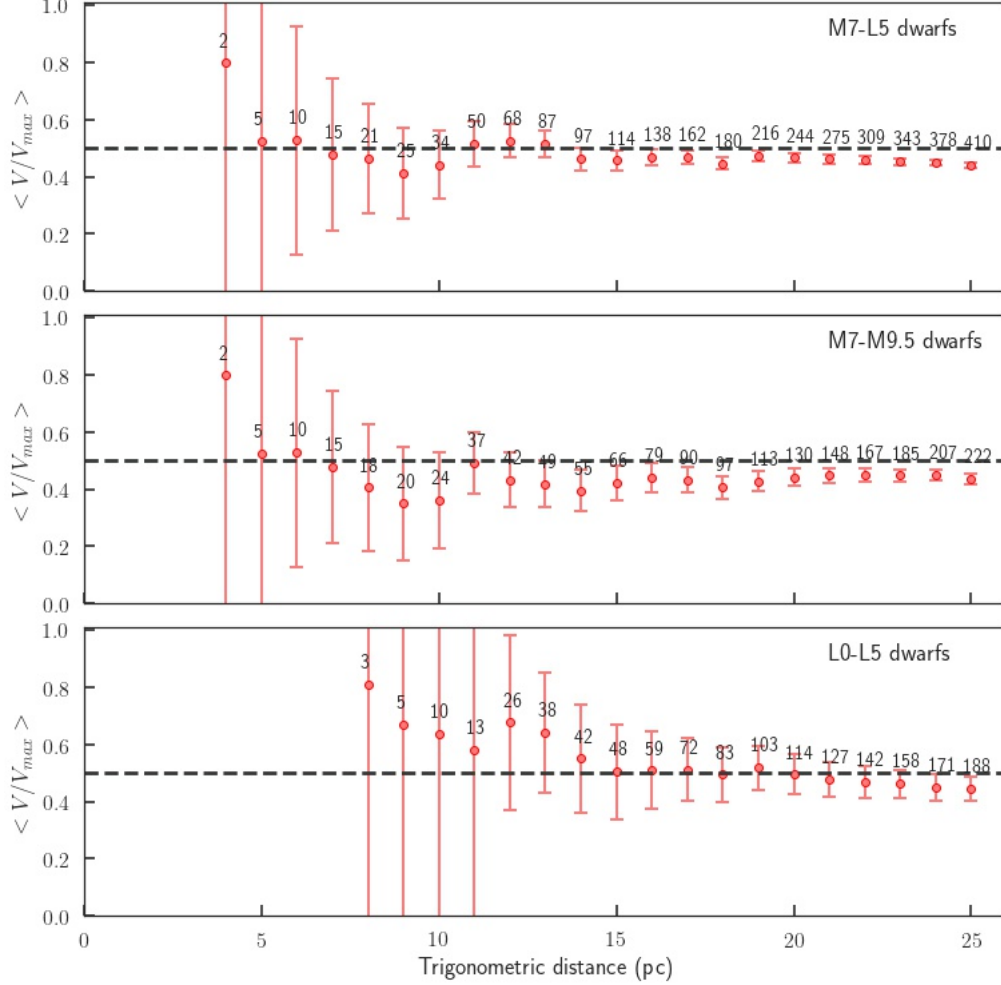


Figure 22. Average $\langle V/V_{max} \rangle$ values for our 25 pc sample, and also for subsamples of M and L dwarf with uncertainties calculated as described in Kirkpatrick et al. (2019). The numbers indicate the cumulative number of sources counted up to that distance. We used the adopted distances for this calculation.

number of sources in each half of a given volume, approaching 0.5 for a uniformly distributed sample with equal counts on each half-volume. Figure 22 shows the distribution of $\langle V/V_{max} \rangle$ values. Uncertainties are calculated as $0.5 - \frac{n/2 - a_{max}}{n}$, where a_{max} is the distance at which the value of $\langle V/V_{max} \rangle$ last equals 0.68 (4 pc for the full sample, and M dwarfs only, and 8 pc for L dwarfs), corresponding to one Gaussian standard deviation. For M dwarfs, the largest distance at which $\langle V/V_{max} \rangle$ approximates 0.5 is 13 pc, suggesting incompleteness of M7–M9.5 dwarfs at larger distances. Conversely, L dwarfs have $\langle V/V_{max} \rangle$ consistent with 0.5 up until 25 pc, indicating a homogeneous distribution of L0–L5 dwarfs in our sample.

5.3. Sample Simulation

Compiling a sample of objects starting from past literature compilations leads to a complicated selection function. Rather than determining the selection function of each selection process separately, we simulate a sample of UCDs in a volume larger

than 25 pc, including unresolved binaries, and apply selections based on our spectral type and distance cuts, from both parallaxes and spectrophotometric estimates. This procedure aims to measure systematic effects in the sample construction.

We simulate 10^6 UCDs, assigning distances drawn from a uniform spatial distribution out to 50 pc. We calculate “true” parallaxes by inverting the distances. An underlying spectral type distribution was derived by population simulations (c.f. [Burgasser 2004](#)) using the [Chabrier \(2005\)](#) IMF, a uniform age distribution, the [Burrows et al. \(2001\)](#) evolutionary models, and the effective temperature to spectral type empirical relations from [Pecaut & Mamajek \(2013\)](#), which cover the full stellar and substellar spectral type range from O3 to Y2. From this distribution, 10^6 “true” spectral types between M5–L7 were randomly drawn and assigned to our simulated UCD sources.

We calculate absolute magnitudes empirically, from the simulated spectral types, using the following linear relations:

$$M_J = 0.37 \times SpT + 4.29, \text{ rms} = 0.35 \quad (1)$$

$$M_H = 0.32 \times SpT + 4.61, \text{ rms} = 0.29 \quad (2)$$

$$M_{K_s} = 0.29 \times SpT + 4.67, \text{ rms} = 0.29 \quad (3)$$

determined from a subset of 230 single M7–L5 dwarfs with parallax measurements, 2MASS magnitudes, not classified as VL-G, INT-G, unusually red, or unusually blue from our 25 pc sample. The scatter in these relations is slightly smaller than in other empirical relations covering broader spectral type ranges (e.g. [Dupuy & Liu 2012](#); $\sigma = 0.4$ mag). To simulate the intrinsic brightness distribution of the population, we add offsets to these empirical absolute magnitudes, drawn from a Gaussian distribution centered at zero and scaled by the scatter in the empirical relations.

Parallax-limited and magnitude-limited samples are subject to different biases affecting the total number of included sample members. The Lutz-Kelker bias affects parallax-limited samples by allowing objects from outside a distance limit into the observed volume ([Lutz & Kelker 1973](#)). For an observed parallax π_0 , there is a range of true parallaxes $\pi_0 \pm \delta\pi$ for normally-distributed measurement uncertainties. Assuming a uniform number density of stars, the number of objects per parallax bin will be proportional to $N_* \propto 1/\pi^4$, implying that the number of stars increases as the parallax decreases, i.e. there are more objects in the volume outside a given distance than within. Subsequently, this means that more stars will appear to have smaller true parallaxes than their observed parallaxes, and that the average distance for sample members will be farther than the distance limit ([Lutz & Kelker 1973](#)).

In magnitude-limited samples, intrinsically brighter sources (i.e. on the high end of the absolute magnitude distribution) and unresolved binaries will be selected in larger numbers than intrinsically fainter sources, again due to the larger volume sampled by the brighter sources, an effect known as the Malmquist bias ([Malmquist 1922](#)). Depending on the relative uncertainty in distance and magnitude measurements, and

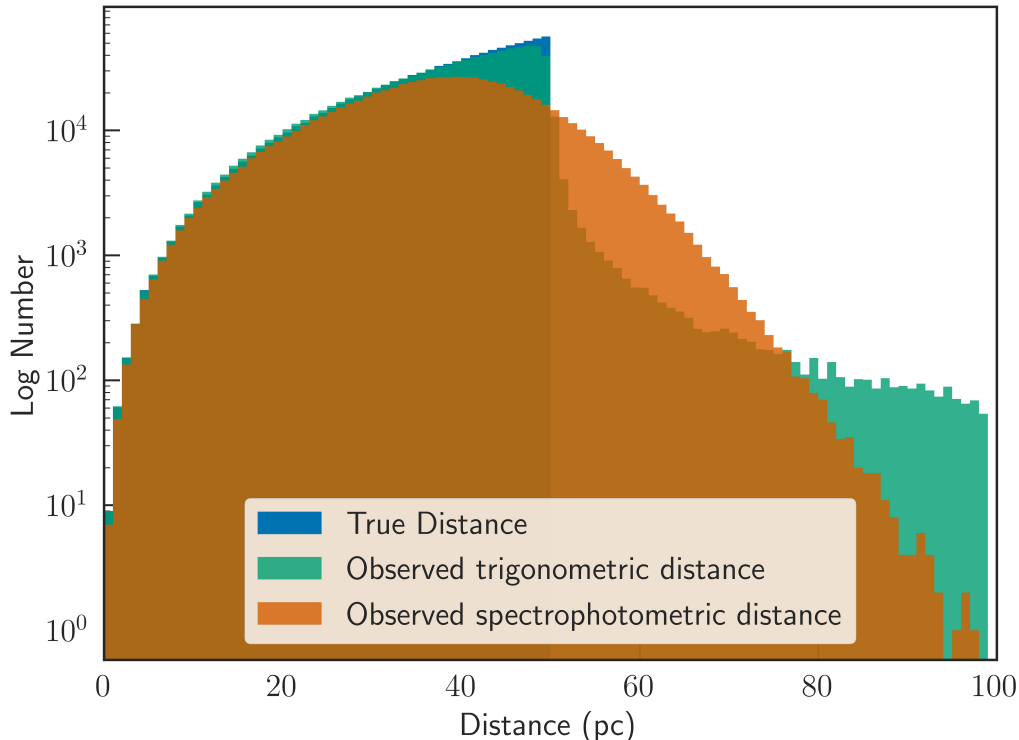


Figure 23. True and observed distances from our simulation. The blue histogram shows the distribution of true distances, following an r^3 shape, defined up to 50 pc. The green histogram shows the distribution of observed trigonometric distances, measured after a Gaussian uncertainty was added to the true parallax, with the scale of the distribution emerging from our sample’s parallax uncertainty distribution. The orange histogram shows the distribution of the observed spectrophotometric distances, measured with spectral types, apparent magnitudes, and empirical absolute magnitude relations. This distribution is affected by the Malmquist bias, including sources located farther than the volume limit.

intrinsic scatter in the population, the effect from the Malmquist bias can be significantly larger than that of the Lutz-Kelker bias. Since our sample is defined by both trigonometric and spectrophotometric distances, both effects are significant in our calculations, although the Lutz-Kelker bias plays a more significant role given the large number of parallaxes in our sample (93% of the sample).

We model the Lutz-Kelker bias in our simulation by adding an uncertainty offset to our parallax measurements drawn from the uncertainty distribution of our observed parallaxes (see Figure 23). We excluded 2246 simulated sources with observed negative parallaxes. We account for unresolved binarity by adding a magnitude offset to 20% of stars in our simulated sample, the fraction based on estimates of the underlying UCD binary fraction (Bouy et al. 2003; Gizis et al. 2003; Burgasser et al. 2007c). We randomly assigned mass ratios from a power law distribution ($\propto q^{1.8}$; Allen 2007) to compute secondary masses. Effective temperatures, spectral types, and absolute

magnitudes for the secondaries were obtained in the same manner as the primaries, resulting in combined system absolute magnitudes. Magnitude offsets ranged between $\Delta m = 0 - 0.75 \text{ mag}$ ¹³. For simplicity, we assumed that the addition of flux to the simulated binaries does not affect the spectral type classification, which is likely true for late-M and early-L dwarf primaries but not necessarily for late-L+T dwarf systems (Cruz et al. 2004; Burgasser et al. 2010). The addition of magnitude offsets for simulated binaries, and uncertainties to the true absolute magnitudes for all simulated sources models the effects from the Malmquist bias.

To model observed spectral types, offsets were drawn from a Gaussian distribution with a standard deviation equal to 0.95 subtypes (see Section 2.2.1). Apparent magnitudes were assigned based on the distance modulus and absolute magnitudes, adding an observational uncertainty drawn from a Gaussian distribution with a standard deviation following the same photometric error distribution from our literature sample. Observed parallaxes were modeled by adding a Gaussian uncertainty to the true parallaxes.

5.4. Selection Function

We quantify four selection functions, one for trigonometric and one for spectrophotometric distance selections as functions of spectral type and absolute magnitude. First, we define our “intrinsic sample” as those simulated sources whose true distances are $d \leq 25 \text{ pc}$. We define “observed samples” by requiring observed trigonometric or observed spectrophotometric distances $d \leq 25 \text{ pc}$. In each sample, we select objects with an observed spectral type between M7–L5, and organize them according to their true spectral type, given that we are concerned with modeling our observations, yet aware that the true subtype may be different from the observed one. For the selection function by absolute magnitudes, we organized this selected sample in bins of 0.5 mag observed absolute magnitudes. Our trigonometric and spectrophotometric selection functions are the ratio of objects selected by observations over the number of objects selected by their true parameters. These selection functions are summarized in Tables 13 and 14 and illustrated in Figure 24.

Our trigonometric selection function is relatively high (92 – 98%) for the central part of the M7–L5 spectral type range, except at the edges where the selection rate drops to 71% for M7 and 69% for L5. The spectrophotometric selection function runs parallel to the trigonometric one, following a similar shape at a lower rate, 77 – 82% for M8–L4 and dropping to 65% for M7 and 53% for L5. The trigonometric selection function based on *J*-band absolute magnitudes steadily increases from 66% at 10.75 mag (roughly equivalent to M7) to 96% at 12.25 mag, then dropping to 92% and 76% in the subsequent fainter bins. The corresponding spectrophotometric

¹³ Systems with a magnitude offset larger than 0.75 (corresponding to an equal mass binary) occurred when the secondary was slightly brighter than the primary in any band as allowed by the added scatter, despite a larger primary mass. This is the case for 33,194 sources, 3.3% of the simulated sample or 16.6% of the simulated binaries. All of these systems were dropped from the simulation, resulting in 964,560 objects total.

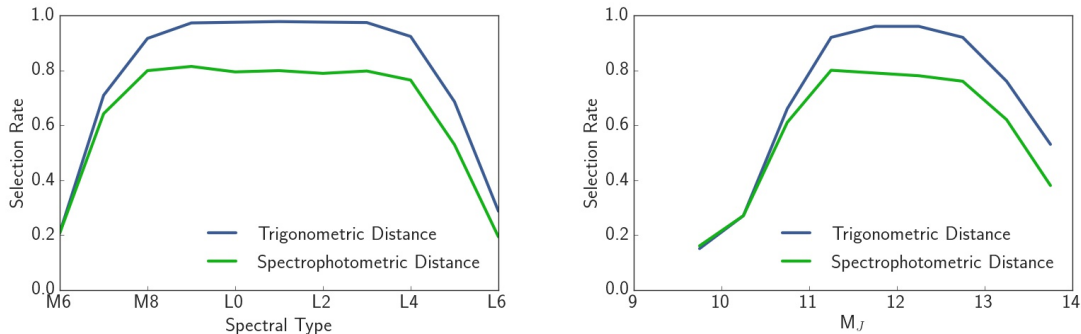


Figure 24. Selection functions from trigonometric (blue) and spectrophotometric (green) distance cuts as a function of spectral type (*Left*) and absolute magnitude in *J*-band (*Right*).

selection function follows a similar shape at a lower rate as well, starting at 61% for 10.75 mag, reaching a peak of 80% at 11.25 mag, and decreasing towards fainter magnitudes down to 62% at 13.25 mag (roughly equivalent to L4). These results are presented in Tables 13 and 14. As expected, the edges of our sample suffer from higher contamination than the bulk of it. Contamination from bright sources that do not belong in the 25 pc M7–L5 sample is most noticeable in the low spectrophotometric selection rate of the brightest absolute magnitude bins.

We also calculated the proportion of true negatives and false positives per spectral subtype and absolute magnitude bin. True negatives are true M7–L5 dwarfs with true distances within 25 pc which are not selected by observed trigonometric or spectrophotometric cuts at 25 pc, i.e. true sources missed by our selections. The true negative fraction is 2% for any spectral subtype using a parallax cut, except for L0 where the missed fraction is 3%. However, for a spectrophotometric cut, the true negative fraction rises with spectral type from 8% to a maximum of 21% at L2, then decreasing again to 17% at L5. The true negative fraction by absolute magnitude bins is also 2% for trigonometric cuts and 7–22% for spectrophotometric cuts, with the maximum at 12.25 mag. False positives are contaminants, either sources outside the M7–L5 spectral range within 25 pc or true M7–L5 dwarfs outside 25 pc selected by observations. The false positive fraction for M7–L5 dwarfs varied between 6–9% for spectral type bins selected by parallax, and 10–31% if selected by spectrophotometric distance. The false positive rates by absolute magnitude bins are 2–8% for trigonometric selections and 14–30% for spectrophotometric selections. Thus, the true negative and false positive rates for trigonometric and spectrophotometric selections are comparable across spectral type and absolute magnitude bins. Tables 15 and 16 show the fraction of simulated sources outside 25 pc with a given spectral type and their observed spectral type as selected by observed trigonometric and spectrophotometric distances. For example, on Table 15, 4% of observed M8 dwarfs are actually M9 dwarfs outside of 25 pc. Overall, it appears that parallax selections are more resistant to scattering of earlier type objects. Diagonal elements indicate objects of matching true and observed spectral subtype, outside of 25 pc but falsely selected

Table 15. False positive fractions per spectral subtypes for observed trigonometric selection.

		Observed Spectral Type								
		M7	M8	M9	L0	L1	L2	L3	L4	L5
True Spectral Type	M5	0.02	0.00	0.00	0.00	0.00	0.00	0.00	0.00	0.00
	M6	0.04	0.01	0.00	0.00	0.00	0.00	0.00	0.00	0.00
	M7	0.03	0.03	0.00	0.00	0.00	0.00	0.00	0.00	0.00
	M8	0.02	0.04	0.01	0.00	0.00	0.00	0.00	0.00	0.00
	M9	0.00	0.03	0.04	0.02	0.01	0.00	0.00	0.00	0.00
	L0	0.00	0.01	0.02	0.03	0.03	0.01	0.00	0.00	0.00
	L1	0.00	0.00	0.00	0.01	0.03	0.03	0.01	0.00	0.00
	L2	0.00	0.00	0.00	0.00	0.02	0.03	0.02	0.01	0.00
	L3	0.00	0.00	0.00	0.00	0.00	0.02	0.03	0.02	0.00
	L4	0.00	0.00	0.00	0.00	0.00	0.00	0.02	0.04	0.02
	L5	0.00	0.00	0.00	0.00	0.00	0.00	0.01	0.03	0.04
	L6	0.00	0.00	0.00	0.00	0.00	0.00	0.00	0.00	0.02

Table 16. False positive fractions per spectral subtypes for observed spectrophotometric selection.

		Observed Spectral Type								
		M7	M8	M9	L0	L1	L2	L3	L4	L5
True Spectral Type	M5	0.25	0.06	0.00	0.00	0.00	0.00	0.00	0.00	0.00
	M6	0.42	0.17	0.01	0.00	0.00	0.00	0.00	0.00	0.00
	M7	0.08	0.20	0.06	0.01	0.00	0.00	0.00	0.00	0.00
	M8	0.01	0.10	0.08	0.03	0.00	0.00	0.00	0.00	0.00
	M9	0.00	0.02	0.08	0.11	0.08	0.01	0.00	0.00	0.00
	L0	0.00	0.00	0.01	0.06	0.16	0.10	0.01	0.00	0.00
	L1	0.00	0.00	0.00	0.00	0.07	0.15	0.06	0.01	0.00
	L2	0.00	0.00	0.00	0.00	0.01	0.06	0.11	0.06	0.01
	L3	0.00	0.00	0.00	0.00	0.00	0.01	0.08	0.14	0.06
	L4	0.00	0.00	0.00	0.00	0.00	0.00	0.01	0.09	0.14
	L5	0.00	0.00	0.00	0.00	0.00	0.00	0.00	0.01	0.09
	L6	0.00	0.00	0.00	0.00	0.00	0.00	0.00	0.00	0.01

to be within the volume, possibly very close to the 25 pc limit (Lutz-Kelker bias) or brighter than most other objects of the same subtype (Malmquist bias).

5.5. Luminosity Function

5.5.1. Luminosity Function with respect to Spectral Types

Luminosity functions are a result of the underlying mass function and stellar birth rates. Calculating a luminosity function of UCDs in the 25 pc volume around the Sun is the first step towards building a field IMF across the stellar/substellar boundary. To measure our luminosity function with respect to spectral types, we prioritize literature optical, SpeX, and literature NIR spectral types in that order, since optical classifications are more precise than NIR ones¹⁴. Since our study is concerned with the areas accessible by SpeX and outside of $\pm 15^\circ$ from the galactic plane, we excluded literature sources outside of these areas, reducing our sample to 331 sources. However, 4 sources do not have unresolved J -band magnitude (see Section 2.2), hence our effective sample includes 327 objects. From these, we find 306 sources in our 25 pc sample with prioritized spectral types within M7–L5 within declinations accessible by SpeX ($-50^\circ \leq \delta \leq +67^\circ$), and outside galactic latitudes $\pm 15^\circ$ from the galactic plane.

To estimate the expected total number of objects in our 25 pc sample per spectral type bin, we scale our counts by our selection functions and completeness. We proportionally apply the trigonometric and spectrophotometric selection functions (SF_{plx} and SF_{phot} , respectively) to each spectral type bin by splitting our counts, $N_{bin} = N_{plx} + N_{phot}$ according to their type of adopted distance (trigonometric or spectrophotometric), and then scaled by the completeness percentage for the 5-15 pc fit from Section 5.2, i.e.,

$$N_{corrected} = \left(\frac{N_{plx}}{SF_{plx}} + \frac{N_{phot}}{SF_{phot}} \right) \cdot \left(\frac{1}{\text{completeness}} \right) \quad (4)$$

These corrected counts were divided over the volume estimated in Section 5.1 to obtain our luminosity function with respect to spectral types. Our number densities are listed in Table 17, and shown in Figure 27 with and without selection function and completeness corrections.

Figure 28 compares our number densities to other UCD field studies, including the 20 pc samples of Cruz et al. (2007) and Reid et al. (2008), and the 8 pc sample of Kirkpatrick et al. (2012), extended into the substellar regime. Our number densities are consistently higher than those of Reid et al. (2008), particularly on the M dwarfs, although their study does not claim completeness on spectral types earlier than L0. Except for the M7 and L5 edges, our number densities are comparable within 2σ to those of Cruz et al. (2007) for all spectral types, albeit they claim only a lower limit on L dwarf densities. However, our densities are on average slightly higher than those of Cruz et al. (2007), except for the M8 bin. Cruz et al. (2007) found 99 objects between M7–L8 in 20 pc with a sky coverage of 36%, which scales to 244 sources at

¹⁴ We made an exception to prioritize literature NIR over SpeX classification for 2MASS J22521073–1730134A, which has a literature NIR spectral type of L4, no literature optical spectral type, and an unresolved SpeX spectral type of T0.

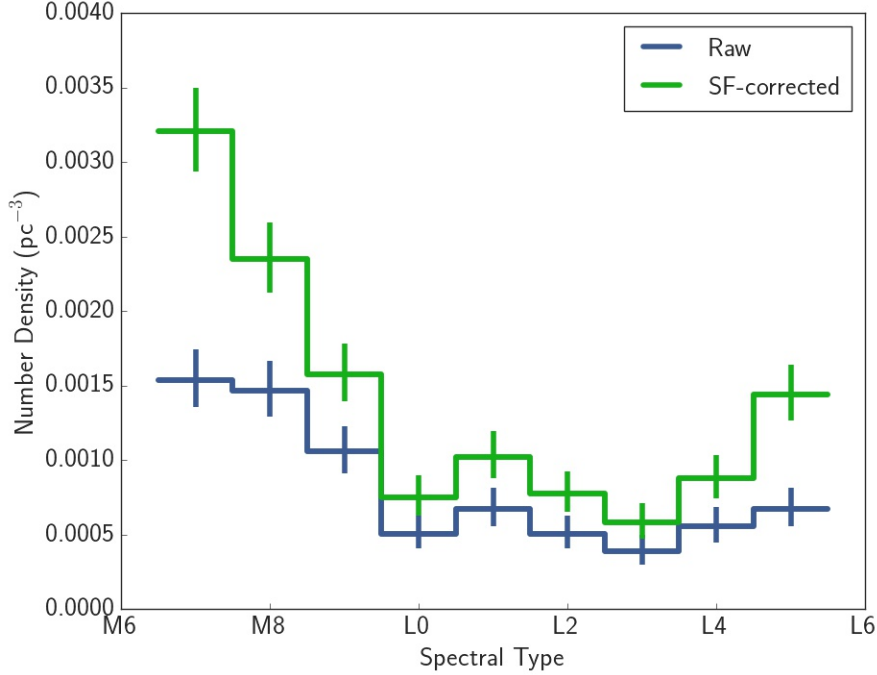


Figure 27. Raw and selection-function corrected number densities per subtype for our 25 pc sample.

25 pc for our sky coverage of 63.5% and 69% completeness, yet we count 327 sources within a shorter spectral type range. This $\geq 34\%$ difference can be attributed to new discoveries, improvements in source color selection (i.e. Schmidt et al. 2015), and broader availability of parallaxes. The 8 pc sample of Kirkpatrick et al. (2012) is sparse on the L dwarf regime, with only one L5 within that volume, and while they include 11 M7–M9.5 dwarfs, they claim no completeness on the M dwarf range. We identify 19 M7–M9.5 sources in the literature within the 8 pc volume and therefore have larger number densities than Kirkpatrick et al. (2012), including a few new discoveries since then.

Table 17 also shows number densities for the M7–M9.5, L0–L5, and M7–L5 ranges. We find that the late-M dwarf raw number density agrees within 20% of Cruz et al. (2007), but our number density corrected by the selection function and incompleteness is $\sim 45\%$ higher, largely driven by the latter. Our L dwarf densities cover a smaller spectral type range than Cruz et al. (2007), and raw and corrected densities follow the same proportions as for the M-dwarf regime. Taking the full range of M7–L5 spectral subtypes, we find 40% higher densities than Cruz et al. (2007), with a raw density of $(7.3 \pm 0.4) \times 10^{-3} pc^{-3}$ and a corrected density of $(12.6 \pm 0.6) \times 10^{-3} pc^{-3}$. Our volume density implies that the total number of M7–L5 dwarfs within the 25 pc volume could be as high as ~ 820 .

5.5.2. Luminosity Function with respect to Absolute Magnitudes

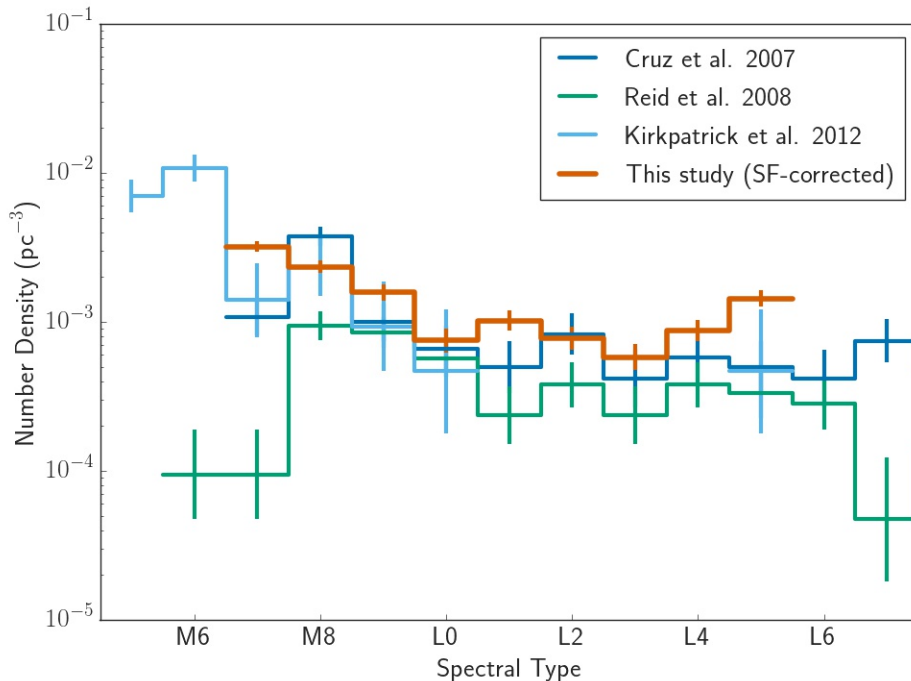


Figure 28. Number densities per subtype for the surveys of Cruz et al. (2007), Reid et al. (2008), Kirkpatrick et al. (2012), and this study.

We follow a similar procedure to calculate the luminosity function with respect to absolute magnitude in J . We use the subsample of 306 sources described in Section 5.5.1, yet we organize it in absolute magnitude bins. Our luminosity function is described in Table 18. Figure 25 shows the resulting luminosity function, including Poisson error bars. Using the Filippazzo et al. (2015) empirical relations, we determine that the 10.3 – 14.2 mag range in J -band encompasses the M7–L5 dwarf range, including the 1σ (0.4 mag) relation uncertainties. Our luminosity function peaks at the 10.25 – 10.75 mag bin, which roughly corresponds to the peak at the M7–M8 spectral class, matching our spectral type distribution from Figure 8. Our luminosity function then tapers off to a plateau after the 12.25 mag bin.

Our luminosity function follows from the faint end of the Reid et al. (2003a) luminosity function, as seen in Figure 26, matching it well within uncertainties. Throughout the 10.75 – 13.75 mag range, our luminosity function resembles the downward slope of the Cruz et al. (2007) corresponding function.

5.6. Towards building a substellar IMF

The IMF is a direct outcome of the formation process. Measurements of the IMF across the hydrogen burning limit have revealed that brown dwarfs are not a significant contributor to dark matter (Reid et al. 2003a), yet brown dwarfs could be as abundant as stars (e.g., Mužić et al. 2017). The efficiency of the star formation process at low masses, and the minimum mass allowed by the gravitational fragmen-

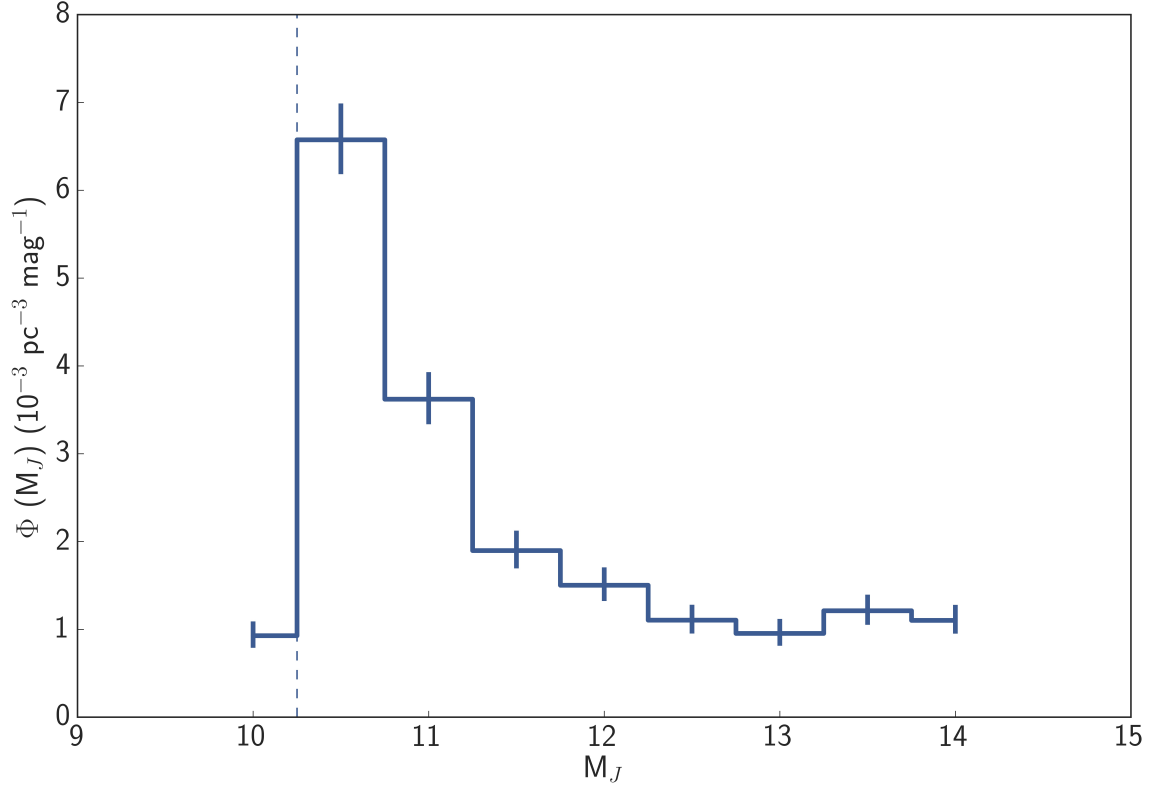


Figure 25. Measured luminosity function for M7–L5 ultracool dwarfs with Poisson error bars, corrected by the selection function and completeness. We do not claim completeness at magnitudes brighter than the dashed line.

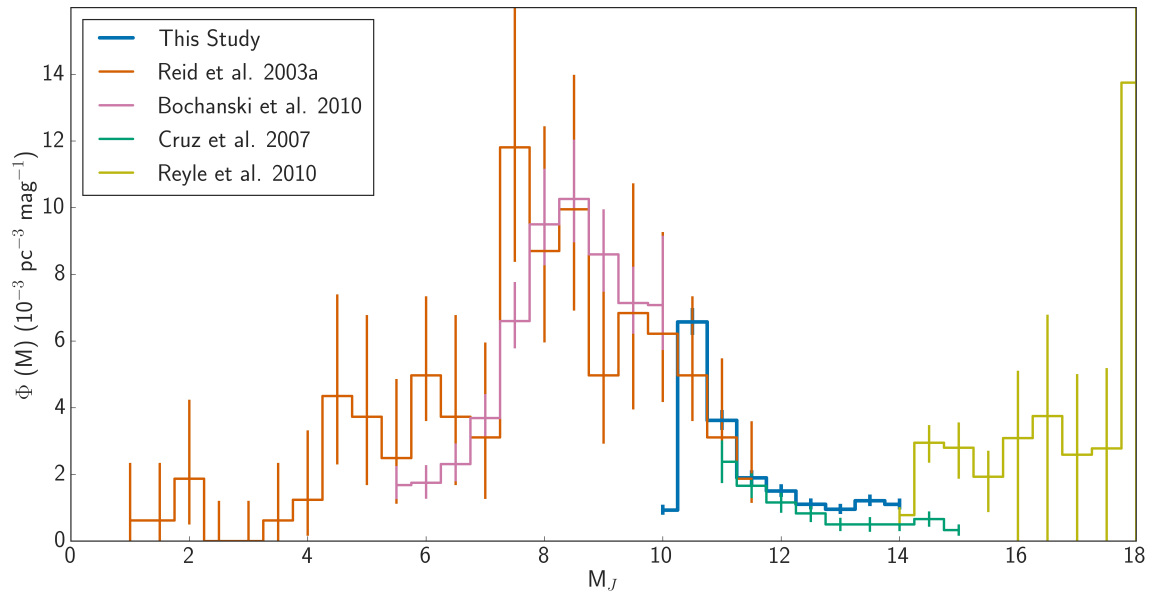


Figure 26. Luminosity functions for ultracool dwarfs according to our study (dark blue), Reid et al. (2003a) (orange), Bochanski et al. (2010) (pink), Cruz et al. (2007) (green), and Reylé et al. (2010) (yellow).

tation of a molecular cloud can be determined by quantifying the IMF. Constraining the IMF at low masses is a necessary step towards determining the prevalence of different brown dwarf formation mechanisms (Reipurth & Clarke 2001; Padoan & Nordlund 2002; Whitworth & Zinnecker 2004; Stamatellos et al. 2007), and whether they depend on environmental conditions or not (e.g., Whitworth et al. 2007; Bate 2019).

Mass functions are typically derived from luminosity functions, a straightforward operation for main sequence stars. For ultracool dwarfs, however, the mapping is no longer one-to-one due to the long lifetimes of very low mass stars and the mass-age-luminosity degeneracy of brown dwarfs. Substellar IMFs can be directly measured in clusters and young moving groups where age is known for all members (e.g., Taurus, Luhman 2000; TW Hydrae, Looper 2011; Gagné et al. 2017). Measuring the substellar field IMF requires assumptions about the age distribution (Burgasser 2004). Nevertheless, the field luminosity function presented here is an important step towards measuring an accurate mass function across the hydrogen-burning limit in the field, and the overall formation history and evolution of UCDs in the Milky Way.

This sample also has the potential to reveal ultracool dwarf hosts to habitable zone terrestrial planets like those orbiting TRAPPIST-1 (Gillon et al. 2016, 2017). Currently, this source is the only example of a planetary system around an ultracool dwarf, and the only planetary system known with 3 potentially habitable terrestrial worlds. With this volume-limited ultracool sample, planetary population studies around the lowest mass stars and brown dwarfs can be approached in a systematic way (e.g., SPECULOOS, Delrez et al. 2018).

6. SUMMARY

We have compiled a volume-limited sample of M7–L5 ultracool dwarfs out to 25 pc, with targets originating from various surveys in the literature. The variety of selection criteria that goes into defining these surveys makes for a potentially complicated selection function with biases difficult to quantify. Nevertheless, we estimate the compiled sample to be $70_{-8}^{+9}\%$ complete to 25 pc, and highly complete for L dwarfs.

The main results of this study are summarized as follows:

1. We find 410 UCDs in 394 systems in the 25 pc volume surrounding the Sun, with 60 more sources in the 1σ periphery of 25 pc. Thanks to *Gaia* DR2, our sample is largely volume-limited, with 93% of the sample having parallaxes.
2. We obtained low-resolution, NIR, SpeX prism spectra for 89% of the observable sample, and uniformly classified them with spectral and gravity standards.
3. We identify 7 very low gravity sources and 26 intermediate gravity sources in our 25 pc spectral sample, corresponding to fractions of $2.1_{-0.8}^{+0.9}\%$ and $7.8_{-1.5}^{+1.7}\%$, respectively. One new very low gravity source, 2MASS J1739+2454, is identified in this study. Thirteen new intermediate gravity sources are also reported.

Eleven other sources identified as having intermediate gravity also have blue $J - K_S$ colors, suggesting instead low metallicity effects.

4. We calculate $J - K_S$ infrared colors and use them to determine the color distribution of our sample, and identify the red and blue color outlier fractions of $1.4^{+0.6}_{-0.5}\%$ for red and $3.6^{+1.0}_{-0.9}\%$ for blue, from 5 and 15 red and blue color outliers, respectively. We do not identify a color bias in our sample given approximately equal numbers of sources with positive and negative $J - K_S$ color excesses.
5. We identify 5 previously confirmed spectral binaries in the 25 pc volume, and 2 new additional candidates outside the 25 pc volume. The resulting spectral binary fraction is $1.8^{+0.6}_{-0.5}\%$. In a future paper, we will explore the significance of this fraction with respect to the true ultracool binary fraction of M7–L5 dwarfs.
6. We also identified 25 resolved binaries and 13 ultracool companions to main sequence stars in the literature. The literature binary fraction from this sample is $7.5^{+1.6}_{-1.4}\%$. We expect that the identification of overluminous binaries and potentially hidden low gravity and small separation systems will increase this fraction closer to an ultracool resolved binary fraction of 10 – 20%.
7. Our sample is $70^{+9}_{-8}\%$ complete for all sources, mostly incomplete for late-M dwarfs. The completeness for M7–M9.5 is $62^{+8}_{-7}\%$, while for L0–L5 dwarfs it is $83^{+11}_{-10}\%$.
8. We have produced a J -band luminosity function for the 25 pc sample that closely agrees with previous work but with smaller statistical uncertainties.
9. We have calculated space densities per subtype and find a 40% increase in our densities compared to [Cruz et al. \(2007\)](#). Our predicted number density of M7–L5 dwarfs is $(12.6 \pm 0.6) \times 10^{-3} \text{ pc}^{-3}$, or ~ 820 objects within 25 pc.

This homogeneous, volume-limited sample of ultracool dwarfs, with uniformly determined spectral types, measured distances, and masses that span the hydrogen burning limit, has important potential for future statistical studies of UCDS, such as the incidence of magnetic activity, binarity, color outliers, young sources, low metallicity sources, and searches for planetary systems around UCDS.

The authors thank telescope operators Brian Cabreira, Dave Griep, and Tony Matulonis at IRTF for their support during observations. DBG and AJB acknowledge funding support from the National Aeronautics and Space Administration under Grant No. NNX15AI75G. This research has made heavy use of the VizieR catalogue access tool and SIMBAD database, operated at CDS, Strasbourg, France. The original description of the VizieR service was published in [Ochsenbein et al. \(2000\)](#),

and the SIMBAD astronomical database was published in Wenger et al. (2000). This publication makes use of data from the SpeX Prism Spectral Libraries, maintained by Adam Burgasser at <http://www.browndwarfs.org/spexprism>. This research has made use of the Washington Double Star Catalog maintained at the U.S. Naval Observatory. This research was worked on at the NYC *Gaia* DR2 Workshop at the Center for Computational Astrophysics of the Flatiron Institute in 2018 April. This research has benefitted from the Ultracool RIZzo Spectral Library, maintained by Jonathan Gagné and Kelle Cruz. The authors acknowledge being on the traditional territory of the Lenape Nations and recognizes that Manhattan continues to be the home to many Algonkian peoples. We give blessings and thanks to the Lenape people and Lenape Nations in recognition that we are carrying out this work on their indigenous homelands. The authors wish to recognize and acknowledge the very significant cultural role and reverence that the summit of Mauna Kea has always had within the indigenous Hawaiian community. We are most fortunate to have the opportunity to conduct observations from this mountain.

Software: Astropy (Astropy Collaboration et al. 2013), Astroquery (Ginsburg et al. 2018), BANYAN Σ (Gagné et al. 2018), Matplotlib (Hunter 2007), Pandas (McKinney 2013), SpeXtool (Cushing et al. 2004), SpeX Prism Library Analysis Toolkit (SPLAT; Burgasser & Splat Development Team 2017), Tool for OPERations on Catalogues and Tables (TOPCAT; Taylor 2005).

Facilities: IRTF (SpeX)

REFERENCES

- Aberasturi, M., Burgasser, A. J., Mora, A., et al. 2014, *AJ*, 148, 129, 129
- Ackerman, A. S., & Marley, M. S. 2001, *ApJ*, 556, 872, 872
- Adelman-McCarthy, J. K., & et al. 2009, *VizieR Online Data Catalog*, 2294
- Aganze, C., Burgasser, A. J., Faherty, J. K., et al. 2016, *AJ*, 151, 46, 46
- Ahn, C. P., Alexandroff, R., Allende Prieto, C., et al. 2012, *ApJS*, 203, 21, 21
- Alam, S., Albareti, F. D., Allende Prieto, C., et al. 2015, *ApJS*, 219, 12, 12
- Allen, P. R. 2007, *ApJ*, 668, 492, 492
- Allen, P. R., Koerner, D. W., McElwain, M. W., Cruz, K. L., & Reid, I. N. 2007, *AJ*, 133, 971, 971
- Allen, P. R., Koerner, D. W., Reid, I. N., & Trilling, D. E. 2005, *ApJ*, 625, 385, 385
- Allers, K. N., & Liu, M. C. 2013, *ApJ*, 772, 79, 79
- Allers, K. N., Liu, M. C., Dupuy, T. J., & Cushing, M. C. 2010, *ApJ*, 715, 561, 561
- Allers, K. N., Jaffe, D. T., Luhman, K. L., et al. 2007, *ApJ*, 657, 511, 511
- Alonso-Floriano, F. J., Morales, J. C., Caballero, J. A., et al. 2015, *A&A*, 577, A128, A128
- Astropy Collaboration, Robitaille, T. P., Tollerud, E. J., et al. 2013, *A&A*, 558, A33, A33

- Bailer-Jones, C. A. L., Rybizki, J., Fouesneau, M., Mantelet, G., & Andrae, R. 2018, ArXiv e-prints, arXiv:1804.10121
- Bardalez Gagliuffi, D. C., Gelino, C. R., & Burgasser, A. J. 2015, *AJ*, 150, 163, 163
- Bardalez Gagliuffi, D. C., Burgasser, A. J., Gelino, C. R., et al. 2014, *ApJ*, 794, 143, 143
- Barrado Y Navascués, D. 2006, *A&A*, 459, 511, 511
- Bartlett, J. L., Lurie, J. C., Riedel, A., et al. 2017, *AJ*, 154, 151, 151
- Basri, G., Mohanty, S., Allard, F., et al. 2000, *ApJ*, 538, 363, 363
- Bate, M. R. 2012, *MNRAS*, 419, 3115, 3115
- . 2019, *MNRAS*, 484, 2341, 2341
- Beamín, J. C., Minniti, D., Gromadzki, M., et al. 2013, *A&A*, 557, L8, L8
- Berger, E. 2006, *ApJ*, 648, 629, 629
- Bessell, M. S. 1991, *AJ*, 101, 662, 662
- Best, W. M. J., Liu, M. C., Magnier, E. A., et al. 2015, *ApJ*, 814, 118, 118
- Best, W. M. J., Magnier, E. A., Liu, M. C., et al. 2018, *ApJS*, 234, 1, 1
- Bihain, G., & Scholz, R.-D. 2016, *A&A*, 589, A26, A26
- Biller, B. A., Kasper, M., Close, L. M., Brandner, W., & Kellner, S. 2006, *ApJL*, 641, L141, L141
- Blake, C. H., Charbonneau, D., & White, R. J. 2010, *ApJ*, 723, 684, 684
- Blake, C. H., Charbonneau, D., White, R. J., et al. 2008, *ApJL*, 678, L125, L125
- Bochanski, J. J., Hawley, S. L., Covey, K. R., et al. 2010, *AJ*, 139, 2679, 2679
- Bochanski, J. J., Hawley, S. L., & West, A. A. 2011, *AJ*, 141, 98, 98
- Bouy, H., Brandner, W., Martín, E. L., et al. 2003, *AJ*, 126, 1526, 1526
- Bowler, B. P., Liu, M. C., & Cushing, M. C. 2009, *ApJ*, 706, 1114, 1114
- Bowler, B. P., Liu, M. C., & Dupuy, T. J. 2010, *ApJ*, 710, 45, 45
- Boyd, M. R., Henry, T. J., Jao, W.-C., Subasavage, J. P., & Hambly, N. C. 2011, *AJ*, 142, 92, 92
- Burgasser, A. J. 2002, PhD thesis,
- . 2004, *ApJS*, 155, 191, 191
- . 2007a, *ApJ*, 659, 655, 655
- . 2007b, *AJ*, 134, 1330, 1330
- Burgasser, A. J. 2014, in *Astronomical Society of India Conference Series*, Vol. 11, *Astronomical Society of India Conference Series*, 7–16
- Burgasser, A. J., Bardalez-Gagliuffi, D. C., & Gizis, J. E. 2011a, *AJ*, 141, 70, 70
- Burgasser, A. J., Blake, C. H., Gelino, C. R., Sahlmann, J., & Bardalez Gagliuffi, D. 2016, *ApJ*, 827, 25, 25
- Burgasser, A. J., Cruz, K. L., Cushing, M., et al. 2010, *ApJ*, 710, 1142, 1142
- Burgasser, A. J., Cruz, K. L., & Kirkpatrick, J. D. 2007a, *ApJ*, 657, 494, 494
- Burgasser, A. J., Kirkpatrick, J. D., Cruz, K. L., et al. 2006, *ApJS*, 166, 585, 585
- Burgasser, A. J., Kirkpatrick, J. D., & Lowrance, P. J. 2005, *AJ*, 129, 2849, 2849
- Burgasser, A. J., Liu, M. C., Ireland, M. J., Cruz, K. L., & Dupuy, T. J. 2008a, *ApJ*, 681, 579, 579
- Burgasser, A. J.,Looper, D. L., Kirkpatrick, J. D., Cruz, K. L., & Swift, B. J. 2008b, *ApJ*, 674, 451, 451
- Burgasser, A. J.,Looper, D. L., Kirkpatrick, J. D., & Liu, M. C. 2007b, *ApJ*, 658, 557, 557
- Burgasser, A. J., Luk, C., Dhital, S., et al. 2012, *ApJ*, 757, 110, 110
- Burgasser, A. J., & Mamajek, E. E. 2017, *ApJ*, 845, 110, 110
- Burgasser, A. J., Reid, I. N., Siegler, N., et al. 2007c, *Protostars and Planets V*, 427, 427
- Burgasser, A. J., Sitarski, B. N., Gelino, C. R., Logsdon, S. E., & Perrin, M. D. 2011b, *ApJ*, 739, 49, 49
- Burgasser, A. J., & Splat Development Team. 2017, in *Astronomical Society of India Conference Series*, Vol. 14, *Astronomical Society of India Conference Series*, 7–12
- Burgasser, A. J., Kirkpatrick, J. D., Burrows, A., et al. 2003, *ApJ*, 592, 1186, 1186

- Burgasser, A. J., Logsdon, S. E., Gagné, J., et al. 2015a, *ApJS*, 220, 18, 18
- Burgasser, A. J., Gillon, M., Melis, C., et al. 2015b, *AJ*, 149, 104, 104
- Burningham, B., Pinfield, D. J., Lucas, P. W., et al. 2010, *MNRAS*, 406, 1885, 1885
- Burrows, A., Hubbard, W. B., Lunine, J. I., & Liebert, J. 2001, *Reviews of Modern Physics*, 73, 719, 719
- Caballero, J. A., Cortés-Contreras, M., Alonso-Floriano, F. J., et al. 2016, in *19th Cambridge Workshop on Cool Stars, Stellar Systems, and the Sun (CS19)*, 148
- Casewell, S. L., Jameson, R. F., & Burleigh, M. R. 2008, *MNRAS*, 390, 1517, 1517
- Castro, P. J., Gizis, J. E., Harris, H. C., et al. 2013, *ApJ*, 776, 126, 126
- Chabrier, G. 2005, in *Astrophysics and Space Science Library*, Vol. 327, *The Initial Mass Function 50 Years Later*, ed. E. Corbelli, F. Palla, & H. Zinnecker, 41
- Chiu, K., Fan, X., Leggett, S. K., et al. 2006, *AJ*, 131, 2722, 2722
- Clarke, F. J., Tinney, C. G., & Hodgkin, S. T. 2003, *MNRAS*, 341, 239, 239
- Clarke, J. R. A., Pinfield, D. J., Gálvez-Ortiz, M. C., et al. 2010, *MNRAS*, 402, 575, 575
- Close, L. M., Siegler, N., Freed, M., & Biller, B. 2003, *ApJ*, 587, 407, 407
- Costa, E., Méndez, R. A., Jao, W.-C., et al. 2005, *AJ*, 130, 337, 337
- Crifo, F., Phan-Bao, N., Delfosse, X., et al. 2005, *A&A*, 441, 653, 653
- Cruz, K., & Gagné, J. 2014, *The Ultracool RIZZO Spectral Library*
- Cruz, K. L., Burgasser, A. J., Reid, I. N., & Liebert, J. 2004, *ApJL*, 604, L61, L61
- Cruz, K. L., Kirkpatrick, J. D., & Burgasser, A. J. 2009, *AJ*, 137, 3345, 3345
- Cruz, K. L., Núñez, A., Burgasser, A. J., et al. 2018, *AJ*, 155, 34, 34
- Cruz, K. L., Reid, I. N., Liebert, J., Kirkpatrick, J. D., & Lowrance, P. J. 2003, *AJ*, 126, 2421, 2421
- Cruz, K. L., Reid, I. N., Kirkpatrick, J. D., et al. 2007, *AJ*, 133, 439, 439
- Cushing, M. C., Vacca, W. D., & Rayner, J. T. 2004, *PASP*, 116, 362, 362
- Cushing, M. C., Kirkpatrick, J. D., Gelino, C. R., et al. 2011, *ApJ*, 743, 50, 50
- Cutri, R. M., Skrutskie, M. F., van Dyk, S., et al. 2003, *VizieR Online Data Catalog*, 2246, 0, 0
- Dahn, C. C., Harris, H. C., Vrba, F. J., et al. 2002, *AJ*, 124, 1170, 1170
- Dahn, C. C., Harris, H. C., Subasavage, J. P., et al. 2017, *AJ*, 154, 147, 147
- Davison, C. L., White, R. J., Henry, T. J., et al. 2015, *AJ*, 149, 106, 106
- Day-Jones, A. C., Marocco, F., Pinfield, D. J., et al. 2013, *MNRAS*, 648, 648
- Deacon, N. R., Hambly, N. C., & Cooke, J. A. 2005, *A&A*, 435, 363, 363
- Deacon, N. R., Hambly, N. C., King, R. R., & McCaughrean, M. J. 2009, *MNRAS*, 394, 857, 857
- Deacon, N. R., Liu, M. C., Magnier, E. A., et al. 2014, *ApJ*, 792, 119, 119
- Delfosse, X., Tinney, C. G., Forveille, T., et al. 1997, *A&A*, 327, L25, L25
- Delorme, P., Willott, C. J., Forveille, T., et al. 2008, *A&A*, 484, 469, 469
- Delrez, L., Gillon, M., Queloz, D., et al. 2018, in *Society of Photo-Optical Instrumentation Engineers (SPIE) Conference Series*, Vol. 10700, *Society of Photo-Optical Instrumentation Engineers (SPIE) Conference Series*, 107001I
- Deshpande, R., Martín, E. L., Montgomery, M. M., et al. 2012, *AJ*, 144, 99, 99
- Dhital, S., West, A. A., Stassun, K. G., Schluns, K. J., & Massey, A. P. 2015, *AJ*, 150, 57, 57
- Dieterich, S. B., Henry, T. J., Jao, W.-C., et al. 2014, *AJ*, 147, 94, 94
- Dittmann, J. A., Irwin, J. M., Charbonneau, D., & Berta-Thompson, Z. K. 2014, *ApJ*, 784, 156, 156
- Dittmann, J. A., Irwin, J. M., Charbonneau, D., & Newton, E. R. 2016, *ApJ*, 818, 153, 153

- Dupuy, T. J., Forbrich, J., Rizzuto, A., et al. 2016, *ApJ*, 827, 23, 23
- Dupuy, T. J., & Liu, M. C. 2012, *ApJS*, 201, 19, 19
- Dupuy, T. J., Liu, M. C., & Bowler, B. P. 2009, *ApJ*, 706, 328, 328
- Dupuy, T. J., Liu, M. C., Bowler, B. P., et al. 2010, *ApJ*, 721, 1725, 1725
- Epchtein, N. 1994, *Experimental Astronomy*, 3, 73, 73
- Faherty, J. K., Burgasser, A. J., Cruz, K. L., et al. 2009, *AJ*, 137, 1, 1
- Faherty, J. K., Cruz, K. L., Rice, E. L., & Riedel, A. 2013a, *Mem. Soc. Astron. Italiana*, 84, 955, 955
- Faherty, J. K., Gagné, J., Burgasser, A. J., et al. 2018, *ApJ*, 868, 44, 44
- Faherty, J. K., Rice, E. L., Cruz, K. L., Mamajek, E. E., & Núñez, A. 2013b, *AJ*, 145, 2, 2
- Faherty, J. K., Burgasser, A. J., Walter, F. M., et al. 2012, *ApJ*, 752, 56, 56
- Faherty, J. K., Riedel, A. R., Cruz, K. L., et al. 2016, *ApJS*, 225, 10, 10
- Fan, X., Knapp, G. R., Strauss, M. A., et al. 2000, *AJ*, 119, 928, 928
- Filippazzo, J. C., Rice, E. L., Faherty, J., et al. 2015, *ApJ*, 810, 158, 158
- Folkes, S. L., Pinfield, D. J., Jones, H. R. A., et al. 2012, *MNRAS*, 427, 3280, 3280
- Forveille, T., Ségransan, D., Delorme, P., et al. 2004, *A&A*, 427, L1, L1
- Forveille, T., Beuzit, J.-L., Delorme, P., et al. 2005, *A&A*, 435, L5, L5
- Freed, M., Close, L. M., & Siegler, N. 2003, in *IAU Symposium*, Vol. 211, *Brown Dwarfs*, ed. E. Martín, 261
- Gagné, J., Burgasser, A. J., Faherty, J. K., et al. 2015a, *The Astrophysical Journal Letters*, 808, L20, L20
- Gagné, J., Lafrenière, D., Doyon, R., Malo, L., & Artigau, É. 2014, *ApJ*, 783, 121, 121
- Gagné, J., Lafrenière, D., Doyon, R., Malo, L., & Artigau, É. 2015b, *The Astrophysical Journal*, 798, 73, 73
- Gagné, J., Faherty, J. K., Cruz, K. L., et al. 2015c, *The Astrophysical Journal Supplement Series*, 219, 33, 33
- Gagné, J., Faherty, J. K., Mamajek, E. E., et al. 2017, *ApJS*, 228, 18, 18
- Gagné, J., Mamajek, E. E., Malo, L., et al. 2018, *ApJ*, 856, 23, 23
- Gaia Collaboration. 2018, *VizieR Online Data Catalog*, 1345
- Gaia Collaboration, Prusti, T., de Bruijne, J. H. J., et al. 2016, *A&A*, 595, A1, A1
- Gaia Collaboration, Brown, A. G. A., Vallenari, A., et al. 2018, *A&A*, 616, A1, A1
- Gaidos, E., Mann, A. W., Lépine, S., et al. 2014, *MNRAS*, 443, 2561, 2561
- Gálvez-Ortiz, M. C., Solano, E., Lodieu, N., & Aberasturi, M. 2017, *MNRAS*, 466, 2983, 2983
- Gálvez-Ortiz, M. C., Clarke, J. R. A., Pinfield, D. J., et al. 2010, *MNRAS*, 409, 552, 552
- Gauza, B., Béjar, V. J. S., Pérez-Garrido, A., et al. 2015, *ApJ*, 804, 96, 96
- Geballe, T. R., Knapp, G. R., Leggett, S. K., et al. 2002, *ApJ*, 564, 466, 466
- Geißler, K., Metchev, S., Kirkpatrick, J. D., Berriman, G. B., & Looper, D. 2011, *ApJ*, 732, 56, 56
- Gillon, M., Jehin, E., Lederer, S. M., et al. 2016, *Nature*, 533, 221, 221
- Gillon, M., Triaud, A. H. M. J., Demory, B.-O., et al. 2017, *Nature*, 542, 456, 456
- Gilmore, G., & Reid, N. 1983, *MNRAS*, 202, 1025, 1025
- Ginsburg, A., Sipocz, B., Parikh, M., et al. 2018, *astropy/astroquery: v0.3.7 release*
- Gizis, J. E. 2002, *ApJ*, 575, 484, 484
- Gizis, J. E., Kirkpatrick, J. D., & Wilson, J. C. 2001, *AJ*, 121, 2185, 2185
- Gizis, J. E., Monet, D. G., Reid, I. N., et al. 2000, *AJ*, 120, 1085, 1085
- Gizis, J. E., Reid, I. N., & Hawley, S. L. 2002, *AJ*, 123, 3356, 3356
- Gizis, J. E., Reid, I. N., Knapp, G. R., et al. 2003, *AJ*, 125, 3302, 3302
- Gizis, J. E., Troup, N. W., & Burgasser, A. J. 2011, *ApJL*, 736, L34, L34
- Gomes, J. I., Pinfield, D. J., Marocco, F., et al. 2013, *MNRAS*, 431, 2745, 2745

- Goodwin, S. P., Whitworth, A. P., & Ward-Thompson, D. 2004, *A&A*, 423, 169, 169
- Goto, M., Kobayashi, N., Terada, H., et al. 2002, *ApJL*, 567, L59, L59
- Gray, R. O., Corbally, C. J., Garrison, R. F., et al. 2006, *AJ*, 132, 161, 161
- Günther, H. M., Cody, A. M., Covey, K. R., et al. 2014, *AJ*, 148, 122, 122
- Hambaryan, V., Staude, A., Schwobe, A. D., et al. 2004, *A&A*, 415, 265, 265
- Han, C., Jung, Y. K., Udalski, A., et al. 2013, *ApJ*, 778, 38, 38
- Haro, G., & Chavira, E. 1966, *Vistas in Astronomy*, 8, 89, 89
- Hartwick, F. D. A., Cowley, A. P., & Mould, J. R. 1984, *ApJ*, 286, 269, 269
- Hawley, S. L., Gizis, J. E., & Reid, I. N. 1996, *AJ*, 112, 2799, 2799
- Hawley, S. L., Covey, K. R., Knapp, G. R., et al. 2002, *AJ*, 123, 3409, 3409
- Hayashi, C., & Nakano, T. 1963, *Progress of Theoretical Physics*, 30, 460, 460
- Henry, T. J., & Kirkpatrick, J. D. 1990, *ApJL*, 354, L29, L29
- Henry, T. J., Subasavage, J. P., Brown, M. A., et al. 2004, *AJ*, 128, 2460, 2460
- Herbig, G. H. 1956, *PASP*, 68, 531, 531
- Hiranaka, K., Cruz, K. L., Douglas, S. T., Marley, M. S., & Baldassare, V. F. 2016, *ApJ*, 830, 96, 96
- Hunter, J. D. 2007, *Computing In Science & Engineering*, 9, 90, 90
- Ireland, M. J., Kraus, A., Martinache, F., Lloyd, J. P., & Tuthill, P. G. 2008, *ApJ*, 678, 463, 463
- Irwin, M., McMahon, R. G., & Reid, N. 1991, *MNRAS*, 252, 61P, 61P
- Jahreiß, H., Scholz, R., Meusinger, H., & Lehmann, I. 2001, *A&A*, 370, 967, 967
- Jameson, R. F., Casewell, S. L., Bannister, N. P., et al. 2008, *MNRAS*, 384, 1399, 1399
- Jeans, J. H. 1902, *Philosophical Transactions of the Royal Society of London Series A*, 199, 1, 1
- Jenkins, J. S., Ramsey, L. W., Jones, H. R. A., et al. 2009, *ApJ*, 704, 975, 975
- Kane, S. R., Henry, G. W., Dragomir, D., et al. 2011, *ApJL*, 735, L41, L41
- Kao, M. M., Hallinan, G., Pineda, J. S., Stevenson, D., & Burgasser, A. 2018, *ApJS*, 237, 25, 25
- Kasper, M., Biller, B. A., Burrows, A., et al. 2007, *A&A*, 471, 655, 655
- Kellogg, K., Metchev, S., Miles-Páez, P. A., & Tannock, M. E. 2017, *AJ*, 154, 112, 112
- Kendall, T. R., Delfosse, X., Martín, E. L., & Forveille, T. 2004, *A&A*, 416, L17, L17
- Kendall, T. R., Jones, H. R. A., Pinfield, D. J., et al. 2007, *MNRAS*, 374, 445, 445
- Kendall, T. R., Maun, N., Azzopardi, M., & Gigoyan, K. 2003, *A&A*, 403, 929, 929
- Kent, S. M., Dame, T. M., & Fazio, G. 1991, *ApJ*, 378, 131, 131
- Khandrika, H., Burgasser, A. J., Melis, C., et al. 2013, *AJ*, 145, 71, 71
- Kirkpatrick, J. D., Dahn, C. C., Monet, D. G., et al. 2001a, *AJ*, 121, 3235, 3235
- Kirkpatrick, J. D., Henry, T. J., & Irwin, M. J. 1997, *AJ*, 113, 1421, 1421
- Kirkpatrick, J. D., Henry, T. J., & Liebert, J. 1993, *ApJ*, 406, 701, 701
- Kirkpatrick, J. D., Henry, T. J., & McCarthy, Jr., D. W. 1991, *ApJS*, 77, 417, 417
- Kirkpatrick, J. D., Henry, T. J., & Simons, D. A. 1995, *AJ*, 109, 797, 797
- Kirkpatrick, J. D., Liebert, J., Cruz, K. L., Gizis, J. E., & Reid, I. N. 2001b, *PASP*, 113, 814, 814
- Kirkpatrick, J. D., McGraw, J. T., Hess, T. R., Liebert, J., & McCarthy, Jr., D. W. 1994, *ApJS*, 94, 749, 749
- Kirkpatrick, J. D., Reid, I. N., Liebert, J., et al. 1999, *ApJ*, 519, 802, 802
- . 2000, *AJ*, 120, 447, 447
- Kirkpatrick, J. D., Cruz, K. L., Barman, T. S., et al. 2008, *ApJ*, 689, 1295, 1295
- Kirkpatrick, J. D., Looper, D. L., Burgasser, A. J., et al. 2010, *ApJS*, 190, 100, 100
- Kirkpatrick, J. D., Cushing, M. C., Gelino, C. R., et al. 2011, *ApJS*, 197, 19, 19

- Kirkpatrick, J. D., Gelino, C. R., Cushing, M. C., et al. 2012, *ApJ*, 753, 156, 156
- Kirkpatrick, J. D., Schneider, A., Fajardo-Acosta, S., et al. 2014, *ApJ*, 783, 122, 122
- Kirkpatrick, J. D., Kellogg, K., Schneider, A. C., et al. 2016, *ApJS*, 224, 36, 36
- Kirkpatrick, J. D., Martin, E. C., Smart, R. L., et al. 2019, *ApJS*, 240, 19, 19
- Knapp, G. R., Leggett, S. K., Fan, X., et al. 2004, *AJ*, 127, 3553, 3553
- Koen, C. 2013, *MNRAS*, 428, 2824, 2824
- Koen, C., Kilkenny, D., van Wyk, F., & Marang, F. 2010, *MNRAS*, 403, 1949, 1949
- Koerner, D. W., Kirkpatrick, J. D., McElwain, M. W., & Bonaventura, N. R. 1999, *ApJL*, 526, L25, L25
- Konopacky, Q. M., Ghez, A. M., Barman, T. S., et al. 2010, *ApJ*, 711, 1087, 1087
- Kumar, S. S. 1963, *ApJ*, 137, 1121, 1121
- Latham, D. W., Mazeh, T., Stefanik, R. P., Mayor, M., & Burki, G. 1989, *Nature*, 339, 38, 38
- Laughlin, G., Bodenheimer, P., & Adams, F. C. 1997, *ApJ*, 482, 420, 420
- Law, N. M., Hodgkin, S. T., & Mackay, C. D. 2006, *MNRAS*, 368, 1917, 1917
- Lawrence, A., Warren, S. J., Almaini, O., et al. 2007, *MNRAS*, 379, 1599, 1599
- Leggett, S. K., Allard, F., Geballe, T. R., Hauschildt, P. H., & Schweitzer, A. 2001, *ApJ*, 548, 908, 908
- Leggett, S. K., Hauschildt, P. H., Allard, F., Geballe, T. R., & Baron, E. 2002, *MNRAS*, 332, 78, 78
- Leinert, C., Allard, F., Richichi, A., & Hauschildt, P. H. 2000, *A&A*, 353, 691, 691
- Leinert, C., Weitzel, N., Richichi, A., Eckart, A., & Tacconi-Garman, L. E. 1994, *A&A*, 291, L47, L47
- Lépine, S., & Gaidos, E. 2011, *AJ*, 142, 138, 138
- Lépine, S., Hilton, E. J., Mann, A. W., et al. 2013, *AJ*, 145, 102, 102
- Lépine, S., Rich, R. M., Neill, J. D., Caulet, A., & Shara, M. M. 2002a, *ApJL*, 581, L47, L47
- Lépine, S., Rich, R. M., & Shara, M. M. 2003, *AJ*, 125, 1598, 1598
- Lépine, S., & Shara, M. M. 2005, *AJ*, 129, 1483, 1483
- Lépine, S., Shara, M. M., & Rich, R. M. 2002b, *AJ*, 124, 1190, 1190
- Lépine, S., Thorstensen, J. R., Shara, M. M., & Rich, R. M. 2009, *AJ*, 137, 4109, 4109
- Liebert, J. 1976, *PASP*, 88, 232, 232
- Liebert, J., & Ferguson, D. H. 1982, *MNRAS*, 199, 29P, 29P
- Liebert, J., Kirkpatrick, J. D., Cruz, K. L., et al. 2003, *AJ*, 125, 343, 343
- Lindgren, L., Lammers, U., Bastian, U., et al. 2016, *A&A*, 595, A4, A4
- Liu, M. C., Dupuy, T. J., & Allers, K. N. 2016, *ApJ*, 833, 96, 96
- Liu, M. C., Fischer, D. A., Graham, J. R., et al. 2002, *ApJ*, 571, 519, 519
- Liu, M. C., & Leggett, S. K. 2005, *ApJ*, 634, 616, 616
- Lodders, K., & Fegley, Jr., B. 2006, *Chemistry of Low Mass Substellar Objects*, ed. J. W. Mason, 1
- Lodieu, N., Espinoza Contreras, M., Zapatero Osorio, M. R., et al. 2017, *A&A*, 598, A92, A92
- Lodieu, N., Scholz, R.-D., McCaughrean, M. J., et al. 2005, *A&A*, 440, 1061, 1061
- Looper, D. L. 2011, PhD thesis,
- Looper, D. L., Kirkpatrick, J. D., Cutri, R. M., et al. 2008, *ApJ*, 686, 528, 528
- Luhman, K. L. 2000, *ApJ*, 544, 1044, 1044
- . 2013, *ApJL*, 767, L1, L1
- . 2014, *ApJL*, 786, L18, L18
- Luhman, K. L., Rieke, G. H., Young, E. T., et al. 2000, *ApJ*, 540, 1016, 1016
- Luhman, K. L., & Sheppard, S. S. 2014, *ApJ*, 787, 126, 126
- Luhman, K. L., Loutrel, N. P., McCurdy, N. S., et al. 2012, *ApJ*, 760, 152, 152
- Lutz, T. E., & Kelker, D. H. 1973, *PASP*, 85, 573, 573
- Mace, G. N., Kirkpatrick, J. D., Cushing, M. C., et al. 2013, *ApJS*, 205, 6, 6
- Mainzer, A., Grav, T., Bauer, J., et al. 2011, *ApJ*, 743, 156, 156

- Malkov, O. Y., Tamazian, V. S., Docobo, J. A., & Chulkov, D. A. 2012, *A&A*, 546, A69, A69
- Malmquist, K. G. 1922, *Meddelanden fran Lunds Astronomiska Observatorium Serie I*, 100, 1, 1
- Marocco, F., Andrei, A. H., Smart, R. L., et al. 2013, *AJ*, 146, 161, 161
- Marocco, F., Jones, H. R. A., Day-Jones, A. C., et al. 2015, *MNRAS*, 449, 3651, 3651
- Martin, E. L., Brandner, W., & Basri, G. 1999, *Science*, 283, 1718, 1718
- Martín, E. L., Delfosse, X., Basri, G., et al. 1999, *AJ*, 118, 2466, 2466
- Martín, E. L., Koresko, C. D., Kulkarni, S. R., Lane, B. F., & Wizinowich, P. L. 2000, *ApJL*, 529, L37, L37
- Martín, E. L., Phan-Bao, N., Bessell, M., et al. 2010, *A&A*, 517, A53, A53
- Mason, B. D., Wycoff, G. L., Hartkopf, W. I., Douglass, G. G., & Worley, C. E. 2001, *AJ*, 122, 3466, 3466
- McCarthy, M. F., Bertiau, F. C., & Treanor, P. J. 1964, *Ricerche Astronomiche*, 6
- McCaughrean, M. J., Scholz, R.-D., & Lodieu, N. 2002, *A&A*, 390, L27, L27
- McElwain, M. W., & Burgasser, A. J. 2006, *AJ*, 132, 2074, 2074
- McKinney, W. 2013, *Python for Data Analysis: Data Wrangling with Pandas, NumPy, and IPython*, 1st edn.
- Metchev, S. A., & Hillenbrand, L. A. 2006, *ApJ*, 651, 1166, 1166
- Metchev, S. A., Kirkpatrick, J. D., Berriman, G. B., &Looper, D. 2008, *ApJ*, 676, 1281, 1281
- Metodieva, Y., Antonova, A., Golev, V., et al. 2015, *MNRAS*, 446, 3878, 3878
- Monet, D. G., Levine, S. E., Canzian, B., et al. 2003, *AJ*, 125, 984, 984
- Montagnier, G., Ségransan, D., Beuzit, J.-L., et al. 2006, *A&A*, 460, L19, L19
- Morin, J., Donati, J.-F., Petit, P., et al. 2010, *MNRAS*, 407, 2269, 2269
- Mužić, K., Schödel, R., Scholz, A., et al. 2017, *MNRAS*, 471, 3699, 3699
- Newton, E. R., Charbonneau, D., Irwin, J., et al. 2014, *AJ*, 147, 20, 20
- Newton, E. R., Charbonneau, D., Irwin, J., & Mann, A. W. 2015, *ApJ*, 800, 85, 85
- Ochsenbein, F., Bauer, P., & Marcout, J. 2000, *A&AS*, 143, 23, 23
- Padoan, P., & Nordlund, Å. 2002, *ApJ*, 576, 870, 870
- Patience, J., White, R. J., Ghez, A. M., et al. 2002, *ApJ*, 581, 654, 654
- Pecaut, M. J., & Mamajek, E. E. 2013, *ApJS*, 208, 9, 9
- Pérez Garrido, A., Lodieu, N., Béjar, V. J. S., et al. 2014, *A&A*, 567, A6, A6
- Phan-Bao, N. 2011, *Astronomische Nachrichten*, 332, 668, 668
- Phan-Bao, N., & Bessell, M. S. 2006, *A&A*, 446, 515, 515
- Phan-Bao, N., Crifo, F., Delfosse, X., et al. 2003, *A&A*, 401, 959, 959
- Phan-Bao, N., Bessell, M. S., Martín, E. L., et al. 2006, *MNRAS*, 366, L40, L40
- . 2008, *MNRAS*, 383, 831, 831
- Pokorny, R. S., Jones, H. R. A., & Hambly, N. C. 2003, *A&A*, 397, 575, 575
- Pokorny, R. S., Jones, H. R. A., Hambly, N. C., & Pinfield, D. J. 2004, *A&A*, 421, 763, 763
- Pravdo, S. H., Shaklan, S. B., & Lloyd, J. 2005, *ApJ*, 630, 528, 528
- Radigan, J., Jayawardhana, R., Lafrenière, D., et al. 2012, *ApJ*, 750, 105, 105
- Radigan, J., Lafrenière, D., Jayawardhana, R., & Doyon, R. 2008, *ApJ*, 689, 471, 471
- Rajpurohit, A. S., Reylé, C., Allard, F., et al. 2013, *A&A*, 556, A15, A15
- Rajpurohit, A. S., Reylé, C., Schultheis, M., et al. 2012, *A&A*, 545, A85, A85
- Rayner, J. T., Toomey, D. W., Onaka, P. M., et al. 2003, *PASP*, 115, 362, 362
- Rebolo, R., Zapatero Osorio, M. R., Madrugá, S., et al. 1998, *Science*, 282, 1309, 1309
- Reid, I. N., Burgasser, A. J., Cruz, K. L., Kirkpatrick, J. D., & Gizis, J. E. 2001, *AJ*, 121, 1710, 1710

- Reid, I. N., Cruz, K. L., & Allen, P. R. 2007, *AJ*, 133, 2825, 2825
- Reid, I. N., Cruz, K. L., Kirkpatrick, J. D., et al. 2008, *AJ*, 136, 1290, 1290
- Reid, I. N., & Gizis, J. E. 2005, *PASP*, 117, 676, 676
- Reid, I. N., Hawley, S. L., & Gizis, J. E. 1995, *AJ*, 110, 1838, 1838
- Reid, I. N., Kirkpatrick, J. D., Gizis, J. E., et al. 2000, *AJ*, 119, 369, 369
- Reid, I. N., Lewitus, E., Allen, P. R., Cruz, K. L., & Burgasser, A. J. 2006, *AJ*, 132, 891, 891
- Reid, I. N., Cruz, K. L., Laurie, S. P., et al. 2003a, *AJ*, 125, 354, 354
- Reid, I. N., Cruz, K. L., Allen, P., et al. 2003b, *AJ*, 126, 3007, 3007
- . 2004, *AJ*, 128, 463, 463
- Reiners, A., & Basri, G. 2009, *ApJ*, 705, 1416, 1416
- Reipurth, B., & Clarke, C. 2001, *AJ*, 122, 432, 432
- Reipurth, B., & Zinnecker, H. 1993, *A&A*, 278, 81, 81
- Reylé, C. 2018, *ArXiv e-prints*, arXiv:1809.08244
- Reylé, C., Scholz, R.-D., Schultheis, M., Robin, A. C., & Irwin, M. 2006, *MNRAS*, 373, 705, 705
- Reylé, C., Delorme, P., Willott, C. J., et al. 2010, *A&A*, 522, A112, A112
- Riaz, B., Gizis, J. E., & Harvin, J. 2006, *AJ*, 132, 866, 866
- Ricci, L., Testi, L., Natta, A., et al. 2014, *ApJ*, 791, 20, 20
- Riedel, A. R., Finch, C. T., Henry, T. J., et al. 2014, *AJ*, 147, 85, 85
- Sahlmann, J., Lazorenko, P. F., Ségransan, D., et al. 2015, *A&A*, 577, A15, A15
- Salim, S., & Gould, A. 2003, *ApJ*, 582, 1011, 1011
- Salim, S., Lépine, S., Rich, R. M., & Shara, M. M. 2003, *ApJL*, 586, L149, L149
- Saumon, D., Bergeron, P., Lunine, J. I., Hubbard, W. B., & Burrows, A. 1994, *ApJ*, 424, 333, 333
- Schmidt, M. 1968, *ApJ*, 151, 393, 393
- Schmidt, S. J., Cruz, K. L., Bongiorno, B. J., Liebert, J., & Reid, I. N. 2007, *AJ*, 133, 2258, 2258
- Schmidt, S. J., Hawley, S. L., West, A. A., et al. 2015, *AJ*, 149, 158, 158
- Schmidt, S. J., West, A. A., Bochanski, J. J., Hawley, S. L., & Kielty, C. 2014, *PASP*, 126, 642, 642
- Schmidt, S. J., West, A. A., Hawley, S. L., & Pineda, J. S. 2010, *AJ*, 139, 1808, 1808
- Schneider, A., Melis, C., Song, I., & Zuckerman, B. 2011, *ApJ*, 743, 109, 109
- Schneider, A. C., Cushing, M. C., Kirkpatrick, J. D., et al. 2014, *AJ*, 147, 34, 34
- Schneider, A. C., Greco, J., Cushing, M. C., et al. 2016, *ApJ*, 817, 112, 112
- Scholz, R.-D. 2014, *A&A*, 561, A113, A113
- Scholz, R.-D., Lodieu, N., Ibata, R., et al. 2004a, *MNRAS*, 347, 685, 685
- Scholz, R.-D., Lodieu, N., & McCaughrean, M. J. 2004b, *A&A*, 428, L25, L25
- Scholz, R.-D., & Meusinger, H. 2002, *MNRAS*, 336, L49, L49
- Scholz, R.-D., Meusinger, H., & Jahreiß, H. 2005, *A&A*, 442, 211, 211
- Seifahrt, A., Mugrauer, M., Wiese, M., Neuhäuser, R., & Guenther, E. W. 2005, *Astronomische Nachrichten*, 326, 974, 974
- Seifahrt, A., Reiners, A., Almaghrbi, K. A. M., & Basri, G. 2010, *A&A*, 512, A37, A37
- Sheppard, S. S., & Cushing, M. 2009a, in *Bulletin of the American Astronomical Society*, Vol. 41, American Astronomical Society Meeting Abstracts #213, 291
- Sheppard, S. S., & Cushing, M. C. 2009b, *AJ*, 137, 304, 304
- Shkolnik, E., Liu, M. C., & Reid, I. N. 2009, *ApJ*, 699, 649, 649
- Siegler, N., Close, L. M., Burgasser, A. J., et al. 2007, *AJ*, 133, 2320, 2320
- Siegler, N., Close, L. M., Cruz, K. L., Martín, E. L., & Reid, I. N. 2005, *ApJ*, 621, 1023, 1023

- Skrutskie, M. F., Cutri, R. M., Stiening, R., et al. 2006, *AJ*, 131, 1163, 1163
- Skrzypek, N., Warren, S. J., Faherty, J. K., et al. 2015, *A&A*, 574, A78, A78
- Smart, R. L., Marocco, F., Caballero, J. A., et al. 2017, *MNRAS*, 469, 401, 401
- Smith, L. C., Lucas, P. W., Contreras Peña, C., et al. 2015, *MNRAS*, 454, 4476, 4476
- Stamatellos, D., Hubber, D. A., & Whitworth, A. P. 2007, *MNRAS*, 382, L30, L30
- Stephenson, C. B. 1986, *AJ*, 92, 139, 139
- Stumpf, M. B., Brandner, W., Henning, T., et al. 2008, *ArXiv e-prints*, arXiv:0811.0556
- Taylor, M. B. 2005, in *Astronomical Society of the Pacific Conference Series*, Vol. 347, *Astronomical Data Analysis Software and Systems XIV*, ed. P. Shopbell, M. Britton, & R. Ebert, 29
- Teegarden, B. J., Pravdo, S. H., Hicks, M., et al. 2003, *ApJL*, 589, L51, L51
- Terrien, R. C., Mahadevan, S., Deshpande, R., & Bender, C. F. 2015, *ApJS*, 220, 16, 16
- Testi, L., Natta, A., Scholz, A., et al. 2016, *A&A*, 593, A111, A111
- Theissen, C. A. 2018, *ApJ*, 862, 173, 173
- Theissen, C. A., West, A. A., Shippee, G., Burgasser, A. J., & Schmidt, S. J. 2017, *AJ*, 153, 92, 92
- Thompson, M. A., Kirkpatrick, J. D., Mace, G. N., et al. 2013, *PASP*, 125, 809, 809
- Thorstensen, J. R., & Kirkpatrick, J. D. 2003, *PASP*, 115, 1207, 1207
- Tinney, C. G. 1993, *ApJ*, 414, 279, 279
- Tinney, C. G., Delfosse, X., Forveille, T., & Allard, F. 1998, *A&A*, 338, 1066, 1066
- Tinney, C. G., Mould, J. R., & Reid, I. N. 1993, *AJ*, 105, 1045, 1045
- Tokunaga, A. T., Simons, D. A., & Vacca, W. D. 2002, *PASP*, 114, 180, 180
- Trimble, V. 1986, *Quarterly Journal of the Royal Astronomical Society*, 27, 38, 38
- Tsuji, T., Ohnaka, K., Aoki, W., & Nakajima, T. 1996, *A&A*, 308, L29, L29
- Vacca, W. D., Cushing, M. C., & Rayner, J. T. 2003, *PASP*, 115, 389, 389
- van Biesbroeck, G. 1961, *AJ*, 66, 528, 528
- van Leeuwen, F. 2007, *A&A*, 474, 653, 653
- Weinberger, A. J., Boss, A. P., Keiser, S. A., et al. 2016, *AJ*, 152, 24, 24
- Wenger, M., Ochsenbein, F., Egret, D., et al. 2000, *A&AS*, 143, 9, 9
- West, A. A., Hawley, S. L., Bochanski, J. J., et al. 2008, *AJ*, 135, 785, 785
- West, A. A., Weisenburger, K. L., Irwin, J., et al. 2015, *ApJ*, 812, 3, 3
- West, A. A., Morgan, D. P., Bochanski, J. J., et al. 2011, *AJ*, 141, 97, 97
- Whitworth, A., Bate, M. R., Nordlund, Å., Reipurth, B., & Zinnecker, H. 2007, *Protostars and Planets V*, 459, 459
- Whitworth, A. P., & Zinnecker, H. 2004, *A&A*, 427, 299, 299
- Wilson, J. C., Miller, N. A., Gizis, J. E., et al. 2003, in *IAU Symposium*, Vol. 211, *Brown Dwarfs*, ed. E. Martín, 197
- Winters, J. G., Henry, T. J., Lurie, J. C., et al. 2015, *AJ*, 149, 5, 5
- Winters, J. G., Sevrinsky, R. A., Jao, W.-C., et al. 2017, *AJ*, 153, 14, 14
- Witte, S., Helling, C., Barman, T., Heidrich, N., & Hauschildt, P. H. 2011, *A&A*, 529, A44, A44
- Wright, E. L., Eisenhardt, P. R. M., Mainzer, A. K., et al. 2010, *AJ*, 140, 1868, 1868
- York, D. G., Adelman, J., Anderson, Jr., J. E., et al. 2000, *AJ*, 120, 1579, 1579
- Zacharias, N., Finch, C. T., Girard, T. M., et al. 2012, *VizieR Online Data Catalog*, 1322
- Zacharias, N., Urban, S. E., Zacharias, M. I., et al. 2003, *VizieR Online Data Catalog*, 1289
- Zapatero Osorio, M. R., Béjar, V. J. S., Martín, E. L., et al. 2000, *Science*, 290, 103, 103
- Zhang, Z. H., Homeier, D., Pinfield, D. J., et al. 2017, *MNRAS*, 468, 261, 261
- Zhang, Z. H., Pokorny, R. S., Jones, H. R. A., et al. 2009, *A&A*, 497, 619, 619

Table 1. Literature sources providing UCD targets to the final sample

Reference	Survey/Compilation	UCD Targets
Burgasser (2014)	SpeX Prism Library (SPL)	510
Best et al. (2015)	L/T Transition Dwarfs from Pan-STARRS1	5
Best et al. (2018)	MLT Dwarfs from Pan-STARRS1	1041
Boyd et al. (2011)	The Solar Neighborhood XXVIII	119
Caballero et al. (2016)	Carmencita, CARMENES Input Catalogue	63
Castro et al. (2013)	High Proper Motion L Dwarfs	29
Chiu et al. (2006)	SDSS L and T Dwarfs	71
Clarke et al. (2010)	Southern ultracool dwarfs in young moving groups	98
Crifo et al. (2005)	Spectroscopy of DENIS nearby candidates	19
Cruz et al. (2003)	Meeting the Cool Neighbors V	304
Deacon et al. (2009)	UKIDSS-2MASS Proper Motion Survey	233
Deacon et al. (2014)	Wide UCD Companions in Pan-STARRS I	98
Dhital et al. (2015)	SLoWPoKES-II	44
Dieterich et al. (2014)	The Solar Neighborhood XXXII	63
Dittmann et al. (2016)	MEarth Photometry Calibration	90
Folkes et al. (2012)	Ultra-cool dwarfs at low Galactic latitudes	90
Gagné et al. (2015c)	List of M6-M9.5 Dwarfs	1570
Gagné et al. (2015c)	List of All Ultracool Dwarfs	335
Gaidos et al. (2014)	CONCH-SHELL	23
Gálvez-Ortiz et al. (2017)	Wide VLM binary systems using Virtual Observatory tools	46
Hawley et al. (1996)	Palomar/MSU Nearby-Star Spectroscopic Survey II (PMSU)	12
Hawley et al. (2002)	M, L, and T Dwarfs in SDSS	25
Kirkpatrick et al. (2010)	2MASS Proper Motion Survey	193
Kirkpatrick et al. (2011)	First Hundred Brown Dwarfs Discovered by WISE	93
Kirkpatrick et al. (2016)	AllWISE Motion Survey	63
Knapp et al. (2004)	NIR Photometry and Spectroscopy of L and T Dwarfs	27
Lépine et al. (2013)	Brightest ($J < 9$) M Dwarfs in the Northern Sky	56
Lépine & Shara (2005)	LSPM North	4042
Lépine & Gaidos (2011)	Bright M Dwarfs	137
Luhman & Sheppard (2014)	WISE High Proper Motion Objects	41
Lodieu et al. (2005)	Red high proper motion objects in the Southern Sky	55
Lodieu et al. (2017)	Ultracool subdwarfs with Virtual Observatory tools	3
Luhman & Sheppard (2014)	High Proper Motion Objects from WISE	239
Mace et al. (2013)	WISE T Dwarfs	91
Marocco et al. (2015)	UKIDSS LAS LT Dwarfs	262
Newton et al. (2014)	Metallicities, Radial Velocities, and Spectral Types for MEarth M Dwarfs	72
Newton et al. (2015)	Cool Dwarf Fundamental Parameters for MEarth M Dwarfs	38
Phan-Bao et al. (2003)	DENIS late-M dwarfs	50
Reid et al. (1995)	Palomar/MSU Nearby-Star Spectroscopic Survey I (PMSU)	7
Reid et al. (2004)	NLTT Catalog	13
Reid & Gizis (2005)	LHS Catalog II	50

Table 1 continued on next page

Table 1 (*continued*)

Reference	Survey/Compilation	UCD Targets
Reid et al. (2008)	Meeting the Cool Neighbors X	227
Reylé et al. (2006)	Optical spectroscopy of high proper motion stars	8
Riaz et al. (2006)	New M Dwarfs in Solar Neighborhood	1080
Riedel et al. (2014)	The Solar Neighborhood XXXIII	4
Schmidt et al. (2010)	SDSS L Dwarfs	484
Schmidt et al. (2015)	BOSS Ultracool Dwarfs	225
Schneider et al. (2016)	NEOWISER Proper Motion Survey	17
Shkolnik et al. (2009)	Young LMS within 25 pc	11
Skrzypek et al. (2015)	Photometric brown-dwarf classification	50
Smart et al. (2017)	The Gaia ultracool dwarf sample	153
Theissen et al. (2017)	LaTE-MoVeRS	1796
Thompson et al. (2013)	WISE MLT Dwarfs	41
Weinberger et al. (2016)	Carnegie Astrometric Planet Search Program	78
West et al. (2008)	SDSS DR5 Low-Mass Star Spectroscopic Sample	922
West et al. (2011)	SDSS DR7 Spectroscopic M Dwarf Catalog	34
West et al. (2015)	Kinematic Analysis of Nearby Mid-to-Late-Type M Dwarfs	58
Winters et al. (2015)	The Solar Neighborhood XXXV	175
Winters et al. (2017)	The Solar Neighborhood XXXVIII	33
Zhang et al. (2009)	SDSS and 2MASS UCD	806
<i>Unrefereed Publications</i>		
Cruz & Gagné (2014)	Ultracool RIZzo Spectral Library	632
dwarfarchives.org	Dwarf Archives (C. Gelino)	404
M. Gillon (priv. comm.)	SPECULOOS Input Target List	732
	SIMBAD M dwarfs $J > 14$ mag	760
	SIMBAD LT dwarfs $J > 14$ mag	115
S. Pineda (priv. comm.)		534

Table 3. Bona fide and 1σ samples of M7–L5 ultracool dwarfs in the 25 pc volume

Designation	SIMBAD Name	Adopted SpT	SpT Flag	J (mag)	$J - K_S$	Distance (pc)	Distance Type	Ref.
<i>Bona fide sample</i>								
LP 584–4	J00020649+0115366	M9.0	NIR	12.17±0.02	1.04±0.03	20.81±0.06	Trig	2
GJ 1001 C	J00043484–4044058B	L5.0	OPT	13.76±0.04	1.7±0.06	12.18±0.06	Trig	2
GJ 1001 B	J00043484–4044058C	L5.0	OPT	13.9±nan	1.6±nan	12.18±0.06	Trig	3
2MASS J00044144–2058298	J000441442–20582984	M7.0	NIR	12.4±0.02	1.01±0.03	15.08±0.04	Trig	4
2MASS J00145575–4844171	J00145575–4844171	L2.5	OPT	14.05±0.04	1.33±0.05	19.96±0.16	Trig	5

References—(1) This paper; (2) Cutri et al. (2003); (3) Leggett et al. (2002); (4) Gaia Collaboration (2018); (5) Kirkpatrick et al. (2008); (6) Kirkpatrick et al. (2000); (7) Cruz et al. (2003); (8) Irwin et al. (1991); (9) McCarthy et al. (1964); (10) Leinert et al. (1994); (11) Reid et al. (2008); (12) Deacon et al. (2005); (13) Gizis et al. (2003); (14) Reid et al. (2000); (15) Wilson et al. (2003); (16) Trimble (1986); (17) Crifo et al. (2005); (18) Theissen et al. (2017); (19) Cruz et al. (2007); (20) Liebert et al. (2003); (21) Ahn et al. (2012); (22) Gizis et al. (2001); (23) Tinney (1993); (24) Basri et al. (2000); (25) Lodieu et al. (2005); (26) Phan-Bao et al. (2006); (27) Kirkpatrick et al. (1997); (28) Kendall et al. (2007); (29) Castro et al. (2013); (30) Adelman-McCarthy & et al. (2009); (31) Hawley et al. (2002); (32) Kirkpatrick et al. (2016); (33) Reid et al. (2004); (34) Lépine et al. (2002b); (35) Pokorny et al. (2004); (36) Kirkpatrick et al. (2014); (37) Salim et al. (2003); (38) Zacharias et al. (2012); (39) Phan-Bao et al. (2008); (40) Gizis et al. (2000); (41) Reylé et al. (2006); (42) Reid et al. (2003b); (43) Scholz (2014); (44) Scholz & Meusinger (2002); (45) Liebert (1976); (46) Haro & Chavira (1966); (47) Lépine & Shara (2005); (48) Shkolnik et al. (2009); (49) West et al. (2008); (50) Schneider et al. (2014); (51) Rebolo et al. (1998); (52) Gizis (2002); (53) Kirkpatrick et al. (1995); (54) Close et al. (2003); (55) Davison et al. (2015); (56) Schneider et al. (2016); (57) Delfosse et al. (1997); (58) Bessell (1991); (59) Gagné et al. (2015c); (60) Koerner et al. (1999); (61) Looper et al. (2008); (62) Phan-Bao et al. (2003); (63) Schmidt et al. (2010); (64) West et al. (2011); (65) Fan et al. (2000); (66) Tinney et al. (1993); (67) Kirkpatrick et al. (1999); (68) Hartwick et al. (1984); (69) Jenkins et al. (2009); (70) Kirkpatrick et al. (1993); (71) Gauza et al. (2015); (72) Burgasser et al. (2015b); (73) Liu & Leggett (2005); (74) Patience et al. (2002); (75) Alonso-Floriano et al. (2015); (76) Schmidt et al. (2007); (77) Kendall et al. (2004); (78) Reid & Gizis (2005); (79) Sheppard & Cushing (2009b); (80) Faherty et al. (2012); (81) Scholz et al. (2004b); (82) Goto et al. (2002); (83) Martín et al. (2000); (84) Kirkpatrick et al. (2011); (85) Reid et al. (2007); (86) Kellogg et al. (2017); (87) Chiu et al. (2006); (88) Pérez Garrido et al. (2014); (89) Zhang et al. (2009); (90) Rajpurohit et al. (2013); (91) M. Gillon (priv. comm.); (92) Gizis et al. (2002); (93) Günther et al. (2014); (94) Martín et al. (2010); (95) Luhman & Sheppard (2014); (96) McElwain & Burgasser (2006); (97) Radigan et al. (2008); (98) Schneider et al. (2011); (99) Zacharias et al. (2003); (100) Costa et al. (2005); (101) Beamín et al. (2013); (102) Newton et al. (2014); (103) Kirkpatrick et al. (2010); (104) Luhman et al. (2012); (105) Folkes et al. (2012); (106) Lépine et al. (2002a); (107) Lépine et al. (2003); (108) Marocco et al. (2015); (109) Gizis et al. (2011); (110) Herbig (1956); (111) Gray et al. (2006); (112) Dupuy et al. (2009); (113) Kirkpatrick et al. (2001a); (114) Dahn et al. (2002); (115) Deshpande et al. (2012); (116) Allen et al. (2007); (117) Pokorny et al. (2003); (118) Phan-Bao & Bessell (2006).

NOTE—This table is available in its entirety in a machine-readable form in the online journal. A portion is shown here for guidance regarding its form and content.

Table 4. Multi-wavelength photometry for bona fide and 1σ samples of M7–L5 ultracool dwarfs in the 25 pc volume

Column Number	Label	Description
1	SIMBAD Name	Source name as listed in SIMBAD
2	Adopted Spectral Type	Adopted spectral type following the preference order described in Section 2.2.1.
3	Spectral Type Flag	Source of spectral type
4, 5	SDSS r (mag)	SDSS r magnitude and uncertainty
6, 7	SDSS i (mag)	SDSS i magnitude and uncertainty
8, 9	SDSS z (mag)	SDSS z magnitude and uncertainty
10, 11	2MASS J (mag)	2MASS J magnitude and uncertainty
12, 13	2MASS H (mag)	2MASS H magnitude and uncertainty
14, 15	2MASS K_s (mag)	2MASS K_s magnitude and uncertainty
16, 17	MKO J (mag)	MKO J magnitude and uncertainty
18, 19	MKO H (mag)	MKO H magnitude and uncertainty
20, 21	MKO K (mag)	MKO K magnitude and uncertainty
22, 23	UKIDSS J (mag)	UKIDSS J magnitude and uncertainty
24, 25	UKIDSS H (mag)	UKIDSS H magnitude and uncertainty
26, 27	UKIDSS K (mag)	UKIDSS K magnitude and uncertainty
28, 29	WISE $W1$ (mag)	WISE $W1$ magnitude and uncertainty
30, 31	WISE $W2$ (mag)	WISE $W2$ magnitude and uncertainty
32, 33	WISE $W3$ (mag)	WISE $W3$ magnitude and uncertainty
34	Reference	Discovery reference

References— (2) Cutri et al. (2003); (3) Leggett et al. (2002); (4) Gaia Collaboration (2018); (5) Kirkpatrick et al. (2008); (6) Kirkpatrick et al. (2000); (7) Cruz et al. (2003); (8) Irwin et al. (1991); (9) McCarthy et al. (1964); (10) Leinert et al. (1994); (11) Reid et al. (2008); (12) Deacon et al. (2005); (13) Gizis et al. (2003); (14) Reid et al. (2000); (15) Wilson et al. (2003); (16) Trimble (1986); (17) Crifo et al. (2005); (18) Theissen et al. (2017); (19) Cruz et al. (2007); (20) Liebert et al. (2003); (21) Ahn et al. (2012); (22) Gizis et al. (2001); (23) Tinney (1993); (24) Basri et al. (2000); (25) Lodieu et al. (2005); (26) Phan-Bao et al. (2006); (27) Kirkpatrick et al. (1997); (28) Kendall et al. (2007); (29) Castro et al. (2013); (30) Adelman-McCarthy & et al. (2009); (31) Hawley et al. (2002); (32) Kirkpatrick et al. (2016); (33) Reid et al. (2004); (34) Lépine et al. (2002b); (35) Pokorny et al. (2004); (36) Kirkpatrick et al. (2014); (37) Salim et al. (2003); (38) Zacharias et al. (2012); (39) Phan-Bao et al. (2008); (40) Gizis et al. (2000); (41) Reylé et al. (2006); (42) Reid et al. (2003b); (43) Scholz (2014); (44) Scholz & Meusinger (2002); (45) Liebert (1976); (46) Haro & Chavira (1966); (47) Lépine & Shara (2005); (48) Shkolnik et al. (2009); (49) West et al. (2008); (50) Schneider et al. (2014); (51) Rebolo et al. (1998); (52) Gizis (2002); (53) Kirkpatrick et al. (1995); (54) Close et al. (2003); (55) Davison et al. (2015); (56) Schneider et al. (2016); (57) Delfosse et al. (1997); (58) Bessell (1991); (59) Gagné et al. (2015c); (60) Koerner et al. (1999); (61)Looper et al. (2008); (62) Phan-Bao et al. (2003); (63) Schmidt et al. (2010); (64) West et al. (2011); (65) Fan et al. (2000); (66) Tinney et al. (1993); (67) Kirkpatrick et al. (1999); (68) Hartwick et al. (1984); (69) Jenkins et al. (2009); (70) Kirkpatrick et al. (1993); (71) Gauza et al. (2015); (72) Burgasser et al. (2015b); (73) Liu & Leggett (2005); (74) Patience et al. (2002); (75) Alonso-Floriano et al. (2015); (76) Schmidt et al. (2007); (77) Kendall et al. (2004); (78) Reid & Gizis (2005); (79) Sheppard & Cushing (2009b); (80) Faherty et al. (2012); (81) Scholz et al. (2004b); (82) Goto et al. (2002); (83) Martín et al. (2000); (84) Kirkpatrick et al. (2011); (85) Reid et al. (2007); (86) Kellogg et al. (2017); (87) Chiu et al. (2006); (88) Pérez Garrido et al. (2014); (89) Zhang et al. (2009); (90) Rajpurohit et al. (2013); (91) M. Gillon (priv. comm.); (92) Gizis et al. (2002); (93) Günther et al. (2014); (94) Martín et al. (2010); (95) Luhman & Sheppard (2014); (96) McElwain & Burgasser (2006); (97) Radigan et al. (2008); (98) Schneider et al. (2011); (99) Zacharias et al. (2003); (100) Costa et al. (2005); (101) Beamín et al. (2013); (102) Newton et al. (2014); (103) Kirkpatrick et al. (2010); (104) Luhman et al. (2012); (105) Folkes et al. (2012); (106) Lépine et al. (2002a); (107) Lépine et al. (2003); (108) Marocco et al. (2015); (109) Gizis et al. (2011); (110) Herbig (1956); (111) Gray et al. (2006); (112) Dupuy et al. (2009); (113) Kirkpatrick et al. (2001a); (114) Dahn et al. (2002); (115) Deshpande et al. (2012); (116) Allen et al. (2007); (117) Pokorny et al. (2003); (118) Phan-Bao & Bessell (2006).

NOTE—This table is available in its entirety in a machine-readable form in the online journal.

Table 5. Bona fide and 1σ samples of M7–L5 ultracool dwarfs in the 25 pc volume

Column Number	Label	Description
1	Source Name	Name of source as shown in SIMBAD
	<i>Literature spectral types</i>	
2	Adopted Spectral Type	Spectral type as reported in the literature adopted in this study
3	Flag of Adopted Spectral Type	Type of spectral classification adopted
4	Optical Spectral Type	Optical spectral classification as reported in the literature
5	NIR Spectral Type	NIR spectral classification as reported in the literature
6	SIMBAD Spectral Type	Spectral classification reported in SIMBAD, either optical or NIR
7	SDSS Spectral Type	Spectral classification as reported in SDSS
	<i>Spectral types by indices</i>	
8, 9	Burgasser (2007a) indices	Spectral type according to Burgasser (2007a) indices and uncertainty
10, 11	Allers et al. (2007) indices	Spectral type according to Allers et al. (2007) indices and uncertainty
12, 13	Reid et al. (2001) indices	Spectral type according to Reid et al. (2001) indices and uncertainty
	<i>Spectral types by standard</i>	
14	Classification by Standard	Spectral type measured by comparison to Kirkpatrick et al. (2010) spectral standards
15	References	References for optical, NIR, SIMBAD, and spectral classification by standard

References— (1) This paper; (5) Kirkpatrick et al. (2008); (6) Kirkpatrick et al. (2000); (7) Cruz et al. (2003); (11) Reid et al. (2008); (13) Gizis et al. (2003); (14) Reid et al. (2000); (15) Wilson et al. (2003); (19) Cruz et al. (2007); (20) Liebert et al. (2003); (22) Gizis et al. (2001); (25) Lodieu et al. (2005); (26) Phan-Bao et al. (2006); (28) Kendall et al. (2007); (29) Castro et al. (2013); (31) Hawley et al. (2002); (32) Kirkpatrick et al. (2016); (33) Reid et al. (2004); (35) Pokorny et al. (2004); (36) Kirkpatrick et al. (2014); (37) Salim et al. (2003); (39) Phan-Bao et al. (2008); (40) Gizis et al. (2000); (42) Reid et al. (2003b); (43) Scholz (2014); (44) Scholz & Meusinger (2002); (47) Lépine & Shara (2005); (48) Shkolnik et al. (2009); (49) West et al. (2008); (50) Schneider et al. (2014); (52) Gizis (2002); (53) Kirkpatrick et al. (1995); (54) Close et al. (2003); (55) Davison et al. (2015); (58) Bessell (1991); (59) Gagné et al. (2015c); (61)Looper et al. (2008); (62) Phan-Bao et al. (2003); (63) Schmidt et al. (2010); (64) West et al. (2011); (65) Fan et al. (2000); (67) Kirkpatrick et al. (1999); (69) Jenkins et al. (2009); (71) Gauza et al. (2015); (72) Burgasser et al. (2015b); (75) Alonso-Floriano et al. (2015); (76) Schmidt et al. (2007); (77) Kendall et al. (2004); (78) Reid & Gizis (2005); (80) Faherty et al. (2012); (82) Goto et al. (2002); (83) Martín et al. (2000); (84) Kirkpatrick et al. (2011); (85) Reid et al. (2007); (86) Kellogg et al. (2017); (87) Chiu et al. (2006); (88) Pérez Garrido et al. (2014); (90) Rajpurohit et al. (2013); (94) Martín et al. (2010); (95) Luhman & Sheppard (2014); (96) McElwain & Burgasser (2006); (97) Radigan et al. (2008); (101) Beamín et al. (2013); (102) Newton et al. (2014); (103) Kirkpatrick et al. (2010); (104) Luhman et al. (2012); (105) Folkes et al. (2012); (106) Lépine et al. (2002a); (107) Lépine et al. (2003); (108) Marocco et al. (2015); (109) Gizis et al. (2011); (111) Gray et al. (2006); (112) Dupuy et al. (2009); (113) Kirkpatrick et al. (2001a); (115) Deshpande et al. (2012); (116) Allen et al. (2007); (118) Phan-Bao & Bessell (2006); (119) Rajpurohit et al. (2012); (120) Forveille et al. (2005); (121) Cruz et al. (2009); (122) Liebert & Ferguson (1982); (123) Bardalez Gagliuffi et al. (2014); (124) Teegarden et al. (2003); (125) McCaughrean et al. (2002); (126) Siegler et al. (2005); (127) Kendall et al. (2003); (128) Gálvez-Ortiz et al. (2010); (129) Lépine et al. (2009); (130) Faherty et al. (2009); (131) Salim & Gould (2003); (132) Thorstensen & Kirkpatrick (2003); (133) West et al. (2015); (134) Bochanski et al. (2011); (135) Dieterich et al. (2014); (136) Hambaryan et al. (2004); (137) Law et al. (2006); (138) Martín et al. (1999); (139) Jahreiß et al. (2001); (140) Koen (2013); (141) Barrado Y Navascués (2006); (142) Metodieva et al. (2015); (143) Winters et al. (2015); (144) Schmidt et al. (2014); (145) Scholz et al. (2005); (146) Henry & Kirkpatrick (1990); (147) Kirkpatrick et al. (1994); (148) Malkov et al. (2012); (149) SpeX Prism Library; (150) Knapp et al. (2004); (151) Marocco et al. (2013); (152) Allers et al. (2010); (153) Terrien et al. (2015); (154) Phan-Bao (2011); (155) Burgasser et al. (in prep.); (156) Allers & Liu (2013); (157) Faherty et al. (2016); (158) Burgasser et al. (2010); (159) Dupuy et al. (2010); (160) Burgasser et al. (2007a); (161) Burgasser et al. (2008b); (162) Aberasturi et al. (2014); (163) Geballe et al. (2002); (164) Stumpf et al. (2008); (165) Gomes et al. (2013); (166) Bowler et al. (2009); (167) Burgasser et al. (2011b); (168) Bowler et al. (2010); (169) Sheppard & Cushing (2009a); (170) Forveille et al. (2004); (171) Witte et al. (2011); (172) Burgasser et al. (2007b); (173) Aganze et al. (2016); (174) Geißler et al. (2011); (175) Kasper et al. (2007); (176) Liu et al. (2002); (177) Ireland et al. (2008); (178) Dupuy & Liu (2012); (179) Liu et al. (2016); (180) Leggett et al. (2001); (181) Leinert et al. (2000); (182) Konopacky et al. (2010); (183) Henry et al. (2004); (184) Burgasser et al. (2005); (185) Stephenson (1986); (186) Kirkpatrick et al. (1991); (187) Koen et al. (2010); (188) Burgasser et al. (2011a); (189) Tinney et al. (1998); (190) Scholz et al. (2004a).

NOTE—This table is available in its entirety in a machine-readable form in the online journal.

Table 6. Trigonometric and spectrophotometric distances of bona fide and 1σ samples of M7–L5 ultracool dwarfs in the 25 pc volume

Source Name	Spectral Type		Parallax	Distance		Ref.
	Adopted	Flag		Trigonometric	Spectrophotometric (NIR)	
<i>Bona fide sample</i>						
LP 584–4	M9.0	NIR	48.05±0.14	20.81±0.06	15±2	191
GJ 1001 C	L5.0	OPT	82.09±0.38	12.18±0.06	11±1	191
GJ 1001 B	L5.0	OPT	82.09±0.38	12.18±0.06	...	191
2MASS J00044144–2058298	M7.0	NIR	66.33±0.16	15.08±0.04	23±3	191
2MASS J00145575–4844171	L2.5	OPT	50.11±0.39	19.96±0.16	20±2	191

References— (1) This paper; (4) Gaia Collaboration (2018); (72) Burgasser et al. (2015b); (80) Faherty et al. (2012); (129) Lépine et al. (2009); (135) Dieterich et al. (2014); (151) Marocco et al. (2013); (178) Dupuy & Liu (2012); (191) Gaia Collaboration et al. (2018); (192) Dittmann et al. (2014); (193) Weinberger et al. (2016); (194) Bartlett et al. (2017); (195) Lindegren et al. (2016); (196) Sahlmann et al. (2015); (197) van Leeuwen (2007); (198) Pravdo et al. (2005).

NOTE—This table is available in its entirety in a machine-readable form in the online journal.

Table 7. SpeX observing log

Designation	2MASS J	2MASS K_s	Slit	Total t_{exp} (s)	Airmass	Obs. Date	Median S/N	A0 Standard
<i>Within 25 pc</i>								
J00130931–0025521	12.167	11.319	0.5x15''	539	1.098	20151006	379.34	HD 1154
J00192626+4614078	12.603	11.502	0.5x15''	539	1.127	20151117	296.67	HD 222749
J00525468–2705597	13.611	12.54	0.5x15''	719	1.461	20150804	186.29	HD 222332
...	0.5x15''	717	1.474	20151116	163.85	HD 225200
J01004911–1933398	13.487	12.755	0.5x15''	478	1.348	20161007	85.90	HD 13433

^a Magnitudes are for combined system.

^b Background source.

NOTE—This table is available in its entirety in a machine-readable form in the online journal.

Table 8. Intermediate gravity and very low gravity sources in the M7–L5 25 pc Sample

Source Name	Literature SpT		SpeX SpT		μ_α (mas/yr)	μ_δ (mas/yr)	RV (km/s)	Trigonometric Distance (pc)	BANYAN Σ	Ref. ^a
	Optical	NIR	Field	Low Gravity						
<i>Very Low Gravity Sources</i>										
2MASSW J0045214+163445	L2 β	L3.5	L3.0	L1.0 γ	358.92±0.4	-48.07±0.24	3.16±0.83	15.38±0.05	Argus (99.9%)	191;157;191;156;216
2MASS J03552337+1133437 ^b	L5 γ	L3 γ	L7.0	L4.0 γ	219.76±1.57	-631.28±0.82	11.92±0.22	9.12±0.06	AB Dor (99.9%)	191;218;191;59
2MASS J05012406–0010452	L4 γ	L3 γ	L7.0	L4.0 γ	189.25±1.52	-145.31±1.16	21.77±0.66	21.24±0.40	Field (0%)	191;157;191;59;156
2MASS J06244595–4521548	L5:	L5	L7.0	L4.0 γ	-35.75±0.89	376.67±1.24	...	12.25±0.07	Argus (95.1%)	191; ... ;191;59
G 196–3B ^b	L3 β	L4 γ	L7.0	L2.0 γ	-137.82±0.93	-208.52±1.67	...	22.55±0.41	Field (45.3%)	191; ... ;191;156

References— (1) This paper; (49) West et al. (2008); (50) Schneider et al. (2014); (56) Schneider et al. (2016); (59) Gagné et al. (2015c); (80) Faherty et al. (2012); (102) Newton et al. (2014); (115) Deshpande et al. (2012); (156) Allers & Liu (2013); (157) Faherty et al. (2016); (191) Gaia Collaboration et al. (2018); (192) Dittmann et al. (2014); (216) Gagné et al. (2014); (217) Seifahrt et al. (2010); (218) Monet et al. (2003); (219) Burgasser et al. (2015a); (220) Blake et al. (2010); (221) Casewell et al. (2008); (222) Reiners & Basri (2009); (223) Jameson et al. (2008); (224) Morin et al. (2010); (225) Hawley et al. (1996); (226) Burgasser & Mamajek (2017).

NOTE—This table is available in its entirety in a machine-readable form in the online journal.

Table 9. Red and blue $J - K_s$ color outliers

Source Name	Adopted SpT	SpT Flag	$J - K_s$	$J - K_s$ Excess	YMG	Ref.
<i>Red Outliers</i>						
2MASS J03552337+1133437 ^b	L5.0	OPT	2.52±0.03	0.77	11;59	
G 196–3B ^b	L3.0	OPT	2.05±0.06	0.44	51	
LHS2397aA	M8.0	OPT	1.28±0.03	0.22	60	
Kelu–1 A	L2.0	OPT	2.41±0.17	0.90	2	
2MASSW J1728114+394859A	L5.0	NIR	2.21±0.09	0.46	6	
2MASS J17410280–4642218A ^b	L5.0	NIR	2.35±0.08	0.60	50;157	
<i>Blue Outliers</i>						
2MASS J09230296–2300415 ^c	M8.0	NIR	0.55±0.03	-0.51	2	
LHS 286	M8.0	OPT	0.82±0.03	-0.24	2	
2MASS J11263991–5003550	L5.0	OPT	1.17±0.04	-0.58	50	
LHS 2839	M7.0	OPT	0.74±0.03	-0.23	2	
2MASS J14162408+1348263	L5.0	OPT	1.03±0.03	-0.72	50	
2MASS J14343616+2202463 ^d	L2.5	NIR	0.97±0.06	-0.54	79	
2MASS J14442067–2019222	M9.0	OPT	0.61±0.04	-0.54	81	
2MASS J15552651+0954099 ^c	M8.0	PHOT	0.73±0.04	-0.33	91	
G 203–50B	L5.0	NIR	1.20±0.07	-0.54	97	
GJ 660.1B ^c	M7.5	NIR	0.82±0.05	-0.24	98	
UCAC2 11845260 ^d	M7.0	OPT	0.50±0.03	-0.47	99	
2MASS J17210390+3344160 ^c	L3.0	OPT	1.14±0.03	-0.47	100	
2MASS J17264070–2737593	L5.0	OPT	1.18±0.04	-0.57	101	
2MASS J17430860+8526594	L5.0	NIR	1.09±0.06	-0.66	104	
LEHPM 2–90 ^c	M9.0	NIR	0.84±0.03	-0.31	35	
GJ 802 b	L5.0	NIR	1.14±0.28	-0.61	2	
LEHPM 6344	M9.5	NIR	0.75±0.03	-0.47	117	

References— (2) Cutri et al. (2003); (6) Kirkpatrick et al. (2000); (11) Reid et al. (2008); (35) Pokorny et al. (2004); (50) Schneider et al. (2014); (51) Rebolo et al. (1998); (59) Gagné et al. (2015c); (60) Koerner et al. (1999); (79) Sheppard & Cushing (2009b); (81) Scholz et al. (2004b); (91) M. Gillon (priv. comm.); (97) Radigan et al. (2008); (98) Schneider et al. (2011); (99) Zacharias et al. (2003); (100) Costa et al. (2005); (101) Beamín et al. (2013); (104) Luhman et al. (2012); (117) Pokorny et al. (2003); (157) Faherty et al. (2016).

^aDiscovery Reference; Young Moving Group Reference.

^b2MASS J0355+1133 and 2MASS J1741–4642 are members of the AB Doradus young moving group, while G 196–3B is a young, unassociated source.

^cAlso classified as INT-G, indicating low metallicity rather than low gravity.

^dMember of extended 25 $pc + 1\sigma$ sample.

Table 10. Spectral binary candidates with M7–L7 primary components.

Designation	Spectral Type			2MASS ΔJ	Confidence	Spectral Indices ^b	References [*]
	Combined	Primary ^a	Secondary ^a				
<i>Within 25 pc</i>							
2MASSW J0320284–044636	M8.0	M9.6±0.2	T5.6±1.0	3.5±0.5	96%	12	202,213;191
WISE J072003.20–084651.2	M9.0	M8.9±0.0	T5.1±0.7	3.5±0.2	100%	6	71;63
2MASS J08053189+4812330	L4.0	L4.3±0.4	T5.0±1.1	1.5±0.3	> 99%	6	214;188
2MASS J13153094–2649513	L5.5	L4.7±0.4	T5.4±3.0	2.1±0.8	95%	12	168;158
2MASS J22521073–1730134	T0.0	L4.8±0.5	T4.4±0.7	1.24±0.25	> 99%	11	... ;205
<i>Outside 25 pc</i>							
2MASS J09311309+2802289	L3.0	L1.4±0.1	T2.3±0.8	2.3±0.1	> 99%	11	...
2MASS J14111847+2948515	L3.5	L4.1±1.0	T3.9±0.9	1.2±0.5	> 99%	6	...
2MASS J14211873–1618201	M7.5	M8.3±0.2	T5.1±1.4	3.7±0.5	95%	5	...
<i>Rejected candidates</i>							
WISE J000622.67–131955.2	L5.0	L5.3±0.7	T5.3±2.6	1.7±0.9	54%	11	...
1RXS J002247.5+055709	M7.0	M6.6±0.0	T6.0±1.2	4.9±0.6	66%	5	...
2MASS J00525468–2705597	M7.5	M8.6±0.3	T6.0±1.1	4.0±0.6	78%	4	...
2MASS J02150802–3040011	M8.0	M7.8±0.3	T6.1±1.3	4.4±0.6	58%	4	...
2MASS J02354955–0711214	M7.0	M7.2±0.1	T6.2±1.3	4.7±0.6	53%	4	...
LSPM J0240+2832	M7.5	M7.2±0.4	T5.6±1.6	4.5±0.6	61%	6	...
SDSS J031225.12+002158.3	M7.0	M7.1±0.1	T6.6±0.8	4.9±0.5	69%	5	...
LP 356–770	M7.0	M7.1±0.1	T6.2±1.4	4.8±0.6	55%	4	...
2MASS J04430581–3202090	L5.0	L4.4±0.1	T1.3±0.3	1.1±0.1	83%	5	...
WISE J044633.45–242956.9	L5.0	L4.8±0.4	T1.9±0.5	0.8±0.2	> 99%	9	...
2MASS J06431685–1843375	M8.0	M8.5±0.0	T6.1±1.3	4.2±0.6	86%	6	...
2MASS J07410681+1738459	M7.0	M7.3±0.0	T3.6±2.9	4.3±0.9	88%	4	...
2MASS J09041916+4554559	M7.0	M6.6±0.0	T6.0±1.9	5.1±0.7	34%	5	...
SDSS J091130.53+224810.7	M7.0	M6.6±0.0	T6.0±1.7	5.0±0.7	39%	5	...
2MASS J09473829+3710178	M7.0	M6.6±0.1	T4.7±1.9	4.5±0.6	88%	6	...
2MASS J11073750–2759385B	M7.0	M7.2±0.1	T5.6±2.0	4.6±0.7	52%	4	...
SDSS J112329.35+015404.0	M7.0	M7.8±0.4	T5.0±2.1	4.1±0.6	41%	5	...
2MASS J12560215–1257217	M7.5	M7.2±0.2	T6.4±1.1	4.8±0.6	45%	4	...
2MASS J13261625+5640448	M7.0	M7.4±0.2	T5.4±1.7	4.3±0.6	67%	4	...
2MASS J13365044+4751321	M8.0	M7.5±0.2	T6.2±1.4	4.6±0.6	67%	4	...
2MASS J14162408+1348263A	L5.0	L4.0±0.2	T2.3±0.5	1.2±0.1	> 99%	10	159; ...
2MASS J14442067–2019222	M9.0	M7.8±0.2	T3.7±1.5	3.5±0.3	99%	6	...
2MASS J15072779–2000431	M7.5	M8.0±0.2	T6.4±1.2	4.5±0.6	45%	5	...

Table 10 continued on next page

Table 10 (*continued*)

Designation	Spectral Type			2MASS ΔJ	Confidence	Spectral Indices ^b	References [*]
	Combined	Primary ^a	Secondary ^a				
SDSS J151500.62+484744.8	L6.0	L4.6±0.4	T1.8±0.6	1.0±0.2	94%	6	...
2MASS J15394189−0520428	L4.0	L2.9±0.9	T4.1±2.6	2.4±0.6	65%	4	...
2MASS J15583862+2211112	M8.0	M7.0±0.3	T4.8±1.9	4.3±0.6	88%	6	...
G 203−50B	L5.0	L4.0±0.2	T2.4±0.6	1.2±0.1	99%	6	79; ...
LHS 3227	M6.0	M6.8±0.1	T5.4±2.0	4.7±0.7	77%	6	...
2MASS J17312974+2721233	L0.0	M8.7±0.0	T6.9±0.7	4.5±0.5	47%	4	...
2MASS J17335314+1655129	M7.0	M6.1±0.1	T5.2±1.8	5.0±0.7	70%	5	...
2MASS J17334227−1654500	L0.5	L0.2±0.3	T4.2±1.7	3.0±0.5	80%	7	...
2MASS J17351296+2634475	M7.5	M8.1±0.1	T5.6±1.3	4.0±0.5	80%	4	...
SDSS J174919.27+475605.3	M7.0	M6.5±0.1	T5.3±1.3	4.6±0.6	90%	5	...
2MASS J18353790+3259545	M8.5	M8.8±0.1	T5.7±2.0	4.1±0.7	41%	4	...
2MASS J18393308+2952164	M6.5	M7.4±0.3	T6.0±1.5	4.5±0.6	57%	4	...
2MASS J18432213+4040209	M8.0	M7.6±0.2	T6.4±1.3	4.6±0.6	32%	4	...
2MASS J18451889+3853248	M8.0	M7.7±0.2	T5.6±2.0	4.4±0.6	77%	5	...
WISE J204027.24+695923.7	L0.0	M7.7±0.3	T5.4±1.4	4.1±0.6	91%	4	...
2MASS J21363029+0515329	M8.5	M8.0±0.2	T5.6±1.9	4.2±0.7	51%	5	...
2MASS J22010456+2413016	M8.0	M7.6±0.5	T4.9±1.7	4.0±0.6	82%	4	...
2MASS J22021125−1109461	M6.5	M7.5±0.1	T5.4±1.7	4.3±0.6	83%	5	...
2MASS J22060209+0311059	M7.0	M6.6±0.0	T5.6±1.5	4.7±0.6	55%	5	...
2MASS J22120703+3430351	L5.0	L3.7±1.0	T5.4±1.9	2.2±0.8	54%	7	...
2MASS J22285440−1325178	M6.5	M6.9±0.5	T5.5±1.5	4.5±0.6	41%	6	...
LP 702−50	M6.0	M6.9±0.2	T6.1±1.3	4.8±0.6	60%	5	...
LP 460−44	M7.0	M7.1±0.1	T5.6±1.7	4.5±0.6	80%	4	...
LHS 3954	M7.0	M7.3±0.4	T6.5±1.1	4.8±0.6	40%	6	...
2MASS J23312174−2749500	M7.5	M8.3±0.1	T6.1±1.3	4.2±0.6	74%	6	...
2MASS J23515044−2537367	M8.0	M8.3±0.4	T5.5±1.5	3.9±0.6	74%	5	...

* Candidate; Confirmed.

^a Primary and secondary spectral types are a weighted average of the best binary template fits, inversely proportional to their ranked χ^2 .

^b Strong candidates have been selected by 8 or more index-index plots up to 12, weak candidates by 4-8.

References— (63) Burgasser et al. (2015b); (79) Radigan et al. (2008); (158) Burgasser et al. (2011b); (159) Bowler et al. (2010); (188) Dupuy & Liu (2012); (191) Burgasser et al. (2008a); (213) Blake et al. (2008); (214) Burgasser (2007b).

Table 11. Ultracool Binaries with M7–L5 Primaries in the 25 pc Sample

Name	Combined	Spectral type			Adopted Distance (pc)	Binary Reference
		UCD Primary	UCD Secondary	UCD		
2MASS J00275592+2219328AB	M7.5	M7	M8		15.27±0.89	120
2MASSW J0320284–044636AB	M8	M8	T5		20.04±0.2	199
2MASS J04291842–3123568AB	...	M7.5:	L1		12±1	126
V* V780 Tau	M7	M7.0	unknown		10.25±0.29	200
2MASS J06523073+4710348AB	L4.5	L3.5	L6.5		9.12±0.04	182
2MASS J07003664+3157266AB	...	L3.5	L6		12.2±0.3	182
LHS 1901AB	...	M7	M7		12.85±0.5	200
2MASS J07200325–0846499AB	M8	M9	T5		6.02±1.02	72
2MASS J0746425+200032AB	L0.5	L1	L1.5		11.6±0.62	150
2MASS J08053189+4812330AB	L5	L4	T5		21.38±0.44	178
DENIS J0823031–491201AB	L3	L1.5	L5.5		20.67±0.2	105
GJ 1116AB	...	M7	M8		5.14±0.0	102
2MASS J09153413+0422045AB	L5	L6	L6		18.23±0.36	201
LHS2397aAB	...	M8	L7.5		15.19±0.47	204
Kelu–1AB	L2	L2	L3.5		18.57±0.25	164
LP 497–33AB	M7	M7	M7.0		16.39±0.75	137
2MASS J12281523–1547342AB	L5	L5	L5.5		20.24±0.78	205
2MASS J12392727+5515371AB	L5	L5	L6		23.58±1.17	13
2MASS J12560215–1257217A B	...	M7.5	L7		15.62±4.39	71
2MASS J13153094–2649513AB	L5	L3.5	T7		18.56±0.39	167

Ultracool Binaries

Table 11 continued on next page

Table 11 (*continued*)

Name	Spectral type				Adopted Distance (pc)	Binary Reference
	Combined	UCD Primary	UCD Secondary	UCD Tertiary		
2MASS J14162408+1348263AB	...	L5	T7.5		9.3±0.03	168
2MASS J15200224-4422419AB	...	L1	L4.5		21±2, 19±2	172
2MASS J16334908-6808480AB	...	M8	M8.5		15.3±0.02	95
2MASS J17072343-0558249AB	...	M9	L3		16±2	96
2MASSW J1728114+394859AB	...	L5	L7		24.1±1.89	211
2MASS J17351296+2634475AB	...	M7.5	L0		14.99±0.31	137
2MASS J18450541-6357475AB	...	M8.5	T6		4.0±0.0	210
2MASS J21321145+1341584AB ^a	L6	L4.5	L8.5		33.33±9.11	211
2MASSW J2206228-204705AB ^a	M8	M8	M8		26.67±2.39	112
2MASS J22521073-1730134AB	L7.5	L4.5	T3.5		16.91±0.24	201
2MASS J22551861-5713056AB ^a	L5.5	L5	L8		12±1	213

<i>Higher Order Multiples Containing Ultracool Dwarf Binaries</i>						
GJ 1001BC	M4+L5+L5	L5	L5		12.18±0.06	150
LP 881-64BC	M6+M9.5+L0	M9.5	L0		7.72±0.15	10
G1 417BC	A3+L4.5+L6	L4.5	L6:		23.33±0.6	203
WDS J10472+4027Bab	M6+M8+L0	M8	L0		24.92±0.08	54
HD 114762B ^a	F9+F8+F4+M9+planet?	M9.0	d/sdM9±1		28±3	74
HD 130948BC	G2+L4+L4	L4	L4		18.17±0.11	208
BD+16 2708Bab	M3+M8.5+M9	M8.5	M9		9.65±0.16	83

<i>Ultracool Companions to Main Sequence Primaries</i>						
GJ 1048B	K3.5+L1.5	...	L1.5		21.47±0.13	22
CD-35 2722 B	M1+L3	...	L3		22.14±0.17	156

Table 11 continued on next page

Table 11 (*continued*)

Name	Spectral type				Adopted Distance (pc)	Binary Reference
	Combined	UCD Primary	UCD Secondary	UCD Tertiary		
G 196–3B	M3+L2	...	L3		22.55±0.41	51
LHS 5166B	M4+L4	...	L4		18.77±0.2	202
2MASS J11240487+3808054B	M4.5+M8.5	...	M8.5		18.47±0.07	54
NLTT 31198 ^a	M5–7+M6–7	...	M7		23.26±3.24	137
LHS 2839	K4+M7	...	M7		22±3	207
G 239–25 B	M3+L0	...	L0		10.97±0.04	170
2MASS J14562776+1755090	M5+M7	...	M7.0		19±2	209
2MASS J15552651+0954099	M3+M8	...	M8.0		22±3	149
VB 8	M3.5+M3.5+M7	...	M7.0		6.5±0.0	207
G 203–50B	M4.5+L5	...	L5		21.08±0.29	97
GJ 660.1B	M1+M7.5	...	M7.5		23.01±0.1	98
2MASS J19165762+0509021BB	M3+M8	...	M8.0		5.92±0.0	207
G1 779B	G0+L4.5	...	L4.5		17.24±0.27	176
LSPM J2010+0632B	M3.5+M4+M8.5	M4	M8.5		16.13±0.05	104
GJ 802b	M+M+L5	...	L5		15.87±1.39	177
G 216–7B	M0+M9.5	...	M9.5		21.0±0.09	212
LEHPM 1–6443C	WD+M4+M9	...	M9		23.22±0.1	189

Table 11 continued on next page

Table 11 (*continued*)

Name	Spectral type				Binary Reference
	Combined	UCD Primary	UCD Secondary	Adopted Distance (pc)	
References —	(10) Leinert et al. (1994); (13) Gizis et al. (2003); (22) Gizis et al. (2001); (51) Rebolo et al. (1998); (54) Close et al. (2003); (71) Gauza et al. (2015); (72) Burgasser et al. (2015b); (74) Patience et al. (2002); (83) Martin et al. (2000); (95) Luhman & Sheppard (2014); (96) McElwain & Burgasser (2006); (97) Radigan et al. (2008); (98) Schneider et al. (2011); (102) Newton et al. (2014); (104) Luhman et al. (2012); (105) Folkes et al. (2012); (112) Dupuy et al. (2009); (120) Forveille et al. (2005); (126) Siegler et al. (2005); (137) Law et al. (2006); (149) SpeX Prism Library; (150) Knapp et al. (2004); (156) Allers & Liu (2013); (164) Stumpf et al. (2008); (167) Burgasser et al. (2011b); (168) Bowler et al. (2010); (170) Forveille et al. (2004); (172) Burgasser et al. (2007b); (176) Liu et al. (2002); (177) Ireland et al. (2008); (178) Dupuy & Liu (2012); (182) Konopacky et al. (2010); (190) Scholz et al. (2004a); (199) Burgasser et al. (2008a); (200) ?; (201) Montagnier et al. (2006); (202) Reid et al. (2006); (203) Seifahrt et al. (2005); (204) Smith et al. (2015); (205) Freed et al. (2003); (206) Martin et al. (1999); (207) Dupuy et al. (2016); (208) van Biesbroeck (1961); (209) ?; (210) Dahn et al. (2017); (211) Bouy et al. (2003); (212) Biller et al. (2006); (213) Siegler et al. (2007); (214) Kirkpatrick et al. (2001b); (215) Burgasser et al. (2006).				

^aMember of extended $25\text{ pc} + 1\sigma$ sample.

Table 13. Selection functions for trigonometric and spectrophotometric distance cuts per spectral type bin.

SpT	Total	Intrinsic		Observed		Selection		Observed		Fraction		Not Intrinsic		Observed		False Positive	
		(3)	(4)	(5)	(6)	(7)	(8)	(9)	(10)	(11)	(12)	(13)	(14)	(15)	(16)		
M5	189460	23612	2129	2123	0.09	0.09	38	44	0.00	0.00	165848	174	2400	0.01	0.12		
M6	173166	21535	4475	4469	0.21	0.21	106	112	0.00	0.01	151631	353	4517	0.02	0.24		
M7	75002	9459	6704	6113	0.71	0.65	181	772	0.02	0.08	65543	490	2417	0.06	0.30		
M8	51619	6490	5946	5210	0.92	0.80	160	896	0.02	0.14	45129	461	1726	0.08	0.31		
M9	80893	10141	9861	8282	0.97	0.82	251	1830	0.02	0.18	70752	763	2347	0.09	0.27		
L0	83302	10572	10305	8427	0.97	0.80	267	2145	0.03	0.20	72730	754	2192	0.08	0.24		
L1	54934	6926	6770	5562	0.98	0.80	156	1364	0.02	0.20	48008	528	1581	0.09	0.26		
L2	44754	5574	5438	4416	0.98	0.79	134	1156	0.02	0.21	39180	392	1296	0.08	0.26		
L3	51654	6413	6248	5146	0.97	0.80	143	1245	0.02	0.19	45241	462	1688	0.08	0.30		
L4	52264	6542	6039	5035	0.92	0.77	149	1153	0.02	0.18	45722	442	1444	0.08	0.25		
L5	55985	7098	4869	3767	0.69	0.53	121	1223	0.02	0.17	48887	400	639	0.07	0.10		
L6	51527	6484	1856	1250	0.29	0.19	47	653	0.01	0.10	45043	160	63	0.03	0.01		

NOTE—Columns: (1) Spectral type bins; (2) Number of objects per bin; (3) Number of true objects per spectral type bin within 25 pc, i.e. intrinsic objects; (4) Number of intrinsic objects selected by an observed parallax cut at 25 pc; (5) Number of intrinsic objects selected by an observed spectrophotometric distance cut at 25 pc; (6) Selection function by parallax, i.e. fraction of intrinsic objects selected by their parallax cut at 25 pc; (7) Selection function by spectrophotometric distance; (8) Number of intrinsic objects not selected by a trigonometric cut at 25 pc; (9) Number of intrinsic objects not selected by a spectrophotometric cut at 25 pc; (10) Fraction of intrinsic objects missed by a spectrophotometric cut at 25 pc; (11) Fraction of intrinsic objects missed by a spectrophotometric cut at 25 pc; (12) Number of objects per spectral type bin outside of 25 pc; i.e. non-members (13) Number of non-members selected by an observed parallax cut at 25 pc; (14) Number of non-members selected by an observed spectrophotometric distance cut at 25 pc; (15) False positive rate for trigonometric selection; (16) False positive rate for spectrophotometric selection.

Table 14. Selection functions for trigonometric and spectrophotometric distance cuts per absolute magnitude bin.

M_J	(2)	(3)	Observed			Selection			Observed			Fraction			Not Intrinsic			Observed			False Positive											
			Selected			Function			Not Selected			Missed			Selected			Fraction			Selected			Fraction								
			Trig	Phot	(4)	Trig	Phot	(7)	Trig	Phot	(8)	Trig	Phot	(9)	Trig	Phot	(10)	Trig	Phot	(11)	Trig	Phot	(12)	Trig	Phot	(13)	Trig	Phot	(14)	Trig	Phot	(15)
9.75	161816	20008	2962	3155	0.15	0.16	39	98	0.00	0.00	0.00	0.00	0.00	0.00	0.00	0.00	141808	272	4129	0.02	0.23	0.02	0.23	0.02	0.23	0.02	0.23	0.02	0.23	0.02	0.23	
10.25	186252	23385	6363	6346	0.27	0.27	128	336	0.01	0.01	0.01	0.01	0.01	0.01	0.01	0.01	162867	451	4531	0.02	0.22	0.02	0.22	0.02	0.22	0.02	0.22	0.02	0.22	0.02	0.22	
10.75	117183	14691	9628	8925	0.66	0.61	221	1099	0.02	0.07	0.02	0.07	0.02	0.07	0.02	0.07	102492	715	3561	0.06	0.28	0.06	0.28	0.06	0.28	0.06	0.28	0.06	0.28	0.06	0.28	
11.25	101656	12726	11672	10136	0.92	0.80	268	1998	0.02	0.16	0.02	0.16	0.02	0.16	0.02	0.16	88930	899	3285	0.08	0.30	0.08	0.30	0.08	0.30	0.08	0.30	0.08	0.30	0.08	0.30	
11.75	94099	11843	11358	9325	0.96	0.79	272	2472	0.02	0.21	0.02	0.21	0.02	0.21	0.02	0.21	82256	811	2585	0.08	0.25	0.08	0.25	0.08	0.25	0.08	0.25	0.08	0.25	0.08	0.25	
12.25	75482	9411	9022	7296	0.96	0.78	218	2080	0.02	0.22	0.02	0.22	0.02	0.22	0.02	0.22	66071	568	2228	0.07	0.27	0.07	0.27	0.07	0.27	0.07	0.27	0.07	0.27	0.07	0.27	
12.75	70205	8823	8099	6675	0.92	0.76	174	1728	0.02	0.20	0.02	0.20	0.02	0.20	0.02	0.20	61382	435	2059	0.06	0.27	0.06	0.27	0.06	0.27	0.06	0.27	0.06	0.27	0.06	0.27	
13.25	71507	8952	6788	5510	0.76	0.62	179	1608	0.02	0.18	0.02	0.18	0.02	0.18	0.02	0.18	62555	199	1122	0.03	0.14	0.03	0.14	0.03	0.14	0.03	0.14	0.03	0.14	0.03	0.14	
13.75	55588	6908	3669	2657	0.53	0.38	86	1278	0.01	0.19	0.01	0.19	0.01	0.19	0.01	0.19	48680	70	270	0.01	0.04	0.01	0.04	0.01	0.04	0.01	0.04	0.01	0.04	0.01	0.04	

NOTE.—Columns: (1) Bins of absolute magnitude in J -band; (2) Number of objects per bin; (3) Number of true objects per absolute magnitude bin within 25 pc, i.e. intrinsic objects; (4) Number of intrinsic objects selected by an observed parallax cut at 25 pc; (5) Number of intrinsic objects selected by an observed spectrophotometric distance cut at 25 pc; (6) Selection function by parallax, i.e. fraction of intrinsic objects selected by their parallax cut at 25 pc; (7) Selection function by spectrophotometric distance; (8) Number of intrinsic objects not selected by a trigonometric cut at 25 pc; (9) Number of intrinsic objects not selected by a spectrophotometric cut at 25 pc; (10) Number of true objects per absolute magnitude bin outside of 25 pc; i.e. extrinsic objects; (11) Number of extrinsic objects with observed trigonometric distances within 25 pc; (12) Number of extrinsic objects with observed spectrophotometric distances within 25 pc; (13) Number of extrinsic objects selected by an observed parallax cut at 25 pc; (14) Number of extrinsic objects selected by an observed spectrophotometric distance cut at 25 pc; (15) False positive rate for parallax selection; (16) False positive rate for spectrophotometric selection.

Table 17. Number Densities by Spectral Subtype in units of *object pc*⁻³.

Spectral Type	Cruz et al. (2007)	Reid et al. (2008)	Kirkpatrick et al. (2012)	N*	Raw	SF-corrected
M5	$6.99^{+2.05}_{-1.59} \times 10^{-3}$
M6	...	$9.50^{+9.50}_{-4.70} \times 10^{-5}$	$1.07^{+0.25}_{-0.20} \times 10^{-2}$
M7	$1.08^{+0.34}_{-0.26} \times 10^{-3}$	$9.50^{+9.50}_{-4.70} \times 10^{-5}$	$1.40^{+1.07}_{-0.61} \times 10^{-3}$	64	$1.54^{+0.21}_{-0.18} \times 10^{-3}$	$3.20^{+0.29}_{-0.27} \times 10^{-3}$
M8	$3.73^{+0.60}_{-0.52} \times 10^{-3}$	$9.47^{+2.37}_{-1.89} \times 10^{-4}$	$2.33^{+1.30}_{-0.84} \times 10^{-3}$	61	$1.47^{+0.20}_{-0.18} \times 10^{-3}$	$2.34^{+0.25}_{-0.23} \times 10^{-3}$
M9	$9.95^{+3.32}_{-2.49} \times 10^{-4}$	$8.53^{+2.26}_{-1.79} \times 10^{-4}$	$9.33^{+9.33}_{-4.66} \times 10^{-4}$	44	$1.06^{+0.17}_{-0.15} \times 10^{-3}$	$1.58^{+0.21}_{-0.18} \times 10^{-3}$
L0	$6.63^{+2.80}_{-1.97} \times 10^{-4}$	$5.68^{+1.89}_{-1.42} \times 10^{-4}$	$4.66^{+7.54}_{-2.88} \times 10^{-4}$	21	$5.04^{+1.23}_{-0.99} \times 10^{-4}$	$7.50^{+1.47}_{-1.23} \times 10^{-4}$
L1	$4.97^{+2.49}_{-1.66} \times 10^{-4}$	$2.37^{+1.32}_{-0.85} \times 10^{-4}$...	28	$6.72^{+1.40}_{-1.16} \times 10^{-4}$	$1.02^{+0.17}_{-0.15} \times 10^{-3}$
L2	$8.29^{+3.07}_{-2.24} \times 10^{-4}$	$3.79^{+1.60}_{-1.12} \times 10^{-4}$...	21	$5.04^{+1.23}_{-0.99} \times 10^{-4}$	$7.75^{+1.50}_{-1.26} \times 10^{-4}$
L3	$4.14^{+2.31}_{-1.48} \times 10^{-4}$	$2.37^{+1.32}_{-0.85} \times 10^{-4}$...	16	$3.84^{+1.10}_{-0.86} \times 10^{-4}$	$5.80^{+1.31}_{-1.07} \times 10^{-4}$
L4	$5.80^{+2.65}_{-1.82} \times 10^{-4}$	$3.79^{+1.60}_{-1.12} \times 10^{-4}$...	23	$5.52^{+1.29}_{-1.05} \times 10^{-4}$	$8.75^{+1.58}_{-1.34} \times 10^{-4}$
L5	$4.97^{+2.49}_{-1.66} \times 10^{-4}$	$3.32^{+1.51}_{-1.04} \times 10^{-4}$	$4.66^{+7.54}_{-2.88} \times 10^{-4}$	28	$6.72^{+1.40}_{-1.16} \times 10^{-4}$	$1.44^{+0.20}_{-0.18} \times 10^{-3}$
L6	$4.14^{+2.31}_{-1.48} \times 10^{-4}$	$2.84^{+1.42}_{-0.95} \times 10^{-4}$
L7	$7.46^{+2.94}_{-2.11} \times 10^{-4}$	$4.70^{+7.70}_{-2.90} \times 10^{-5}$
L8	$4.97^{+2.49}_{-1.66} \times 10^{-4}$	$1.42^{+1.09}_{-0.62} \times 10^{-4}$
M7–M9.5	169	$(4.1 \pm 0.3) \times 10^{-3}$	$(7.1 \pm 0.5) \times 10^{-3}$
L0–L5	137	$(3.3 \pm 0.3) \times 10^{-3}$	$(5.4 \pm 0.4) \times 10^{-3}$
M7–L5	306	$(7.3 \pm 0.4) \times 10^{-3}$	$(12.6 \pm 0.6) \times 10^{-3}$

*Number of sources within 25 pc, declinations accessible by SpeX ($-50^\circ \leq \delta \leq +67^\circ$), and galactic latitudes outside of $\pm 15^\circ$ from the plane.

NOTE—The units for all values are pc^{-3} . These number densities take into account the sky coverage in each survey, but not the survey incompleteness. For the 20 pc sample of Cruz et al. (2007) the volume coverage is 36%, for the Reid et al. (2008) survey of the same volume, the coverage is 63%. For the Kirkpatrick et al. (2012) 8 pc sample, the volume coverage is 100%. For this study, the volume coverage is $63.6 \pm 0.59\%$. Uncertainties are calculated from Poisson statistics.

Table 18. Luminosity Function.

M_J	N	N_{trig}	N_{phot}	SFplx	SFphot	$N_{corrected}$	Density (mag pc^{-3})
9.75	4	4	0	0.15	0.16	38.65	$9.28^{+1.62}_{-1.39} \times 10^{-4}$
10.25	51	41	10	0.27	0.27	273.75	$6.57^{+4.14}_{-0.39} \times 10^{-3}$
10.75	68	60	8	0.66	0.61	150.76	$3.62^{+0.31}_{-0.29} \times 10^{-3}$
11.25	50	49	1	0.92	0.80	79.00	$1.90^{+0.23}_{-0.20} \times 10^{-3}$
11.75	41	39	2	0.96	0.79	62.55	$1.50^{+0.20}_{-0.18} \times 10^{-3}$
12.25	30	28	2	0.96	0.78	45.99	$1.10^{+0.18}_{-0.15} \times 10^{-3}$
12.75	25	24	1	0.92	0.76	39.71	$9.54^{+1.65}_{-1.41} \times 10^{-4}$
13.25	26	24	2	0.76	0.62	50.44	$1.21^{+0.18}_{-0.16} \times 10^{-3}$
13.75	16	14	2	0.53	0.38	45.91	$1.10^{+0.18}_{-0.15} \times 10^{-3}$